FINE SPATIAL RESOLUTION FOREST INVENTORY FOR GEORGIA:

REMOTE SENSING BASED GEOSTATISTICAL MODELING

AND K NEAREST NEIGHBOR METHOD

by

QINGMIN MENG

(Under the Direction of Chris J. Cieszewski)

ABSTRACT

The main objective of forest inventory is to acquire and maintain accurate and up-to-date forest information. Updating forest inventory information also is an important aspect of land use dynamics. In the process of large area forest inventory, the development and application of suitable technologies to estimate forest variables with fine spatial resolution are important for natural resources management and characterizing land use dynamics. Although ground inventory often has higher accuracy, it has two obvious disadvantages, i.e., time consuming and expensive. Combining geographic information systems (GIS), remote sensing, geospatial statistics, and ground inventory data, I develop and apply two up-to-date forest inventory approaches with fine spatial resolution (i.e., a 25-meter cell size) for the state of Georgia. One is a systematic geostatistical approach using remote sensing imagery for prediction. I develop this systematic approach including spatial/aspatial data exploration, semivariogram modeling, and kriging. Four typical kriging methods (i.e., ordinary kriging, universal kriging, Cokriging, and regression kriging) are compared and evaluated for spatially forecasting forest variables. Regression kriging is tested as the best kriging method. The second approach is the popular K nearest neighbor

method. I explored and improved two disadvantages (i.e., the selection of K and computation cost) of K nearest neighbor method before using it to estimate forest variables. Another two important aspects of the K nearest neighbor method (i.e., the distance metrics and weight schemes) also are explored and discussed to improve forecast performance. Next, a weighted K nearest neighbor method to forecast the volume of trees for the whole state of Georgia with a 25-meter cell size using 12 scenes of Landsat TM imagery as auxiliary data was used. Forecast evaluation conducted using 10,000 random sample pixels outside the training dataset and the mean estimations of volume compared with the results from US Forest Service indicate that the estimations from this research are reasonable. These estimations also are compatible with other studies for large area forest inventory. I believe the remote sensing based geostatistical modeling and weighted K nearest neighbor are efficient approaches to studying other aspects of land use dynamics and natural resources management.

INDEX WORDS: Up-to-date forest inventory, Fine spatial resolution, Remote sensing, GIS, Geostatistics, Weighted K nearest neighbor method, Hardwood volume, Softwood volume.

FINE SPATIAL RESOLUTION FOREST INVENTORY FOR GEORGIA: REMOTE SENSING BASED GEOSTATISTICAL MODELING AND K NEAREST NEIGHRBOR METHOD

by

QINGMIN MENG

MS, University of Georgia, 2005

PhD, Peking University, China, 2001

MS, Lanzhou University, China, 1997

BS, Shandong Normal University, China, 1994

A Dissertation Submitted to the Graduate Faculty of The University of Georgia in Partial Fulfillment of the Requirements for the Degree

DOCTOR OF PHILOSOPHY

ATHENS, GEORGIA

2006

FINE SPATIAL RESOLUTION FOREST INVENTORY FOR GEORGIA: REMOTE SENSING BASED GEOSTATISTICAL MODELING AND K NEAREST NEIGHBOR METHOD

by

QINGMIN MENG

Major Professor: Chris J. Cieszewski

Committee: Bruce E. Borders
Marguerite Madden
Barry D. Shiver
Mike R. Strub

Electronic Version Approved:

Maureen Grasso
Dean of the Graduate School
The University of Georgia
December 2006

Dedicated to My Parents

ACKNOWLEDGEMENTS

First of all, I would like to express my sincere appreciation to my advisor, Dr. Chris J. Cieszewski, for giving me four years' research assistantship throughout my graduate study in forest biometrics, GIS, remote sensing, and statistics. I thank him very much for giving me free time to do research in forest biometrics, forest health monitoring, geospatial statistics, and GIS.

I would like to extend my sincere appreciation to the committee members, Drs. Bruce E. Border, Marguerite Madden, Barry D. Shiver, and Mike R. Strub. I sincerely appreciate the time they spend evaluating and editing my dissertation. I thank Drs. Borders and Shiver for advising on forest inventory and management. I thank Dr. Strub for the help of supplying data for one of my research papers. I thank Dr. Madden for the advice on my studying and researching in GIS and remote sensing, and she always saves time to help me with research relating to GIS and remote sensing.

. There are so many people I would like to thank for their help. Thanks go to Dr. Clifton W. Pannell for his generosity and encouragement during my graduate study at UGA. Thanks go to Dr. E. Lynn Usery for his generosity and help for my job applications. Thanks go to Dr. Harold E. Burkhart and Mr. Ralph Amateis for their supplying data, reviewing, and editing one of my research papers.

I appreciate the support and encouragement by Drs. Aimin Wang, Chengge Lin, Wenying Wei, Decheng Peng, and Guoping Li. I appreciate Dr. Pete Bettinger's help of giving me an opportunity to design and instruct the course FORS7210, *Spatial Analysis for Natural Resources*

(*Advanced GIS*). I did enjoy that good time of teaching and studying with those 15 graduate students.

I would like to thank to my parents and families in China for their patience, understanding, encouragement, and support. My wife, Yanbing Tang, is such a wonderful woman and gives me a great family and support. Her continued support has always meant the world to me. I would like to acknowledge my son, Alan F. Meng, for providing me the indirect motivation to succeed, and I want him to be as proud of me as I am of my father. I deeply appreciate all their love and support.

TABLE OF CONTENTS

Page

LIST OF TABLES

Page

LIST OF FIGURES

Page

CHAPTER 1

RESEARCH BACKGROUND AND OBJECTIVES

1.1 Introduction

Forest inventory is one of the most important parts of forest management. Its purpose is to acquire and maintain accurate and up-to-date forest information. Updating forest inventory information is an important part of land management. Generally, there are three approaches to forest inventory. The most traditional one is ground inventory. The development of remote sensing techniques including Landsat TM, SPOT, and other satellite remote sensing makes it is possible to obtain resource information for a large area. Forest inventory using satellite imagery has been applied frequently in practice. Compared to the approaches using satellite remote sensing, ground inventory and traditional methods of air photo interpretation are usually time-consuming and expensive, especially for large forest areas. Remotely sensed data can supply up-to-date information and can be used to acquire many types of information about forests. However, ground inventory provides better accuracy than that obtained from remote sensing data. To obtain up-to-date and accurate inventory data for large areas, the most efficient way can be to combine the information from ground inventory and remotely sensed data using geospatial technologies, geographic information systems (GIS), remote sensing, and geospatial statistics.

In the 1970s scientists began to use remote sensing imagery for forest inventory. The first attempts used the newly available Landsat multispectral scanner (MSS) imagery for forest cover mapping (Kleinn). One of the most popular methods applied in forest inventory is the K nearest neighbor (KNN) prediction and classification. The KNN method was first applied in forest

inventory for estimation of timber volume, basal area, tree species, mean height, and mean diameter (Tokola et al 1996, Tomppo 1991, Tomppo et al 1999). It is becoming more and more widely used to acquire almost all types of forest characteristics, such as stem volume and basal area (Holmgren et al. 2000), single tree characteristics from photograph interpretation (Holmstrom 2002), wood volume, age and biomass (Reese et al. 2002), forest fuels (Baath et al. 2002), and defoliation (Heikkila et al. 2002). The most similar neighbor method (Moeur and Stage 1995) applied in forest inventory is very similar to the K nearest neighbor method.

Another approach for forest inventory is geostatistical modeling. It is not widely used though it is a very useful interpolating approach for unmeasured points (Tuominen et al. 2002). The most promising geostatistical technique for forest inventory is the use of variograms with remotely sensed data for classifying image texture (Curran 1988, Jupp et al. 1988, Woodcock et al. 1988a/b, Lark 1996, Chica-Olmo and Abarca-Hernandez 2000).

The prerequisites of applying geostatistics in forest inventory are often overlooked. For example, the basic prerequisite is general regionalized variables. A general regionalized variable is a kind of random variable to describe or model a spatial attribute, which must be indexed by location. It is reasonable to consider forest parameters as random variables, so that statistics can be applied for their analysis. General regionalized variables have two special characteristics, spatial dependence and spatial heterogeneity, which determine the neighborhood selection and the characteristics of semivariogram analysis in geostatistical research in forest inventory. They have been overlooked in the past research in forest inventory. For example, spatial autocorrelation is not considered in the national forest inventory in US.

Spatial dependence can be described as what happens at one place is correlated with events in nearby places. This relationship can be positive or negative, and it is measured by so-

called spatial autocorrelation. The most famous geographic first law, called Tobler's First Law, is "all things are related but nearby things are more related than distant things"(Miller 2004, Tobler 1970). This law describes positive correlation, and a world without positive spatial dependence would be an impossible world (Goodchild 2003). This relationship indicates that nearby things are more similar than distant things. Spatial dependence can be used to improve classification and spatial prediction.

Spatial heterogeneity is ubiquitous in nature. Spatial heterogeneity describes this geographic variation in the constants or parameters of relationships and indicates that the basic attribute of geographical phenomena is nonstationarity. This characteristic is an important aspect in the process of forest inventory since we can think forest variables as geographical phenomena.

1.2 Technological Background or Literature Review

1.2.1 Geostatistics in forest inventory

Geostatistics is not new. Typically, geostaistics is one of the technique used to analyze and predict values of a spatially distributed variable. Geostatistical analysis has been widely applied by geologists, geographers, and social scientists. Geostatistical techniques have been proved to be essential tools for analyzing the spatial variation of remotely sensed data (Curran and Atkinson 1998). Kriging is the best linear unbiased predictor (BLUP). Some studies have demonstrated the efficacy of this suite of quantitative techniques for estimating the optimum spatial resolution using remotely sensed data (Curran 1988, Atkinson 1993). These techniques also have been used as tools to model the spatial variation within images (Chica-Olmo and Abarca_Hernandez 2000, Coburn and Roberts 2004, St-Onge and Cavayas 1995, Woodcock et al. 1988b, Wulder et al. 1996, 1998).

Atkinson (1993) made a good summarization of geostatistical techniques for the applications of remote sensing data. In his review, Atkinson discussed in detail the geostatistical methods (i.e., semivariogram modeling) without discribing kriging. This might because there is not much research using kriging based on remotely sensed data. Although many studies used variograms to classify remotely sensed images based on image texture, these methods have obvious shortcomings. For example, texture classifiers based on the semivariogram work reliably only if the regions of each class are sufficiently large and homogenous, while the classes are heterogenous and texturally diverse. There is no guarantee that the extra data on texture will yield useful information, and for the veriogram analysis applied in smoothing there are also problems that need to be overcome (Atkinson 2000). The more important point is that the optimal method associated with geostatistical techniques is kriging, while kriging might not be applied for image classification only using image data. Therefore, in this study I combined remotely sensed data and ground data and applied both semivariogram analyses and kriging methods.

There is little research in which the geostatistical methods are applied in forest inventories. Magnusen et al. (2002) applied geostatiscal methods to contextual classification of Landsat TM images in order to discern forest cover types. Coburn and Roberts (2004) applied similar techniques to improve forest stand classification at multiple scales, and their research indicated that there was no single window size that would adequately characterize the range of textural conditions present in the one image they were using, which is a problem in contextual classification using geostatistical techniques.

Without using remotely sensed data, kriging (Poso 2001) has been used to estimate forest variables in forest management planning (Czaplewski et al. 1994, Gunnarsson et al 1998, Hock

1993, Holmgren and Thuresson 1997, Samra et al 1989). Tuominen et al. (2003) also used this technique to estimate forest stand variables. Hock et al (1993) applied kriging to estimate site index for pinus radiata. Czaplewski et al (1994) estimated the growth of pine stands, and Samra et al (1989) estimated the height of Dharek (*Melia azedarach*). These studies were all conducted at stand level. Nanos and Montero (2002) presented a geostatistical approach for the prediction of diameter distributions, which made it possible to predict the diameter at other locations without additional variables being measured, and kriging was used for the interpolation of parameters of the diameter distributions over the study area. Later, Nanos et al. (2004) derived a method for spatially predicting the height/diameter relationship by combining mixed models and geostatistical methodology. They found it is possible to predict random stand effects of a height/diameter model without additional stand measurements. Meng et al. (2006), for the state of Georgia, analyzed spatial pattern characteristics of tree mortality, such as spatial dependence and spatial clusters using semivariogram modeling with nugget, range, sill, and other parameters.

As relates to research using remotely sensed data, the semivariogram is more often applied than kriging, but the application of the semivariogram has obvious shortcomings, as discussed above. Kriging used for forest inventory and forest management planning is mainly based on ground inventory data and does not take the advantage of satellite data (i.e. more up-to-date, large area, cheap, and so on). Therefore, a systematic study of geostatistical modeling is needed for forest inventory analysis. In this research, combining ground inventory and remotely sensed data, I used geostatistical techniques focusing on kriging and emphasizing the need for spatial autocorrelation in forest inventory.

1.2.2 Research using K nearest neighbor methods

The K nearest neighbor method has become a practical method for forest inventory techniques including classification, parameter estimation, forest landscape dynamics, and forest

health monitoring. This method has been developed, employed, and improved in both theoretical and practical fields, and has been successfully used in forest inventory (Tomppo et al. 2002, Katila and Tomppo 2002 and 2001, Halme and Tomppo 2001, Katila et al. 2001).

The K nearest neighbor method is one of the most extensively used methods for forest classification and other forest inventory techniques (Atta-Boateng and Jr 1997, Franco-Lopez and Bauser 2000, Franco-lopez and Bauer 2001, and Trotter et al. 1997) . Tomppo and other researchers improved this method (Tomppo 1991, Katila and Tpmppo 2002), the big difference being that distance is not necessarily based on Euclidean distance, and weights are computed based on land use map strata. They described the method as follows: a distance measure *d* is defined in the feature space of the satellite image data. The K nearest field plot pixels (in terms of *d*), i.e., pixels that cover the center of some field plot, are sought for each pixel in the cloud-free satellite image. The neighbors must belong to the same map stratum as the target pixel.

The K nearest neighbor method is an extension of the nearest neighbor method, which is a basic and more powerful method for resampling and image classification. The nearest neighbor method is widely used in GIS and remote sensing. For example, sample and classification functions based on the nearest neighbor method are built in ArcInfo, ArcView, ERDAS Imagine, and Idrisi. If multi-band (i.e., *N* band) imagery data is analyzed using the K nearest neighbor method, then, this method is called the *N*-dimensional K nearest neighbor method, or the *N* K-classification method. This classifier has been used successfully as part of the national-scale boreal forest inventory in Finland (Tomppo and Katila 1991).

The K nearest neighbor method (KNN) is used in estimating basal area and volume (Fazakas and Nilsson 1996, Katila and Tomppo 2001, Tokola 2000, Tolola et al1996, Tomppo

1991, and Trotter et al 1997). Franco-Lopez et al (2000), Franco-lopez et al (2001), and Trotter et al (1997) reported using the KNN technique to classify satellite image data.

One characteristic of the KNN method is that it is a non-parametric approach to predicting values of point variables on the basis of the similarity in a space between the point and other points with observed values of the variables. This in a certain way decides its advantages and disadvantages for analyzing image data. Therefore, three advantages can be concluded based on the above review. (1) The first one is that its theory is simple and easy to understand, and it also is easy to be applied in image classification and other aspects. (2) The second one is that there is no assumption about the distribution of the variables involved in the process of image data analysis. So, it may be more extensively used in image data analysis in the future. However, if sample size is big enough and the normal assumption is not violated, then, a parameter estimation method is more suitable. (3) Instead of first summarizing the training classes before the pixel assignment step in the process of parametric classification, the information of all the training pixels is stored and the unlabelled pixels are classified by “taking a vote” among the neighboring training pixels (Franco-lopez et al. 2001). (4) K nearest neighbor methods are not only suitable for estimation at small scale, such as forest stand and individual tree (Holmstrom 2002, Katila et al 2000), but also can be used at large scale (Katila and Tomppo 2001, Tomppo 2002, Trotter et al 1997).

K nearest neighbor methods also have some disadvantages, although these disadvantages are little discussed in the applications of forest research. One obvious disadvantage is the selection of K. It is the K values that determine how many nearest neighbors used for prediction is efficient, but it has been overlooked in past forest research. The second disadvantage is computation cost. This disadvantage is a problem when the K nearest neighbor method is applied

for large region forecasts using remotely sensed data.

1.3 Data sources

1.3.1 Ground inventory data

Ground inventory data used in this study were mostly supplied by forest industry. Inventory variables include basal area, dominant height, forest types, timber volume, and other stand characteristics. Since the data is confidential, locations of ground inventory data cannot be displayed exactly. I use Figure 1.1 to show the basic spatial pattern of the ground inventory.

1.3.2 Landsat TM data

Twenty-five meter resolution Landsat TM data acquired in 2005 are used as predictors to spatially forecast volume of trees for the whole State of Georgia. The TM imagery used is displayed in Figure 1.2 including path17 row 37, path17 row 38, path17 row 39, path18 row 36, path18 row 37, path18 row38, path18 row39, path19 row36, path19 row37, path19 row38, path19 row39, and path20 row36.

One problem with these TM data is that part of the imagery is covered with cloud and cloud shadows (Figure 1.3). With the cloud and cloud shadows, it is impossible to predict forest variables. I developed a nearest neighbor imputation approach to remove cloud and cloud shadows in the images, and then used the TM data in the further steps of image analysis.

Figure 1.1. The Distribution of Ground Inventory Data

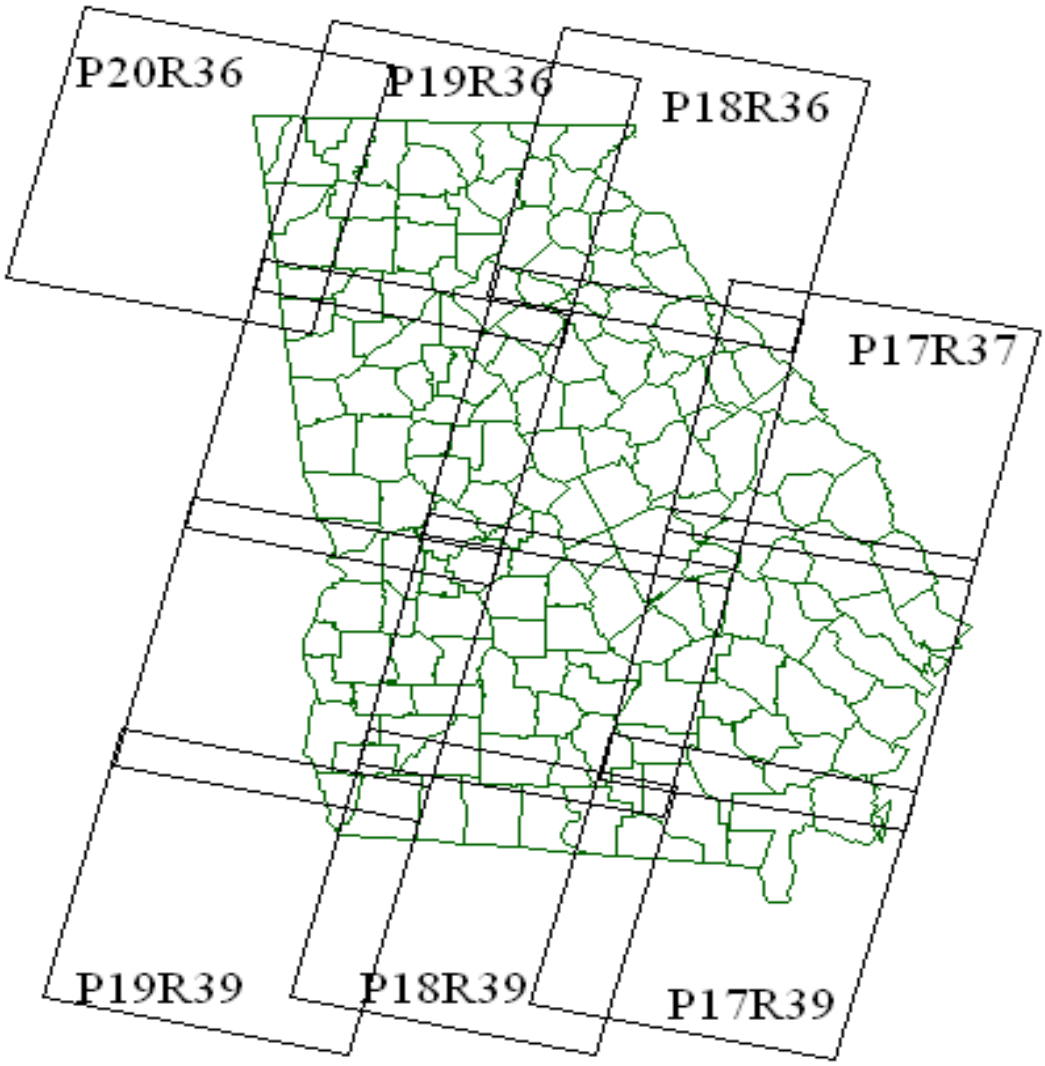

Figure 1.2. Landsat TM Imagery Applied in this Research.

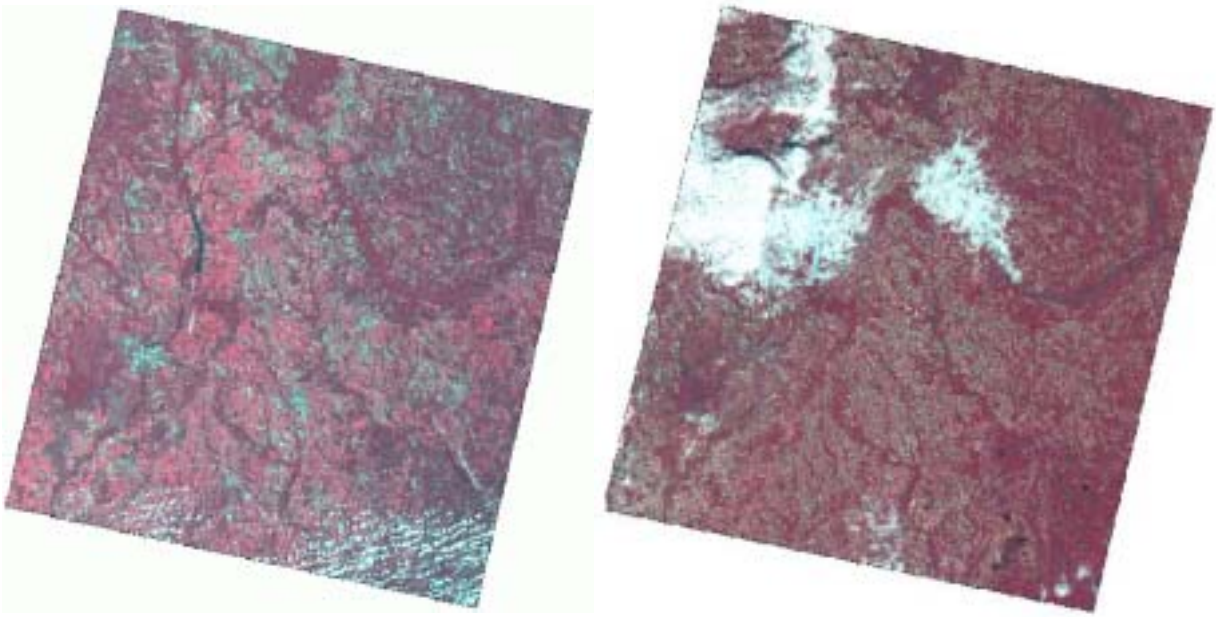

Figure 1.3. Clouds and Cloud Shadows in the Landsat Imagery.

1.3.3 Other auxiliary data

The Georgia Gap Analysis Program supplied basic land cover data used as a type of reference data in the classification process using Landsat TM imagery. The land cover data is derived from remote sensing and modeling for general assessment of land resources (Kramer et al 2003).

1.4 Objectives

The primary objective of this research is to achieve fine spatial resolution forest inventory (i.e., 25-meter resolution) using the KNN imputation approach and geostatistical approaches. Toward this end I integrate the use of remote sensing and ground inventory data. I use the Landsat TM imagery as auxiliary data to spatially forecast forest variables of interest, but before implementing the forecast I need to achieve three sub-objectives.

1) The traditional approach to replacing cloud and cloud shadows is (i.e., cut-and-paste) to use cloud-free images acquired at different times. I decide not to use this approach since every scene of satellite imagery has its individual spectral characteristics and this traditional approach introduces an unacceptable degree of variability. I therefore need to develop a better method to remove cloud and cloud shadows in satellite images.
2) Although the K nearest neighbor method is a popular and powerful method used for large area forest inventory employing remotely sensed imagery, the spatial autocorrelation and spatial dependence among the forest variables are not considered. Kriging models, on the other hand, are developed for capturing the spatial autocorrelation and dependence of forest variables. In addition, kriging methods are

the best linear unbiased predictors (BLUP) of spatial variables. I therefore develop my own kriging-based approach for estimating fine spatial resolution forest variables.

3) The K nearest neighbor imputation has been widely applied for forest inventory, but the disadvantages of K nearest neighbor are little explored. The two main disadvantages are the selection of K and computation cost. The computation cost can be partly solved using fast computation algorithms or data reduction methods. The more important point is the selection of K, which is the number of nearest neighbors. This number helps determine the accuracy of the forecasted variables. I therefore explore methods of selecting K.

1.5 Methodology

1.5.1 K nearest neighbor imputation

The nearest neighbor approach is one of the most popular methods applied in GIS and remote sensing. The basic functions based on the nearest neighbor approach are widely built into GIS and remote sensing software, such as ArcInfo, ArcView, ERDAS Imagine, and Idrisi. The nearest neighbor approach is also extensively applied in forest inventory. K nearest neighbor imputation, an extension of the nearest neighbor method, is the nearest neighbor method when K=1. Wong and Lane (1983) used the K nearest neighbor method to evaluate the most likely number of species clusters within the population covered by their data, and discussed in detail the procedures of statistical techniques used. Recently, K nearest neighbor imputation has also become widely used in forest inventory as I discussed earlier. The basic steps of this method employed in forest classification and forest inventory and the theme of K nearest neighbor can be described as follows.

The Euclidean distance, $d_{pi,p,}$ is computed in the feature space (explanatory variable space) from pixel p (a pixel to be predicted) to each pixel p_i whose ground truth is known (i.e., pixels within field plot i). Take K in the feature space nearest field plot pixels and denote the distances from pixel p to the nearest field plot pixels by

$$d_{(p\,1),\,p}\,,\ldots,\ d_{(pk),p},\ (d_{(p\,1),p}\leq\cdots\leq d_{(pk),p}\,),\ k\sim 5\text{–}10. \tag{1-1}$$

The features (i.e., explanatory variables) are typically the original spectral values or their functions in spectral or spatial space (Tomppo 1996). Ground variables, e.g. stand age, years after thinning, can also be applied if the values are known for each pixel of the area to be analyzed. Tomppo (1996) determined the weight for each pixel in order to get a better estimation of forest inventory variables. He calculated the weight for each pixel using:

$$w_{(i),p}=\frac{1}{d^{2}_{(pi),p}\sum_{j=1}^{k}\frac{1}{d^{2}_{(pj),p}}} \tag{1-2}$$

Sums of weights $w_{i,p}$ are calculated according to requirements. The weight of plot i in the computation unit u yields:

$$c_{i,u}=\sum_{p\in u}w_{i,p} \tag{1-3}$$

Inventory results, by operation units, are computed utilizing the digital boundaries of units and the weight coefficients (Formula 1-2) of the field sample plots estimated in the image process. The area estimates for forestry land strata by computation units are obtained from the estimated plot weights by the equation:

$$A_{s,u} = a\sum_{i \in I_s} c_{i,u} \qquad (1\text{-}4)$$

where *a* is the area of one pixel, *s* is a forestry land stratum, *Is* is the set of field sample plots of the stratum and *u* is a computation unit. Note that the field plots of *Is* do not necessarily belong to the unit *u*. The forestry land strata are defined just as in the case of field sample plots based inventory, i.e. using the field data variables and their values.

The volume estimates are computed by computation units and by strata in the following way. First, mean volumes are estimated by the formula:

$$v_t = \frac{\sum_{i \in I_s} c_{i,u} v_{i,t}}{\sum_{i \in I_s} c_{i,u}} \qquad (1\text{-}5)$$

where $v_{i,t}$ is the volume per hectare of the timber assortment *t* on the sample plot *i*. The corresponding total volumes are obtained by substituting the denominator in Equation (1-5) with the number of pixels per hectare. Mean and total volume increments are similarly estimated, if necessary. Pixel-wise estimates for some forest variables are stored in the form of a digital map during the estimation procedure. The variables entered by the operator are estimated in the following way for forestland: Define the estimate $m_{(j),p}$ of the variable *m* for the pixel:

$$\hat{m}_p = \sum_{j=1}^{k} \omega_{(j),p} . m_{(j),p} \qquad (1\text{-}6)$$

where $m_{(j),p}$, j=1, . . . , k, is the observed value of the variable M in the sample plot j corresponding to the pixel (p_j) which is the jth closest (field plot) pixel in the spectral space to the pixel p (Tomppo 1996). The mode value is used instead of the mean value for possible qualitative variables.

1.5.2 Geostatistical methods

1.5.2.1 Semivariograms

Semivariograms can be calculated as:

$$\gamma(h) = \frac{1}{2N}\sum_{i=1}^{N}[Z(x_i) - Z(x_{i+h})]^2 \qquad (1\text{-}7)$$

where x_i is a data location, h is a vector of distance, $Z(x_i)$ is the data value of one kind of attribute at location x_i , N is the number of data pairs for a certain distance and direction of h units.

Many geographic phenomena have one common spatial characteristic that can be represented by the spherical semivariogram model associated with a finite spatial correlation. The spherical semivariogram model was calculated by the following function (Carr 1995):

$$\gamma(h) = C_0 + C\left(\frac{3h}{2a} - \frac{h^3}{2a^3}\right), \quad if \quad 0 < h \le a$$
$$\gamma(h) = C_0 + C = sill, \quad if \quad h > a \qquad (1\text{-}8)$$

Where h is the lag distance, C_0 is the nugget effect, C is equal to the sill minus C_0, and a is the range. There are 4 semivariogram parameters, namely range, sill, nugget, and spatial dependence (calculated as C/sill), to depict the spatial characteristics of tree attributes. Range is the distance beyond which there are no spatial effects. Sill is the total degree of spatial variation for spatial

phenomena. Nugget is the nearest variability of attributes. Theoretically, the nugget is equal to zero. However, the nugget may also represent the close distance continuity of one attribute, or result from sampling errors, in which cases, the nugget may not equal 0. Spatial dependence reflects the strength of spatial correlation within the range.

Another important measurement relating to semivariograms is spatial covariance. Sometimes spatial covariance is used instead of the semivariogram. Spatial covariance of X referenced to a separation distance *h* can be described as:

$$C_X(h) = E\{[\, X(u_i) - \mu_i \,][\, X(u_{i+h}) - \mu_{i+h} \,]\} = E[X(u_i)X(u_{i+h})] - \mu_i\mu_{i+h} \qquad (1\text{-}9)$$

This spatial covariance can be estimated from a data set by grouping the data pairs into lag "bins" or "sets" and then calculating as follows:

$$\hat{C}_X(h) = \frac{1}{n_h}\sum_{i=1}^{n_h}(x_i)(x_{i+h}) - \overline{x}_i\overline{x}_{i+h} \qquad (1\text{-}10)$$

where: n_p = number of pairs in h lag bin, generally: $\hat{C}_X(0) \approx \mathrm{var}(X)$ and $\hat{C}_X(\underset{h\to\infty}{h}) = 0$

Additionally, other kinds of models, the exponential model, the Gaussian model, and linear model are also usually used to fit semivariograms, and they are listed as equations (1-11), (1-12), and (1-13) respectively.

$$\gamma(h) = \sigma^2\left[1 - e^{-(h/c)}\right] \qquad (1\text{-}11)$$

$$\gamma(h) = \sigma^2\left[1 - e^{-(h/c)^2}\right] \qquad (1\text{-}12)$$

$$\gamma(h) = \sigma^2\left[1 - e^{-(h/c)^2}\right] \qquad (1\text{-}13)$$

1.5.2.2 Kriging

Kriging relates the covariance between samples, the covariance between each sample to the location to be estimated, and the unknown weights. The covariance matrix is inverted to solve for the weights.

Kriging is a class of linear estimators, traditionally obtained by minimizing the local error variance. Take simple kriging (SK) as an example.

$$Z_{SK}^{*}(u)=\sum_{\beta=1}^{n}\lambda_{\beta}(u)Z(u_{\beta}) \tag{1-14}$$

where $Z_{SK}^{*}(u)$ is the simple kriging estimator for the point *u*; $\{Z(u_{\beta}),\beta=1,2,...,n\}$ are random variable sampled values, and $\{Z(u_{\beta}),\beta=1,2,...,n\}$ are one of their realizations.

The SK system is determined by:

$$\sum_{1}^{n}\lambda_{\beta}(u)C(u_{\alpha}-u_{\beta})=C(u_{\alpha}-u),\alpha=1,...,n \tag{1-15}$$

Where $C(h)=Cov\{Z(u)-Z(u+h)\}$ is the covariance model. The error variance of SK is:

$$\sigma_{SK}^{2}(u)=Var\{Z_{SK}^{*}(u)-Z(u)\}=C(0)-\sum_{1}^{2}\lambda_{\alpha}(u)C(u_{\alpha}-u) \tag{1-16}$$

The covariance of any two estimators, i.e., $Z_{SK}^{*}(u)$ and $Z_{SK}^{*}(u')$ however does not reproduce the model value $C(u-u')$ (Journel 2000). Furthermore, the autocovariance defined using equation 1-17:

$$Cov\{Z_{K}^{*}(u),Z_{k}^{*}(u)\}=C(0)-\sigma_{SK}^{2}(u)<Cov\{Z(u),Z(u)\}=C(0) \tag{1-17}$$

is smaller than the model variance $C(0)$. A map estimated by the kriging interpolator is always smoothed, which is the well-known smoothing effect. Additionally, when the value for a point, such as point u, is estimated, the kriging method does not take into consideration the estimated values of any of the other points. Therefore, kriging is not directly used for mapping the spatial distribution of an attribute. It is used, however, for building conditional distributions for stochastic simulations.

In this study, I also try to use cokriging and regression kriging. They are applied in those cases when other, usually more abundantly sampled data, can be used to help in the predictions. Such data are called auxiliary data (as opposed to primary data) and I can assume they are correlated with the primary data. In such situations, you can try cokriging and regression kriging approaches, but generally the results from cokriging and regression kriging are not as smooth as those without using auxiliary variables. To perform cokriging and regression kriging, one needs to model not only the variograms of the auxiliary and primary data, but also the cross-variograms between the primary and auxiliary data.

1.5.3 Remote Sensing and GIScience

Both remote sensing and GIS technologies are extensively applied in this research. For example, unsupervised ISODATA (Iterative Self-Organizing Data Analysis Techniques) classification is applied in order to obtain the optimal classes, and then supervised classification is conducted to obtain hardwood and softwood classes using Landsat TM imagery. Based on ground inventory data and remote sensing imagery, I process the massive dataset using GIS and remote sensing software including ArcGIS 9.1 and Leica-Geosystems ERDAS Imagine and statistical software (i.e., SAS, Splus, and R-programming). The main process technologies include GIS data combination, projection and re-projection, transformation, extraction, mosaic,

subset, and mapping. The geostatistical models and nearest neighbor/K nearest neighbor methods are implemented using SAS, Splus, and R-programming.

1.6 Chapter Organization

My dissertation is objective-oriented and problem-oriented. In other words, I designed one approach using the weighted K nearest neighbor method and one approach using the systematic geostatistical modeling. In both approaches I use Landsat TM imagery to achieve the primary objective, i.e., fine-spatial-resolution forest inventory for the state of Georgia. I four important points in this dissertation: cloud and cloud shadow removal in the TM data, i.e., the problem in the remote sensing data source; the problems in K nearest neighbor imputation methods; the development of the systematic geostatistical approach; and the use of the weighted K nearest neighbor method to forecast volume of trees in Georgia.

I describe concisely the background, the data sources, the objectives, and the methodologies in Chapter 1. In Chapter 2, I first review the literature relating to cloud and cloud shadow removal in remote sensing data, and then develop a simple and powerful nearest neighbor method approach to remove cloud and cloud shadows in Landsat images. In Chapter 3, I explore the two disadvantages of the K nearest neighbor method using remote sensing data for forest inventory after reviewing the applications of this method in forestry. In Chapter 4, I develop a systematic geostatistical forest inventory approach using remotely sensed data. I discuss four types of kriging methods including ordinary kriging, universal kriging, cokriging and regression kriging using remote sensing data as auxiliary data. In Chapter 5, I use the weighted K nearest neighbor method to forecast volume of trees using a cell size of 25-meter for the state of Georgia. Using the mean volume of hardwood/softwood estimated by the USDA

Forest Inventory and Analysis Program (FIA) as the objective, I adjust my estimations to the cell size level and obtain the unbiased estimation of hardwood/softwood volume. Then, I summarize these estimations at the county level.

Finally, I summarize this research in Chapter 6. I discuss the performance and significance of my work finished in Chapter 2, 3, 4, and 5. I also talk about the limitations of this research, and point out the further studies of this research in the future.

CHAPTER 2

CLOUDS AND CLOUD SHADOWS REMOVAL FROM SATELLITE IMAGERY*

2.1 Introduction

Completely cloud-free remotely sensed images are not always available, especially in tropical, neo-tropical, or humid climates, posing complications and perhaps serious constraints to image analysis. The average cloud coverage for the entire world is about 40% (The American Society of Photogrammetry). It is important to study removing cloud and its shadow, because the data of interest in the scene is under cloud, and the cloud free scene cannot be obtained at an appropriate time. This review first summarizes three approaches applied for the removal of clouds and their shadows from satellite images

Approaches to reduce cloud and shadow are rarely studied. Mitchell et al (1977) built a filtering procedure to remove cloud cover in satellite imagery. Liu and Hunt (1984) followed Michell's research and improved this filtering procedure. However, Chanda and Majumder (1991) did not agree on one assumption in Mitchell's procedure, and they also pointed out that the algorithm in the research of Liu and Hunt may not be optimum. Then, they discussed out an iterative algorithm for removing the effect of cloud. Recently, new approaches have been developed to removing cloud based on image fusion with additive wavelet decomposition. Song and Civeo (2002) developed another new approach to reducing cloud and shadow from satellite images.

* This research has been submitted to IEEE *Geoscience and Remote Sensing Letters*, and it is in revision now.

2.2 Available Methods

Although different algorithms were developed in the studies of Mitchell (1977), Liu and Hunt (1984), Chanda and Majumder (1991), these approaches are cloud distortion models and filtering procedures. Image-fusion-based cloud removing procedures are another approach. Song and Civeo (2002) developed the approach of removing cloud area by pixel replacing from a secondary image.

2.2.1 Filtering procedures

Mitchell (1977) applied the Homomorphic filtering process and the Wiener filter functions as follows. To apply this procedure, he made the following assumptions. (1) The cloudy regions were generally brighter than the noncloudy regions; and (2) Compared to other ground reflectance, the clouds had relative low spatial frequencies, and thresholds could be set in both the picture and spatial-frequency domains to allow an estimate of the noise statistics from the cloudy image.

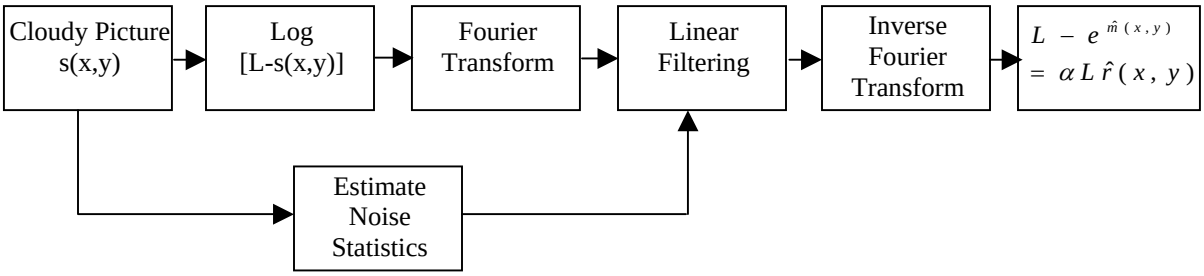

Figure 2.1 Diagram of the Wiener Filter Process

$$s(x,y) = \alpha L r(x,y) t(x,y) + L[1 - t(x,y) \leq L \tag{2-1}$$

$$\log[\, L - s(x,y)] = \log[\, t(x,y)] + \log[\, L - \alpha L r\,(x,y)] \tag{2-2}$$

$$H(u,v) = \frac{S_{MP}(u,v)}{S_{PP}(u,v)} \tag{2-3}$$

$$S_{PP}(u,v) = S_{MM}(u,v) + S_{NN}(u,v) + 2\eta_M \eta_N \delta(u,v) \tag{2-4}$$

$$S_{MP}(u,v) = S_{MM}(u,v) + \eta_M \eta_N \delta(u,v) \tag{2-5}$$

$$H(u,v) = \frac{S_{PP}(u,v) - S_{NN}(u,v) - \eta_M \eta_N \delta(u,v)}{S_{PP}(u,v)} \tag{2-6}$$

Where *s(x,y)* is the scanner image;

r(x,y) is the ground reflectance;

t(x,y) is the attenuation due to the cloud;

L is the sun illumination;

a is sunlight attenuation.

H(u,v) is the Wiener filter function;

$S_{MP}(u,v)$ is the cross power spectrum between signal and the signal plus noise;

$S_{PP}(u,v)$ is the power spectrum of the signal plus noise;

$S_{NN}(u,v)$ is the power spectrum of the noise;

η_M and η_N are the means of the signal and noise;

u and *v* are the two spaital frequency components;

Liu and Hunt (1984) relaxed the first assumption, because sometimes clouds are dark or the scene is bright. Also, the Wiener filter is applicable in a stationary image field and images with clouds are not stationary. Then, they developed a new approach (i.e., equation 2-7) to

simplify the procedure by solving equations (2-1) and (2-2), and then apply it to create the desired image.

$$Lr(x,y) = \Phi^{-1}[s(x,y)] = \frac{L}{\alpha} - \frac{L - s(x,y)}{\alpha t(x,y)} \quad (2\text{-}7)$$

Chanda and Dutta Majumder (1991) agreed that the first assumption in Michell et al is not always true, and pointed out that the results obtained with the method developed by Liu and Hunt may not be optimum. They developed a tapered-shaped low-pass filter whose parameters can be tuned to yield a solution of minimum errors. Shape of the filter assigned to be tapered and circularly symmetric, because the cloud-free image of the earth surface also contains some low-frequency components. The filter function was obtained by rearranging equation (2-2).

$$Log[f'(x,y)] = \log[t(x,y)] + \log[r'(x,y)] \quad (2\text{-}8)$$

$$F(u,v) = T(u,v) + R(u,v) \quad (2\text{-}9)$$

Where (2-10)

$$f'(x,y) = 1 - f(x,y)/L$$

$$r'(x,y) = 1 - r(x,y) \quad (2\text{-}11)$$

$$F(x,y) = \Im\{\log[\, f'(x,y)]\} \tag{2-12}$$

$$T(x,y) = \Im\{\log[t(x,y)]\} \tag{2-13}$$

$$R(x,y) = \Im \log\{[r(x,y)]\} \tag{3-14}$$

2.2.2 Image fusion approach

The multi-spectral image, for example, Landsat and Spot, are applied visible, near infrared, and infrared range. These waves cannot penetrate through clouds so the data fusion of multi-times can compensate the lost data. The procedures include (1) multi-spectral image is transformed to Intensity-Hue-Saturation (HIS) component in order to make histogram matching, (2) the image is decomposed on wavelet transform, and (3) high order coefficients are combined with the image that contained cloud for compensation the data in the hidden regions. These procedures are relatively simple and easy to apply.

2.2.3 Song and Civeo's Approach

Song and Civeo (2002) built a knowledge-based approach to reducing cloud and shadow. Two date images are selected. The main image is referred to the principal image to be used for additional analysis, and the secondary image is applied to supplement the values for cloud and shadow regions in the main image.

This procedure includes the following parts. (1) The brightness and contrast of a secondary image was adjusted to be the same as the main image, (2) a knowledge base is applied to detect the presence of clouds and shadows in the main image in areas not present in the secondary image. (3) A composite image was generated with minimal cloud and shadow by replacing the brightness values of detected areas in the main image with those of the secondary

image. Additionally, equation (2-15) is applied for topographical normalization. Equation (2-16) is applied for multi-time effect brightness correction.

$$DN_{norm} = DN_{orig} + DN_{orig} * (1 - \gamma / \gamma_{mean}) \quad (2\text{-}15)$$

where DN_{norm} is the brightness value after normalization;

DN_{orig} is the original brightness value;

γ is the relief values;

γ_{mean} is the mean value of the whole relief image.

$$DN_{corr} = \mu_{main} + (DN_{\sec d} - \mu_{\sec d}) * \frac{SD_{main}}{SD_{\sec d}} \quad (2\text{-}16)$$

Where DN_{corr} is the corrected brightness of the secondary image,

DN_{secd} is the original brightness from the secondary image,

μ_{main} and SD_{main} is the mean and standard deviation of the main image;

$\mu_{\sec d}$ and $SD_{\sec d}$ is the mean and standard deviation of the secondary image.

2.2.4 Discussion of available methods

Mitchell et al. (1977) developed a cloud distortion model and filtering procedures to remove cloud cover in satellite imagery. Liu and Hunt (1984) and Chanda and Majumder (1991) further improved the distortion model and filtering procedures. However, their methods are used for removing thin clouds, and it is difficult to determine the range of cloud densities in which clouds and cloud shadows (CCS) are removed efficiently.

Cihlar and Howarth (1994) and Simpson and Stitt (1998) developed special methods for detecting and removing cloud contamination from AVHRR images. However, these methods are not suitable for removing CCS in other satellite imagery, such as Landsat imagery. For example,

one prerequisite of their methods is that there is at least one single maximum or a single minimum for the seasonal trajectory of a satellite-derived variable.

The multi-date effect brightness correction method is another approach to removing CCS. Song and Civco (2002) used this method to replace CCS with appropriate pixel values. This approach is built on the sample mean and standard deviation (SD) of band values. However, the mean and SD can only be estimated as approximations for the whole images since CCS cover parts of the images.

2.3 Nearest Neighbor Approach

A significant obstacle to extracting information from remotely sensed imagery is the presence of clouds and their shadows. Sometimes cloudy imagery has to be used because it is all that is available. For example, satellite multispectral scanner imagery of the earth's surface such as those obtained from Landsat is often corrupted by clouds due to nadir-only observing satellites having relatively infrequent revisiting periods.

I developed a nearest neighbor analysis (NNA) technique for replacing CCS pixels with the most similar pixels at cloud-free areas in the same image. Nearest neighbor analysis is one kind of popular data imputation algorithm. The technique is then applied to remove CCS covering parts of a Landsat TM image and is then diagnostically checked.

Two satellite images covering the same area and acquired at different times are needed. The base image is the one with relatively less CCS, and should retain the new information that is acquired. Also, the base image is the one to be used for further applications. The other image will be called the auxiliary image. As much as possible cloudy areas in the base image should be cloud free in the auxiliary image. Both images are selected for this criteria based on visual

estimation. It is impossible to select the most similar pixels for the pixels whose signatures are distorted by cloud and cloud shadow using only the base image, since CCS have corrupted the real energy received and recorded by the satellite sensor. The auxiliary image is used as a medium to determine the relationship in the base image of the most similar pixels to those pixels whose signatures are distorted by cloud and cloud shadow.

The procedures of applying the nearest neighbor analysis technique to remove CCS in images are depicted in Figure 2.2 The conceptions, algorithms and steps used for NNA are as follows.

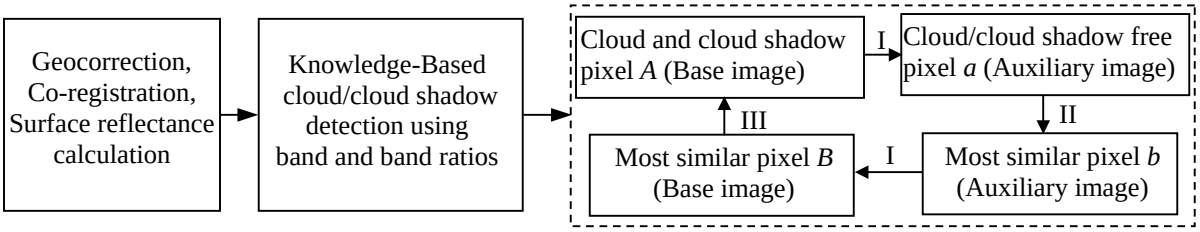

Figure 2.2 The Procedure of Cloud and Cloud Shadow Removal Using Nearest Neighbor Analysis Technique.
I, location based one-to-one correspondence between pixel *A* and *a*, and pixel *B* and *b*;
II, reflectance based nearest neighbor correspondence, pixel *a* and *b*;
III, the replacement of pixel *A* using its most similar pixel *B*.

Step 1. Georegistration

The base and auxiliary satellite images often need to be geo-rectified using U.S. Geological Survey (USGS) digital orthophoto quarter quads (DOQQs) as the sources of control (i.e., root mean square errors should be less than 10 m). Then, the two images are registered with each other, which also is called co-registration.

Step 2. Surface reflectance calibration

Landsat images with the spectral values being represented by digital number (DN) contain substantial noise. To remove the solar illumination cosine effects and the topographic

effects, the algorithms developed by Chander and Markham (2003) are applied to transform DN to radiance. I then use the available atmospheric correction package FLAASH to derive the surface reflectance from these images more consistently.

Step 3. Knowledge-based CCSs detection

Using the relationship of location based one-to-one correspondence I determine and record, in ascii tables, CCS areas in the base image that are cloud- and cloud-shadow free in the auxiliary image.

For Landsat TM imagery the bands 1, 3, 4 and 6 were indicated as the best for the detection of clouds and cloud shadows respectively. The threshold of band 1 should be greater than a value of 5500 for dense clouds in the base image. The thin clouds are generally with in the range (10000, 11300) of band 6. The values of these thresholds might vary for images acquired at different times. Band 3 and 4 were used for checking cloud shadows in the base image with band 3 less than 600 and the ratio of band 4 to band 3 bigger than 1.5. Cloud shadows and water areas might have similar reflectance values in band 4. However shadow areas generally have much higher values in band 4 than those in band 3, while water areas have relatively close values in band 4 and band 3. The ratio of band 4 to band 3 therefore is used for detecting cloud shadows.

Step 4 Nearest neighbor analysis

Nearest neighbor analysis examines the distances between each point and the closest point to it. In an image, if pixel *j* has the closest surface reflectance value to that of pixel *i*, then, *j* is called the nearest neighbor to pixel *i* (i.e., pixels *i* and *j* are more similar to each other than to any other pixels in the image). Similarly, based on the surface reflectance, the most similar pixel *b* in the auxiliary image can be identified for a given pixel *a*, in the auxiliary image. In other

words, the nearest neighbor algorithm determines the most similar pixels for all the corresponding pixels identified in step 3 in the auxiliary image. The relationship of the most similar pixels *a* and *b* in the auxiliary image can be called reflectance based nearest neighbor correspondence.

The distance from pixel to pixel measured in reflectance is a type of point-to-point distance. The smaller the distances are between pixels, the more similar the pixels are. Two pixels are identical to each other if the distance between them is 0. Euclidian distance (ED) is used in this nearest neighbor analysis technique since ED is widely applied in image processing and classification.

$$D = \sqrt{\sum_{L=1}^{n} (i_L - j_L)^2} \qquad (2\text{-}17)$$

where D is the Euclidian Distance between pixels *i* and *j*, *L* indicates satellite bands, and *n* is the number of bands for the satellite imagery being used, such as *n* =7 for Landsat TM.

Step5 Transfer of reflectance based nearest neighbor correspondence

When the relationship of reflectance based nearest neighbor correspondence is built for pixels in the auxiliary image, it is transferred to the base image to match the cloud-free and cloud-shadow-free pixels in the base image to those pixels covered by CCS in the base image. For example, suppose pixel *A* is covered with CCS. Pixel A in the base image and pixel *a* in the auxiliary image are in location based one-to-one correspondence; likewise, pixel *B* in the base image and *b* in the auxiliary image. Pixels *A* and *B* should be in reflectance based nearest neighbor correspondence in the base image because pixels *a* and *b* are in reflectance based nearest neighbor correspondence in the auxiliary image. I can therefore use the reflectance values of pixel *B* to replace the reflectance of pixel *A*.

Step 6 Compose an image in which clouds and cloud shadows have been removed

At last, an image in which CCS has been removed can be composed for the base image using remote sensing software. Filtering functions need to be applied to obtain a smooth view of the composed image.

2.4 An Example and Diagnostic Check

Two Landsat TM images, the base image (Path 18/Row 38, collected on August 17, 2004, Figure 2. 3 A) and the auxiliary image (Path 18/Row 38, collected on December 29, 2004, Figure 2.3 B), have areas covered with CCS, but I have determined visually that most of them are not overlapping. I replaced CCS in the base image with the values obtained using the above procedures.

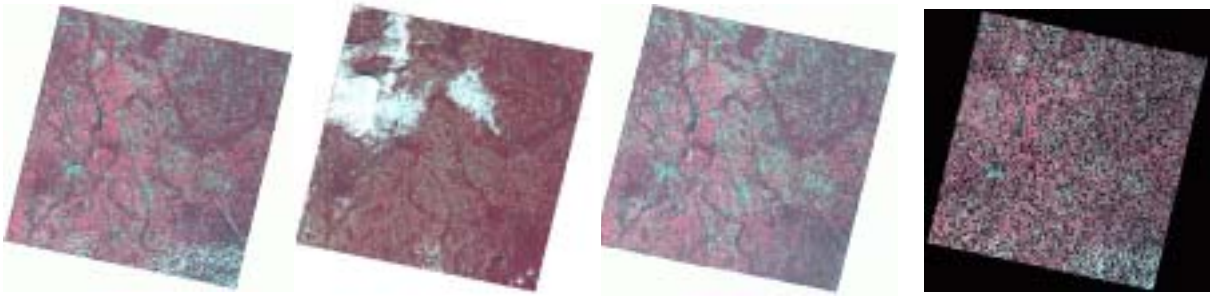

Figure 2.3. Cloud Removal Using Landsat TM images of Path 18Row 38.
Bands 4, 3, and 2 are portrayed as R-G-B, respectively. A, base image acquired on August 17, 2004; B, auxiliary image acquired on December 29, 2004; C, The base image after removing cloud and cloud shadow; D, randomly sampled pixels (black dots) used to check accuracy.

The results of replacing cloud and shadow pixels are pictured in Figure 2.3 C. The CCSs are almost completely removed, but some unsmooth views of the areas initially covered by CCS are achieved. A focal median analysis with a 3x3 size window using ERDAS Imagine 8.7 was applied in order to smooth the images.

In order to separate the pixels in the black background, surrounding the image, from pixels in the image itself, I generated 10,000 random pixels in the area that framed both the image and the black background areas surrounding it. I deleted the 3387 pixels that fell within the black background located outside of the image and within the cloud areas, and then used the remaining 6613 pixels to check the accuracy of pixel replacements (Figure 2.3 D). I applied the nearest neighbor technique, i.e., I found pixel *A* (say, a given pixel in base image) and its location-corresponding *a* (say, a pixel in the auxiliary image having the same location as *A*). I then found the nearest neighbor *b* (say, a pixel in the auxiliary image) to *a* and found *b*'s location-corresponding *B* in the base image. Recalling that in the cloud removal procedure, *B* was used to replace the value of *A* (Figure 2.2), the objective now, this being the diagnostic check, is to examine the difference between the surface reflectance value of *B* and the original value of A.

Two kinds of criteria including bias error (BE) and the standard deviation of the errors (SD) are used to directly compare values between the forecasted reflectance (i.e., the most similar pixel *B*) obtained using NNA and the surface reflectance (i.e., *A*) in the base image. Bias error is used to measure either the model's under-forecast or over-forecast of a parameter and is defined by the equation:

$$BE(X) = \frac{1}{N}\sum_{n=1}^{N}(X_f - X_o) \qquad (2\text{-}18)$$

where N is the total number of comparisons, X_f is the forecast value, and X_o is the observed value. A positive BE indicates a tendency to over-forecast while a negative BE implies under-forecasts.

$$SD = \left[\frac{1}{N-1} \sum_{n=1}^{N} (X_n - \overline{X})^2 \right]^{1/2} \quad (2\text{-}19)$$

where N is the sample size (i.e., the numbers of pixels), X_n is the error value and $\overline{X}$ is the mean of the errors. The larger the SD, the larger the dispersion of error is from its mean.

The mean and SD of the seven bands were listed in Table 2.1. The SD of the errors is relatively bigger than the SD of band values (Table 2.2). The ratio of bias error to the mean of surface reflectance also was added to indicate the magnitude of the bias. The CCS pixels are generally forecasted well for the seven bands and much better in band 4 and 5 with very small errors. There are relatively bigger errors in band 1, 2, 3, 6, and 7, but the relative bias indicates that the bias errors of these bands only take less than 6% of the mean values of these bands (Table 2.2).

Table 2.1. Mean and Standard Deviation (SD) of Seven Bands

	Band 1	Band 2	Band 3	Band 4	Band 5	Band 6	Band 7
Mean	1511.6948	1776.3170	1482.0680	8089.1096	4709.5521	12227.0380	-1903.0271
SD	1011.5340	1317.9344	1403.8653	2647.6156	2089.6100	510.2356	115.3499

Table 2. 2. Bias error (BE), Relative Bias (RB), and Standard Deviation of Error (SDE)

	Band 1	Band 2	Band 3	Band 4	Band 5	Band 6	Band 7
BE	56.1017	75.2797	81.8465	6.4771	36.9239	-158.0803	55.9088
RB	0.0371	0.0424	0.0552	0.0008	0.0078	-0.0129	-0.0294
SDE	1462.0777	1783.8106	1957.2035	3306.5799	2322.4156	2032.1710	331.9547

RB, the relative bias is the ratio of bias error to the mean of observed band values.

2.5 Conclusions

A nearest neighbor analysis technique has been developed and conducted in order to remove CCS, and compose a remotely sensed image with very few CCSs. The example and diagnostic check indicate that the NNA technique is an efficient approach. It is simple and easy to understand and practice. The CCS were almost completely removed in the example using Landsat image Path 18/Row 38. An additional image acquired at a different time can be used again to remove CCS if there are overlaps of CCS in the base and auxiliary images. The nearest neighbor analysis also can be used to remove CCS for other satellite images other than Landsat.

The reflectance based nearest neighbor correspondence in the base image and auxiliary image should be the same or very similar. The two images cover the same area, were obtained using the same remote sensor, and have been processed using the same procedures.

The threshold of band 1 is used for detecting clouds. The threshold of band 4 and the ratio 2 of band 4 to band 3 are used to distinguish cloud shadows in satellite imagery. The ratio improved the discrimination between cloud shadows and water areas. The three criteria are flexible and adjustable from image to image.

The nearest neighbor analysis technique is a simple and efficient method to remove CCS from satellite imagery. Another advantage of NNA is that its efficiency (i.e., the accuracy of removing clouds and cloud shadows) can be diagnostically checked as it is applied. The errors and the standard deviations of errors in forecasting band values indicate whether some of them could be used for further applications. It is unwise to use the forecasting band values for further applications when big errors and standard deviations of errors exist.

CHAPTER 3

K NEAREST NEIGHBOR METHOD

FOR FOREST INVENTORY USING REMOTE SENSING DATA[*]

3.1 Introduction

The K nearest neighbor (KNN) method of image analysis is practical, relatively easy to implement, and is becoming one of the most popular methods for conducting forest inventory using remote sensing data. The KNN is often named K nearest neighbor classifier when it is used for classifying categorical variables, while KNN is called K nearest neighbor regression when it is applied for predicting non-categorical variables. As an instance-based estimation method, KNN has two problems: the selection of K values and computation cost. We address the problems of K selection by applying a new approach, which is the combination of the Kolmogorov-Smirnov (KS) test and cumulative distribution function (CDF) to determine the optimal K. Our research indicates that the KS tests and CDF are much more efficient for selecting K than cross validation and bootstrapping, which are more commonly used today. We use remote sensing data reduction techniques—such as principal component analysis, layer combination, and computation of a vegetation index—to save computation cost. We also consider the theoretical and practical implications of different K values in forest inventory.

[*] This research has been submitted to *GIScience and Remote Sensing*. Now it is in revision.

The K nearest neighbor (KNN) method of image analysis is widely used in the estimation of single tree characteristics and stand attributes, and its algorithm and procedures are discussed in a number of studies (Fazakas and Nilsson, 1996; Holmstrom, 2002; Katila et al. 2000; Katila and Tomppo, 2001; Tokola, 2000; Tokola, et al. 1996; Tomppo, 1991; Tomppo and Halme 2004; and Trotter, et al., 1997). The KNN method has two advantages in that it uses a nonparametric approach and allows for the use of robust to noisy training data. It is therefore becoming one of the most popular methods applied for forest inventory using large-area remote sensing data. Tomppo et al. (1999), Franco-Lopez and Bauer (2001), and Trotter, et al. (1997) reported using the KNN technique to classify satellite image data for large areas. Tomppo (1991) and other researchers first applied the KNN method for forest classification and forest inventory.

As a kind of instance-based data mining approach it still has two problems: the selection of K values and computation cost (James 1985). The two problems are little discussed although a great number of studies of KNN using remote sensing data are available. Computation cost results from the distance computation of each query instance to all training samples. Hardin and Thomson (1992) explore a fast nearest neighbor classification approach using a k-d tree and partially solved the problem of computation cost, but remote sensing data reduction is still important when a large dataset is applied. Jensen (1986) discusses in detail the methods of band reduction and selection. We discuss and then apply remote sensing data reduction in this paper in order to partially resolve the disadvantage of computation cost. The reduction techniques might include determining an optimal combination of bands, performing principal component analysis

(PCA) of multi-bands, and calculating a vegetation index, all three of which can reduce data size significantly while keeping almost all the useful information in the original data.

We explore the problem of the selection of K in the context of KNN being used for spatial prediction using remotely sensed imagery. KNN predictions are based on the intuitive assumption that objects close in distance (say, vector space) are potentially similar. It is an extension of the nearest neighbor method, which is widely used in image processing and classification. KNN methods are applied not only for grand mean estimation, but also for spatial prediction. The bigger the K values, the closer is the estimation to the mean of a forest variable, but as K grows we lose variability in the field data. The smaller the K values, the more the estimation is able to maintain the variation in the field data.

Several important points relating to the selection of K must be considered. For example, what values of K result in estimations retaining the range of variability present in the field data? Also, does a relatively larger standard deviation indicate the estimations significantly cover the variability in the field data? Compared with the field data, are the estimations using different K values significantly different from each other?

KNN is used not only for grand mean estimation of forest stand characteristics but also for spatial estimation and classification of spatial characteristics of forests (e.g., fine-spatial-resolution estimation of basal area, timber volume, species, age, mortality, etc.), providing important information for forest management. It is the selection of K that determines the accuracy of the predictions in forest inventory. In order to resolve the above questions, the selection of K must be answered; i.e., how big or how small of a K value is an optimal selection?

3.2 Objectives

The objectives of this research include the following:

(1) We discuss the available K selection methods and we explore the shortcomings of root mean square error (RMSE) and re-sampling statistics for K selection.

(2) For selecting K for forest inventory applications we use a new approach, which is a combination of the Kolmogorov-Smirnov (KS) test and cumulative distribution functions (CDF). We determine that when using this combination, the estimates of forest variables obtained from KNN will have the same or similar distribution as the observed samples. We also discuss other advantages of the KS test and CDF for selecting K.

(3) We discuss principal component analysis and normalized difference vegetation index, which are both data reduction techniques for remote sensing to save computation cost.

3.3 Study Area and data sources

The study area is Marion County located in southwestern Georgia (Fig. 1). The test area is relatively flat terrain and the vegetation is uneven-aged coniferous stands with the dominant species being Loblolly pine (*Pinus taeda*). The range of average monthly temperatures is from 35º F to 90º F, and the range of average monthly precipitation is from 5.842 to 14.224 cm.

A private timber company inventoried the ground data in September 1999. The plot size was 30.5×30.5 m (100×100 ft) and the location of each plot was archived by differential Global

Positioning System (GPS) techniques with an accuracy of approximately ±5 m. The total 128 plots are mapped in UTM zone 17 (black polygons in Fig. 1). Within each plot, basal area and tree height were measured and used to estimate volume. In this research only basal area was used as ground truth data to evaluate the predicted basal area from Landsat ETM+ data, path19 row37, acquired on September 10, 1999.

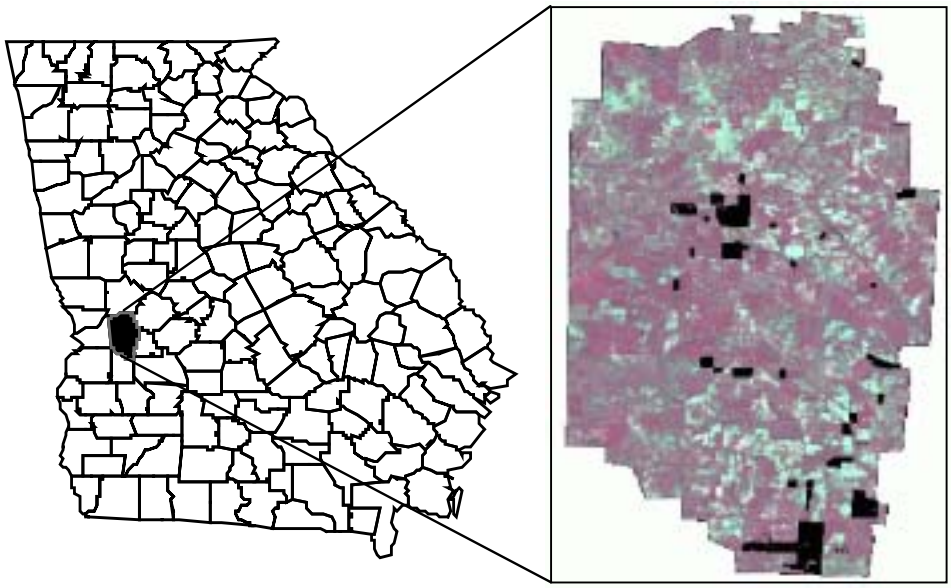

Figure 3.1. The Study Area Is Marion County, Georgia. Ground inventoried plots are indicated as black polygons superimposed on a mosaic of Landsat images.

The image of the Marion County region was a subset from the ETM+ scene path19 row37 after georectification using U.S. Geological Survey (USGS) digital orthophoto quarterquads (DOQQs) as the sources of control (RMSE less than 10 m). This resulted in a 6-band (band 1~5 and 7) image for the KNN analysis. Three types of data — two principal component layers (PCA), a normalized difference of vegetation index (NDVI) image, and the combination of two principal component layers and the NDVI image (NDVIPCA)— were derived using band

reduction and transformation methods. The Landsat image and ground data associated with GPS point locations had been projected in UTM zone17. We overlaid the GPS and ground data on the image and then attached the nearest pixel values of Landsat images including the 6 band data, PCA, NDVI and NDVIPCA to the ground inventory data using ArcInfo grid functions. Then we applied the KNN methods to estimate the basal area.

3.4 Methodology

3.4.1 KNN Algorithms

Our KNN algorithm that is memory-based and has been widely used for data mining requires no model to be fit (Hastie et al. 2001). This algorithm can be depicted as follows: given a query point x_i, we need to find the K training points $x_j, j = 1, 2, \ldots, k$, closest in distance to x_i. For categorical variables we then classify x_i using the majority vote among the K neighbors. For non-categorical variables, we predict x_i calculating an average or weighted average of the K neighbors. The KNN is often named K nearest neighbor classifier when it is used for classifying categorical variables, while KNN is called K nearest neighbor regression when it is applied for predicting non-categorical variables.

In using the KNN algorithm as a procedure for forest inventory, if the objective of our research is to obtain a value of basal area of a pixel *i* (a plot or stand), this KNN algorithm will find K other pixels that have basal area values and that also have the most similar spectral values (we use Euclidian distance as the measure of spectral difference between pixels) to pixel *i* in the multispectral imagery. Then, an average value of basal area from the K other pixels is used as a

prediction for pixel *i*.

The selection of values of K is essential to accurately use KNN to analyze remote sensing data for forest inventory. Generally, the results of using a particular K are evaluated by examining prediction errors, which can be done in several ways. For example, direct calculation of RMSE is commonly used to evaluate the prediction results of different Ks (Katila and Tomppo, 2001; McRoberts et al., 2002; Tomppo, et al., 2002). Re-sampling statistics such as leave-one-out cross validation and bootstrapping (Franco-Lopez et al. 2001; Katila and Tomppo, 2001 and 2002; Trotter, et al., 1997) also are applied to evaluate the results of different K's.

In this paper, we developed a new approach for selecting K, wherein the choice of K is based on the combination of the Kolmogorov-Smirnov (KS) test and cumulative distribution functions (CDF). The KS test is a powerful evaluation that is generally used to determine whether two data samples are compatible. We use it here to determine the significance of the difference between the estimation and sample data. Displays of the empirical CDF can be used to check whether the predictions based on different Ks have the same or similar distributions as the sample data.

3.4.2 Direct Calculations of RMSE and Comparisons of Mean and SD

The RMSE and the mean and standard deviation (SD) of basal area were examined using equations (3-1), (3-2), and (3-3) in the evaluation of the results of different K.

$$RMSE = \sqrt{\sum_{i=1}^{n} (y_i - \hat{y}_i)^2 / n} \quad (3\text{-}1)$$

$$\bar{y} = \frac{1}{n}\sum_{i=1}^{n} y_i \qquad SD = \sqrt{\frac{1}{n-1}\sum_{i=1}^{n} (y_i - \bar{y})^2} \quad (3\text{-}2)$$

$$\bar{\hat{y}} = \frac{1}{n}\sum_{i=1}^{n} \hat{y}_i \qquad SD = \sqrt{\frac{1}{n-1}\sum_{i=1}^{n} (\hat{y}_i - \bar{\hat{y}})^2} \quad (3\text{-}3)$$

where y_i is the response variable (basal area) of the ith observation and $\hat{y}_i$ is the predicted value corresponding to y_i by using KNN. If the observed response variables and predicted variables are normally distributed, both SD and the means of the response variables are considered adequate criteria for measuring whether K is the optimal choice. However, it is unwise to assume the observations and predictions are normally distributed. In forest inventory we do not know whether the samples are from the Gaussian populations, and sometimes the assumptions of non-normal distributions might be more reasonable. For example, distributions of some tree species or tree mortality might be Poisson distributed. Furthermore, all-aged stands tend to have reversed J-shaped diameter distributions, while mound-shaped distributions with varying degrees of left or right skewness exist in even-aged stands (Clutter et al. 1983). Therefore, the simple calculation of RMSE and comparisons of SD and mean, are not optimum ways of selecting K in forest applications.

Typically, the smaller the RMSE, the closer our model follows the data; the RMSE is zero if a model goes through each data point exactly. However, KNN might easily overfit the data since it is flexible, and then KNN will not give satisfactory predictions even if a smaller RMSE is obtained. Furthermore, a dilemma may present itself in the case of a smaller RMSE but a

significantly different SD from that of the sample data. For forest resource management, it is important to obtain an SD that is similar to that of the sample data in order to keep variation information in the sample data.

3.4.3 Resampling Statistics to Estimate Generalization Errors

As an alternative to the direct calculation of RMSE, leave-one-out cross validation (equation 3-4) can be used for model selection, allowing the researcher to choose one of several models that has the smallest estimated generalization error (RMSEcv),

$$RMSE_{cv} = \sqrt{\sum_{i=1}^{n} (y_i - \hat{y}_i^{-i})^2 / n} \qquad (3\text{-}4)$$

where $\hat{y}_i^{-i}$ is the estimated value of the *i*th observation using the KNN rule fitted without considering observation *i*. It also is a popular method used to estimate the generalization error in KNN analysis. Leave-one-out cross validation is *k*-fold cross validation taken to its logical extreme, with *k* equal to *n*. However, this method has several disadvantages that should be considered. We must run the learning algorithm *n* times, which is infeasible for large data sets. Each fold only has one example, and it is impossible to guarantee that each class is properly represented in the test set. Leave-one-out cross validation might perform poorly for discontinuous error functions, such as the number of misclassified cases. Another problem with this method is a lack of continuity—a small change in the data may cause a large change in the model selection (Breiman, 1996). In linear regression, leave-one-out cross validation is similar to Akaike's Information Criterion (AIC). Since some studies have found that AIC overfits badly in small samples (Shao and Tu, 1995), it can be inferred that leave-one-out cross validation also

might overfit in small samples.

Bootstrapping is another resampling technique used in KNN estimation. Bootstrapping, an improvement on cross validation, typically achieves better estimates of generalization error (RMSE_Boot) at the cost of more computing time. Efron and Tibshirani (1997) proposed the ".632+" estimator (equation 3-5), which combines the leave-one-out bootstrap ($RMSE_{LOOB}$) with a measure of over-fitting.

$$RMSE_{0.632} = 0.368RMSE + 0.632RMSE_{LOOB} \quad (3\text{-}5)$$

The coefficients $0.632 \approx 1\text{-}(1\text{-}1/n)^n$ and 0.368 are suggested by the argument that bootstrap samples are supported on approximately 0.632n of the original data points. In extensive simulations it has been shown to be the best-performing bootstrap and offers some gains over cross validation (Arana et al. 2005). The .632+ bootstrap is one of the currently favored methods for estimating generalization error in the classification problem. It has the advantage of performing well even when there is severe overfitting.

It is important to consider that every bootstrapping iteration requires a run of the algorithm, thereby raising the question of whether the bootstrap is worth the large amount of required computer time. Nevertheless, it is an improvement over the calculation of simple RMSE. No matter how accurately the RMSE is calculated, it cannot be used as an optimum criterion to determine the same or similar distributions of sample data and estimated data because the dilemma of smaller RMSE and significantly different SD to sample data might present itself depending on the K value.

3.4.5 KS Test and CDF Plots

As stated previously, the KS test is used to determine if two datasets are compatible. The KS test has the advantage of making no assumption about the distribution of data, or technically speaking, it is non-parametric and distribution free. It is a robust test that relies on the relative distribution of the data. In using the KS test, we are interested in whether the predictions of basal area, based on different Ks, have similar distributions to the sample data. The null hypothesis of the KS test is that both the basal area predictions and sample data are drawn from the same continuous distribution. The predictions and sample data will have the same or similar mean and SD if the null hypothesis cannot be rejected. Therefore, the K values used for these predictions are the optimal selections. To compare two experimental cumulative distributions (S(x) and W(y)) that both contain n events, the KS test uses the maximum vertical deviation between the two curves as the statistic D:

$$D = \max | S(x_i) - W(y_i) | \quad i = 1,2,...,n \tag{3-6}$$

The KS test also is used to check whether the sample data are normally or lognormally distributed. The empirical CDF plots are used to graphically compare the distributions and the quantiles of the sample data and estimated data. All the CDF plots of the different predictions (K=1, K=2, K=3,…, K=13) based on different types of remote sensing data are drawn and compared with the sample data.

3.5 Data reduction

3.5.1 Principal Component Analysis

The principal components analysis (PCA) is a linear transformation used for data compression. It is practical and helpful in the remote sensing realm because sometimes there are redundant data in the different bands of a multispectral image. PCA reduces the dimensionality of the dataset, compacts the data into fewer bands which are noncorrelated and independent, and without losing significant information saves on storage space and speeds up processing. The first few components of the PCA usually capture the majority of the information, so the number of bands in a Landsat ETM+ image may be reduced from 7 to 2 or 3. In this research we ran PCA in Leica Geosystems' ERDAS Imagine using the built-in model. The first two components explained 95% of the variation in the 6-band image.

3.5.2 Normalized Difference Vegetation Index

The Normalized Difference Vegetation Index (NDVI) image (equation 3-7) provides the phenological "greenness" measure. It is one of many vegetation indices that can aid in visualization of an image and can be used to monitor the health of vegetation on the ground. It also is the most important index used to estimate volume and basal area in forest inventory. The NDVI has an added benefit of reducing the number of bands for an image down to one.

$$NDVI = \frac{NIR - RED}{NIR + RED} = \frac{Band\,4 - Band\,3}{Band\,4 + Band\,3} \qquad (3\text{-}7)$$

In this research, using KNN we analyzed a 6-band Landsat ETM+ image, then a PCA image and a NDVI image, and then finally we implemented KNN using the combined PCA and NDVI.

3.6 Results

The sample data included 128 plots of loblolly pine stands for which basal area was measured to serve as ground truth data for evaluating predicted basal area from Landsat ETM+ data. The mean basal area of observations was 25.81 m^2/ha, and the standard deviation was 10.13 m^2/ha. The KS test indicated that it is very unlikely that the sample was normally distributed: P= 0.04 where the normal distribution had a mean equal to 26.86 and standard deviation equal to 9.80. Furthermore, it is not likely that it was lognormally distributed: P= 0.04 where the lognormal distribution had a geometric mean of 22.74 and a multiplicative standard deviation of 0.39. Thus, in this situation, the mean and standard deviation (SD) were not adequate indices for selecting K.

Results of direct calculation of basal area and re-sampling statistics of estimated errors from the 6-band image, PCA image, NDVI image, and NDVIPCA images, are summarized in Tables 3.1 to 3.4. These tables reveal that the estimated standard deviation decays quickly as K increases. The three kinds of errors, RMSE, RMSEcv, and $RMSE_{LOOB}$ have the same trends as the estimated standard deviation and decrease as K increases. There is not much difference among estimated means of basal area from K=1 to 13.

Table 3.1. Estimated Generalization Errors of Basal Area Using 6-band Data (unit: m^2/ha).

K	1	2	3	4	5	6	7	8	9	10	11	12	13
Mean_ Esti	27.11	26.89	26.82	26.84	26.90	26.99	27.05	27.06	26.97	26.94	26.83	26.83	26.72
SD_Esti	10.39	8.86	8.18	7.59	7.46	7.40	7.13	6.97	6.85	6.80	6.66	6.61	6.51
RMSE	10.75	9.35	8.77	8.40	8.40	8.28	8.13	7.98	7.91	7.86	7.78	7.82	7.83
$RMSE_{cv}$	10.81	9.41	8.82	8.45	8.45	8.32	8.18	8.02	7.95	7.90	7.82	7.86	7.87
$RMSE_{\_Boot}$	10.79	9.39	8.80	8.43	8.43	8.31	8.16	8.01	7.94	7.89	7.81	7.84	7.86

K, # of neighbors in K nearest neighbor methods.

SD_esti, the standard deviation of the estimations.

Mean_Esti, the mean of the estimations.

RMSE, root mean square error of estimations; $RMSE_{cv}$, RMSE based on leave-one-out cross validation; $RMSE_{\_Boot}$, RMSE based on boot strapping methods.

Table 3. 2. Estimated Generalization Errors of Basal Area Using PCA (unit: m^2/ha).

K	1	2	3	4	5	6	7	8	9	10	11	12	13
Mean_Esti	26.60	26.45	26.33	26.39	26.49	26.57	26.66	26.67	26.62	26.58	26.53	26.55	26.50
SD_Esti	9.33	7.80	7.30	7.13	6.96	6.88	6.74	6.69	6.63	6.54	6.43	6.35	6.32
RMSE	10.53	9.34	8.85	8.76	8.56	8.54	8.50	8.32	8.29	8.21	8.16	8.17	8.11
RMSEcv	10.59	9.39	8.90	8.81	8.61	8.58	8.55	8.37	8.33	8.25	8.21	8.22	8.15
$RMSE_{\_Boot}$	10.56	9.38	8.88	8.79	8.60	8.57	8.53	8.35	8.31	8.24	8.19	8.20	8.14

The notes are the same as those in Table 3.1.

Table 3.3. Estimated Generalization Errors of Basal Area Using NDVI (unit: m^2/ha).

K	1	2	3	4	5	6	7	8	9	10	11	12	13
Mean_Esti	24.69	24.83	25.03	25.60	25.94	26.18	25.99	26.25	26.14	26.05	26.01	29.89	30.22
SD_Esti	8.21	6.74	6.39	6.20	5.23	4.81	4.80	4.53	4.25	4.17	4.15	0.01	0.01
RMSE	13.30	12.06	11.46	11.04	10.61	10.46	10.26	10.14	9.88	9.91	10.20	10.69	10.80
RMSEcv	13.37	12.13	11.53	11.10	10.67	10.52	10.32	10.19	9.93	9.96	9.96	10.75	10.86
$RMSE_{\_Boot}$	12.81	11.62	11.05	10.64	10.22	10.08	9.89	9.77	9.52	9.55	9.64	10.30	10.41

The notes are the same as those in Table 3.1.

Table 3.4. Estimated Generalization Errors Of Basal Area Using NDVIPCA (unit: m^2/ha).

K	1	2	3	4	5	6	7	8	9	10	11	12	13
Mean_Esti	26.60	26.45	26.33	26.39	26.49	26.57	26.66	26.67	26.62	26.58	26.53	26.55	26.50
SD_Esti	9.33	7.80	7.30	7.13	6.96	6.88	6.74	6.69	6.63	6.54	6.43	6.35	6.32
RMSE	10.53	9.34	8.85	8.76	8.57	8.54	8.50	8.32	8.29	8.21	8.16	8.11	8.11
RMSEcv	10.59	9.39	8.90	8.81	8.61	8.55	8.37	8.37	8.33	8.25	8.21	8.22	8.15
$RMSE_{\_Boot}$	10.56	9.38	8.88	8.79	8.60	8.54	8.42	8.35	8.31	8.24	8.19	8.18	8.14

The notes are the same as those in Table 3.1.

3.6.1 K Selection Using Direct Calculation of RMSE and Resampling Statistics

It is difficult to select K based on direct calculation of RMSE and re-sampling statistics. The optimal choices of K from the different images are summarized in Table 3.5. If the smallest RMSE is used as the criterion to select K, the optimal K is 9, 11, 12, or 13; if the smallest SD of the estimated data is used as the criterion, the optimal K is 12. When using similar SDs between the estimated and sample data, the optimal K is 1. When using a similar mean of estimations as the sample data to select K, there is not much difference for different Ks. However, we prefer the standard deviation of estimated data (i.e., K's estimations selected by some criteria) and sample data to be similar because the same or similar distributions of the estimated data and sample data play important roles in spatial prediction. A dilemma therefore exists in the selection of optimal K values. In other words, although one prediction method results in the smallest RMSE, there is a significantly different SD from the sample data.

Table 3.5. Optimal Selection Of K From Different Images.

	Smallest RMSE	Smallest SD	Similar mean	Similar SD
6-band	11	13	1~13	1
PCA	13	13	1~13	1
NDVI	9	13	1~13	1
NDVIPCA	12	13	1~13	1

6-band, band 1~5 and 7 of Landsat ETM+.
PCA, 2 principal layers based on principal analysis from 6-band data.
NDVI, data of normalized difference of vegetation index.
NDVIPCA, the combined data of NDVI and PCA.

Table 3.6. Kolmogorov-Smirnov (KS) Test For The Distribution Analogous Analysis Between Field Data And Estimations Of The K Nearest Neighbor Method.

K		1	2	3	4	5	6	7	8	9	10	11	12	13
NDVIPCA	D	0.044	0.167	0.222	0.244	0.256	0.278	0.278	0.289	0.289	0.289	0.278	0.278	0.278
	P	1.000	0.164	0.023	0.009	0.006	0.002	0.002	0.001	0.001	0.001	0.002	0.002	0.002
6-band	D	0.067	0.144	0.200	0.278	0.289	0.289	0.289	0.289	0.289	0.289	0.289	0.289	0.289
	P	0.988	0.305	0.055	0.002	0.001	0.001	0.001	0.001	0.001	0.001	0.001	0.001	0.001
NDVI	D	0.178	0.267	0.233	0.233	0.256	0.289	0.289	0.344	0.356	0.356	0.333	0.567	0.644
	P	0.116	0.003	0.015	0.015	0.006	0.001	0.001	0.000	0.000	0.000	0.000	0.000	0.000
PCA	D	0.044	0.168	0.223	0.243	0.257	0.278	0.279	0.289	0.290	0.289	0.279	0.279	0.280
	P	1.000	0.164	0.023	0.009	0.006	0.002	0.002	0.001	0.001	0.001	0.002	0.002	0.002

D, the values of the statistic D using KS test;
P, the P value using KS test;
Other notes are the same as those in Table 3.5.

3.6.2 K Selection Based on the KS Test and CDF Plots

We determined that the sample data are neither normally nor lognormally distributed, and then we used a KS test to check whether the sample data and the estimated data had the same distribution. The CDF plots graphically indicate how they are distributed. These results are summarized in Table 3.6. At the significance level of $\alpha = 0.05$, the estimations of K=1 and K=2 from the 6-band image had the same distribution as the sample data (the *p*-value for K=3 is

0.05465, which is on the boundary of significance level of 0.05). Estimation of K=1 and K=2 from the PCA image had the same distributions as the sample data. Likewise, the estimations of K=1 from the NDVI image and the estimations of K=1 and K=2 from NDVIPCA images had the same distributions as the sample data. Therefore, the selection of K based on the 6-band, PCA, and NDVIPCA images are K=1 and K=2. The selection of K for the NDVI image is 1. In addition, an obvious trend of these KS tests is that the *p*-value (P) decreases quickly as K increases from 1 to 13, and D increases from K=1 to 13. This means that the estimations differ more from the sample distribution as K increases (Figures 3.2 and 3.3 show the obvious differences of K=1, 2, and 13). In addition, for the same K, the NDVI image gave the largest estimate of D, which indicates that the distribution of basal area estimated using the NDVI is much different from estimations using 6-band, PCA, and NDVIPCA images. In other words, the NDVI image was not a good data reduction method for basal area estimation in this study, when compared with PCA and NDVIPCA.

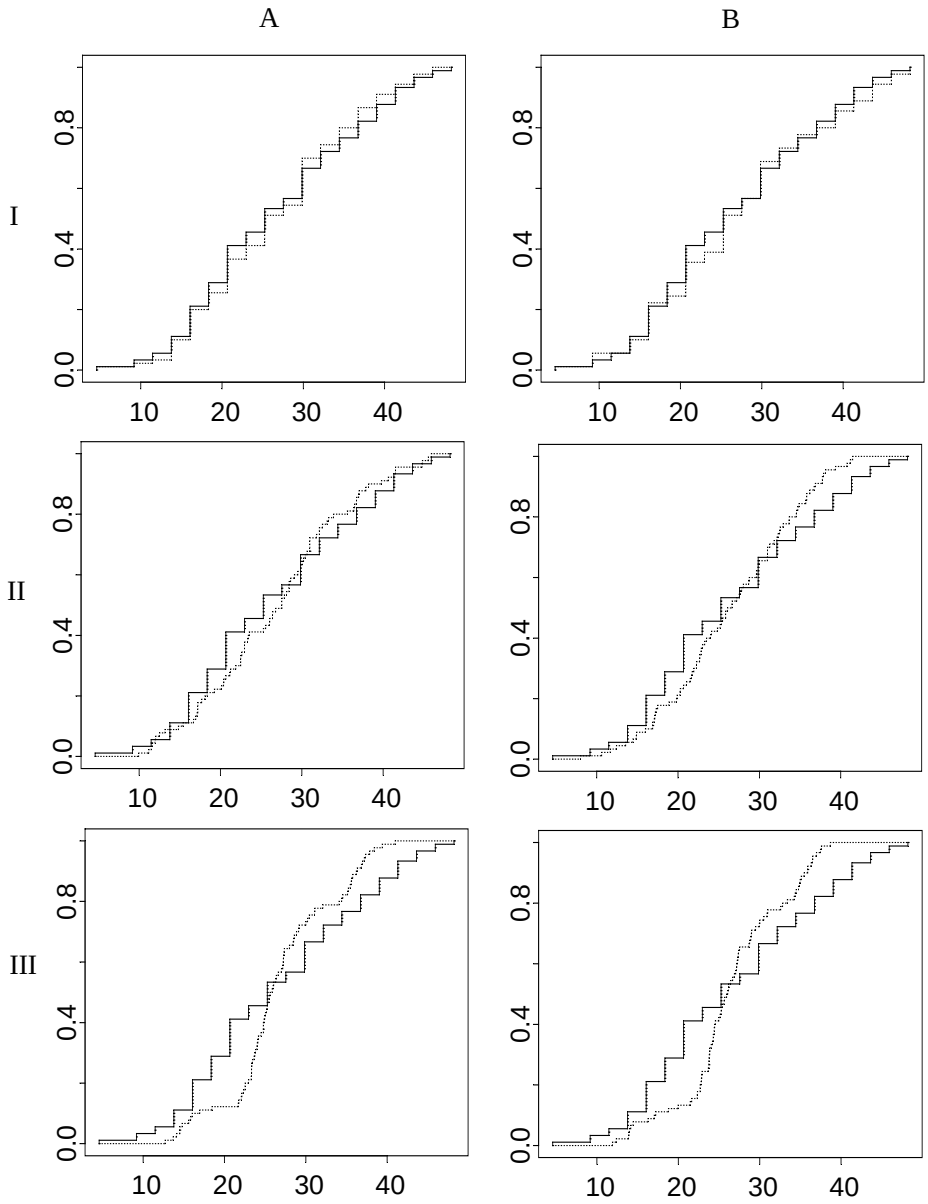

Figure 3.2. Comparison Of Cumulative Distribution Functions Of Sampled Basal Area Vs. Estimated Basal Area. Solid line is the observed basal area, dotted line in column A consists of estimations from the 6-band image, and dotted line in column B consists of estimations from the NDVIPCA image; I shows K=1, II shows K=2, and III shows K=13.

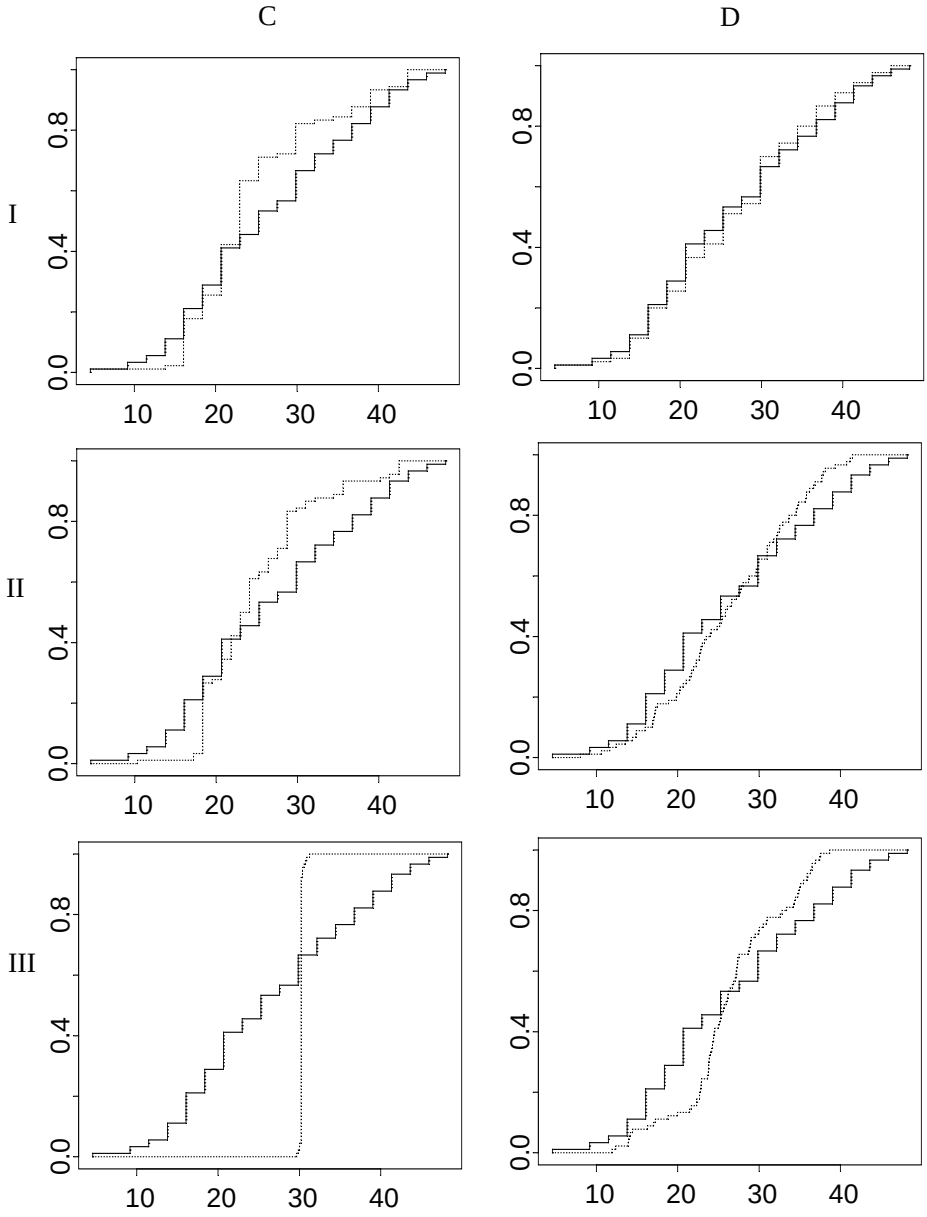

Figure 3.3. Comparison Of Cumulative Distribution Functions Of Sampled Basal Area Vs. Estimated Basal Area. Solid line is the observed basal area, and dotted line in column C consists of estimations from the NDVI image, dotted line in column D consists of estimations from the PCA image; I shows K=1, II shows K=2, and III shows K=13.

The KS tests indicate significant differences between the distributions based on K=1 or K=2 and those estimations based on K>2. When K=1 or K=2, the distributions of the estimated data have almost the same distributions as the sample data. However, the distributions of the estimated data differ greatly from the sample data distribution when K > 2 (Table 3.6). As K increases, the difference between the estimated and sample distributions also increases, although the RMSE decreases. The estimated data from NDVI when K=13 shows the extreme situation, as the vast majority of the data are compacted into a very narrow fraction of the plot (III, C in Fig. 3).

Based on the KS test results and the comparison of the CDF plots, we achieved very similar estimations based on PCA, NDVIPCA, and 6-band images. The PCA image has two layers and the NDVIPCA image has three layers, but the 6-band image has 6 layers. PCA and NDVIPCA images save much more time in the computation process. PCA is a good method of data reduction in image analysis. Therefore, we recommend remote sensing data reduction or transformation and then conduct the KNN analysis using the transformed image for basal area estimation.

3.7 Conclusions

This research focused on the problems of KNN methods, which are the selection of K values and computation cost. The selection of K values was discussed comparing KS tests and CDF plots. The PCA, NDVI, and the combination of PCA and NDVI images were used to save the computation cost. K=1 or K=2 was the optimal selection according to the KS tests and CDF plots

in this research since estimations of basal area using K=1 and K=2 both have almost the same distributions as the sample data.

We discussed and applied three methods of band reduction and transformation: PCA, NDVI, and the combination of PCA and NDVI. Results indicate PCA was the optimal data reduction method for this research because it produced similar basal area estimations to the 6-band and NDVIPCA images. Since it has only two layers, much time is saved in distance computation. The CDF plots show that the NDVI image is not a satisfactory method of data reduction for this research. Although the estimation of K=1 has a similar distribution to the sample data, of the four types of basal estimations using 6-band, PCA, NDVI, and NDVIPCA images, estimations based on the NDVI image have the largest difference from sample data (Table 3.6, Figures 3.2 and 3.3), when the estimations are compared to the sample data.

Overall, the comparison of KS tests and CDF plots is a relatively effective method of selecting K when KNN is used for estimating, classifying, and mapping forest parameters. This method seems more efficient than the available re-sampling statistics because the KS test is a powerful test of whether the estimated and the sample data have the same or similar distributions. The KS test and CDF plots also help us check the agreements of distributions between sample and estimated data, which is useful for selecting an efficient data reduction approach. It is difficult to determine which type of data reduction is better simply comparing SD and RMSE using the available methods for selecting K values (Tables 3.1-5).

The critical point of K selection in forest inventory using KNN is whether the estimation has the same or similar distribution as the sample. KNN is not only useful for global estimation, but

also for classification and spatial prediction in forest inventories. We believe that KNN can be extensively applied in forest inventory and other related natural resource prediction and classification. The characteristics of local vs. regional and place vs. space are also very important in forest or natural resources management. Therefore, the estimations based on the selected K should not only have smaller RMSE, but also similar distributions as the sample data.

It is difficult to select the optimal K based on direct calculation of RMSE and re-sampling statistics because it seems that there are some trade-offs between choosing the smallest RMSE and similar standard deviation (i.e., the similar distributions between the sample data and estimated data). The KS test makes no assumptions on the distribution of data. The KS test and CDF plots indicate the degree of differences in estimations for different Ks. As K increases, the difference between the estimated distributions and the sample distribution also increases. A suitable way to select K is the combination of KS test and CDF comparisons of the samples and estimations. We advise using the KS test and CDF comparisons to select K values. Deciding on the optimal K values, however, depends on the significance of the KS test and the CDF comparisons between samples and estimations in the particular research. In this research, K=2 was the optimal choice, since its estimations have a similar distribution to the sample data and smaller RMSE than that of K=1.

CHAPTER 4

GEOSTATISTICAL PREDICTION AND MAPPING FOR LARGE AREA FOREST INVENTORY USING REMOTE SENSING DATA*

4.1 Introduction

Large area forest inventory is important for understanding and managing forest resources and ecosystems. The purpose of traditional large area forest inventory is to provide unbiased and reliable forest resource information, though typically these inventories lack fine spatial resolution. Remote sensing, the Global Positioning System (GPS), and geographic information systems (GIS) provide new opportunities for forest inventory. By integrating remote sensing, GPS, and GIS, it is possible to predict forest parameters at fine spatial resolutions. The research described here develops a new systematic geostatistical approach for large area forest inventories, where one type of forest parameter, such as basal area, height, health conditions, biomass, or carbon can be incorporated as a response variable and the geostatistical approach can be used to predict un-inventoried points. Using basal area as an illustration, this approach includes univariate kriging (ordinary kriging and universal kriging) and multivariable kriging (cokriging and regression kriging). The combination of bands 4, 3, and 2, as well as the combination of bands 5, 4, and 3, along with normalized difference vegetation index (NDVI) and principal components

* This research has been published online at www.ucgis.org/summer2006/studentpapers/Mengqm_July03_2006.pdf. It has been submitted to *GIScience and Remote Sensing*.

(PCs) are used in cokriging and regression kriging. Cross validation using the training dataset and validation based on 200 random sampling points indicates that the regression kriging is the best geostatistical method for spatial predictions of pine basal area. Finally, pine basal area is mapped using regression kriging, and standard errors also are mapped to assess the dispersions of the spatial prediction.

Large area forest inventories generally are based on plot sampling, and small area forest inventories usually are processed forest stand units. These two traditional inventories can be integrated by combining ground inventory and remote sensing data and processing them in geographical information systems (GIS).

Remote sensing, the Global Positioning System (GPS), and GIS provide new opportunities for forest inventory. It is now easy to measure the locations of survey plots, forest stands, and stand boundaries in the field with an accuracy rate of ±5m using differential GPS. Developments in sensor technology have also enabled acquisition of remotely sensed data at a range of scales. Remote sensing data are available from satellite sensors providing images with medium spatial resolution of 20~30 m (Landsat TM, Landsat ETM+, SPOT HRVIR) as well as high spatial resolution of less than 5 m (Ikonos, QuickBird, LIDAR, and others). Integration of these technologies allows achievements in forest metrics using raster data with cell sizes of 30 m, 20 m, 10 m, 5 m, or 1 m. These raster data can be estimated from remote sensing data by modeling the relationships between the image's digital numbers (DN) and the forest variables inventoried with GPS. Geographic information systems and spatial modeling are efficient tools to model, estimate, map, and predict spatial characteristics of stands or trees. Generally, the two

ways to obtain the fine spatial forest information are spatial modeling and nonspatial modeling.

Nonspatial modeling methods have been widely applied in forest research. Ordinary least-squares (OLS) regressions are the common models applied for estimations of forest variables (Ardö, 1992; Dungan, 1998; Trotter, Dymond & Goulding, 1997). K nearest neighbor (KNN) methods for achieving forest metrics using remote sensing data have been applied in Finland and America for forest inventories (Franco-Lopez, et al. 2001; Holmström and Fransson, 2003; Moeur and Stage, 1995; Tomppo, 1991). Artificial neural networks also are used for estimating forest variables using remote sensing data (Foody & Boyd, 1999; Foody, 2000; Tatem *et al*., 2001).

Tokola et al. (1996) applied both linear regression and the KNN method on forests in the southern boreal vegetation zone in Finland using data from Landsat TM and SPOT. The authors reported standard errors of stem volume prediction from 70 to 80 m^3/ha (more than 60% of the mean) at the plot level. Trotter et al. (1997) used Ordinary Least Squares to predict stem volume of mature plantations in New Zealand and reported a root mean square error (RMSE) greater than 100 m^3/ha (with a mean stem volume of 413 m^3/ha) for pixel predictions. The K nearest neighbor method was applied by Holmström & Fransson (2003) to predict forest variables using a combination of SPOT-4 and low-frequency radar data from the airborne CARABAS system. The study by Holmström & Fransson (2003) used data from a coniferous forest in southwest Sweden and reported RMSEs of 64% (of the mean) of stem volume using optical data and 53% using the combination of optical and radar data. The stem volume of the sample plots (10 m radius) was in the range of 0-750 m^3/ha with a mean value of 171 m^3/ha.

Many studies have conducted spatial predictions using remotely sensed data (Atkinson et al. 1994; Atkinson and Lewis, 2000; Chica-Olmo and Abarca-Hernandez, 2000; Curran, 1988; Curran and Atkinson 1998; Dungan 1998; Dungan, et al.1994; Lark, 1996). Few studies have been conducted on estimations of forestry relevant variables using spatial models, though, a large number of spatial-statistical and prediction models are available in the literature (e.g. Cressie, 1993; Goovaerts, 1997; Odeh, et al. 1995; Odeh and McBratney, 2000; Wackernagel, 1994). Berterretche et al. (2005), Tuominen et al.(2003), and Zhang et al (2004) applied geostatistical models to estimate forest variables, leaf area index, and classify forest lands based on remote sensing data. Gilbert & Lowell (1997) used kriging to predict stem volume in a 1500 ha balsam fir (*Abies balsamea*) dominated forest. Prediction based on 5.6 m and 11.3 m radius plots resulted in a prediction RMSE of 54% (of the mean) and 39-46%, respectively. Similar accuracy was obtained by prediction using the sample average only. Methodologically, the accuracy rate of the predicted variable could be improved by incorporating close field observations as predictors in spatial modeling.

Rarely has research explored the integration of remote sensing data, GPS, ground data, GIS, and geostatistics to estimate forest parameters at a fine spatial resolution for large areas. One systematic geostatistical approach for spatial forest inventory is developed and explored in this research. Compared to the typical ordinary kriging (OK) and universal kriging (UK) using only one variable, this research develops a systematic geostatistical approach—co-kriging (CoK) and regression kriging (RK) using remotely sensed data as predictors—to improve spatial predictions of forest variables by integrating GPS, ground inventory data, remote sensing, and

GIS. This systematic geostatistical approach is summarized in a flow chart (Figure 4.1), and provides new insights for forest parameter estimation, and not only considers the associations between one forest parameter and DN but also incorporates the spatial dependence of the forest parameter into the process of spatial prediction. In this study, basal area is used as the response variable to conduct this geostatistical approach.

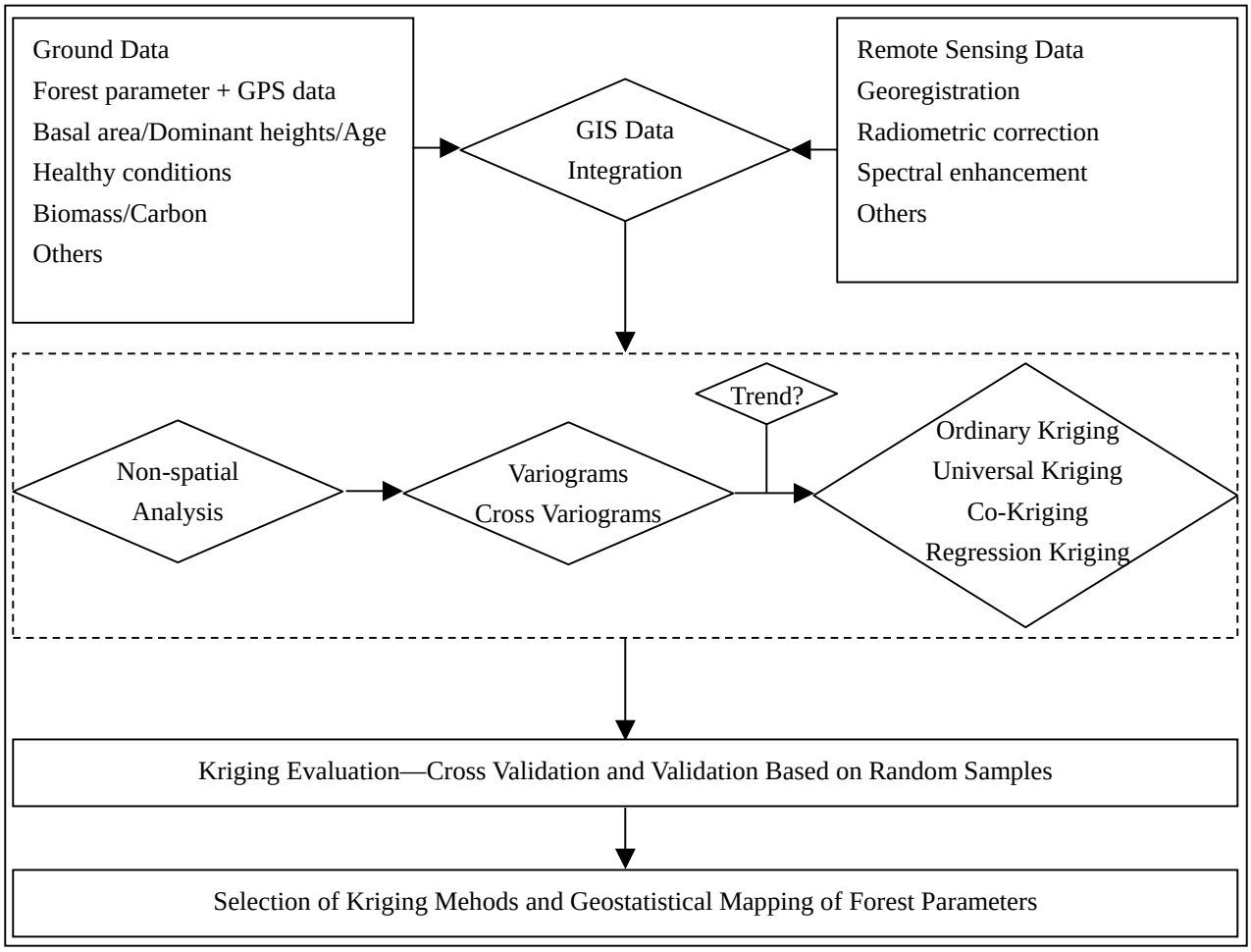

Figure 4.1 A Systematic Geostatistical Approach For Predicting Forest Parameters Using Remotely Sensed Data.

In addition to analyzing spatial characteristics of an integrated GIS with ground and remote sensing data, it is also necessary to analyze nonspatial data; for example, the selection of

band combinations and data reduction of remotely sensed imagery. What is the association between the response variable and independent variables i.e., the remotely sensed data? Distribution tests may be needed. However, the kriging equations are derived without being based on any distributional assumptions (Myers, 1996). Correlation diagnostics are important for multivariable geostatistics. The variogram models are fitted to check spatial autocorrelation and dependence. Cross variograms need fitting if multivariable geostatistical approaches are conducted. Additionally, it is important to check whether a spatial trend exists in the data of the response variable. Both universal kriging and regression kriging are efficient to incorporate the trend in geostatistical predictions.

4.2 Data Sources

4.2.1 Ground data

Ground data covering 20 counties in west Georgia were inventoried in 1999 (Figure 4.2). These locations of ground data were collected using differential Global Positioning System (DGPS) units with errors of about ±5 m. The coordinates of the ground data were converted to the Universal Transverse Mercator to match those of the Landsat ETM+ images (Figure 4.3). There were 2822 ground records used in this study with a mean of 13.99 m^2/ha and a range from 0.038 to 29.84 m^2/ha. The basal area and dominant height were measured, and volume of trees was calculated according to tree species. Basal area of pines is used as the only response variable in this study. Basal area at the Landsat pixel level (30 m) is predicted for the un-inventoried areas in these 20 counties.

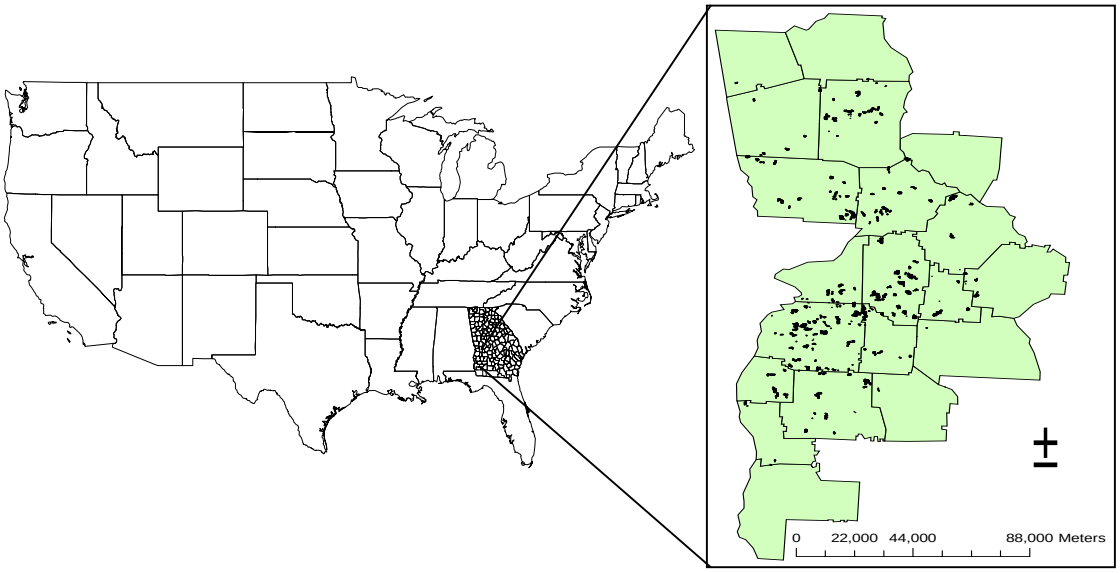

Figure 4.2. The Study Area Includes 20 Counties In The State Of Georgia.
The ground inventory locations are indicated as the dark dotted places in these 20

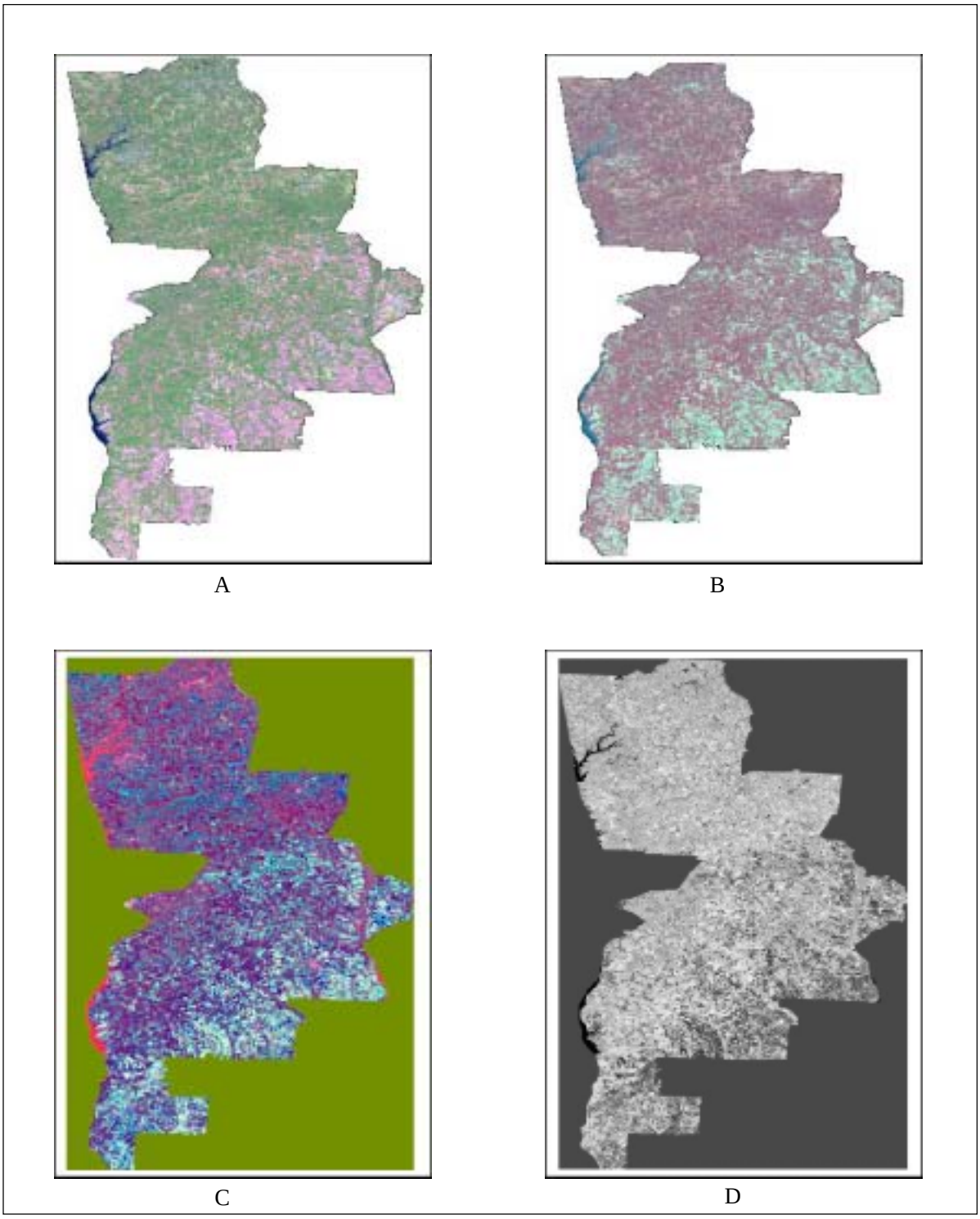

Figure 4. 3. Landsat ETM+ Images Used for Pine Basal Area Prediction.
A, a 543 band combination; B, a 432 band combination; C, the three PCs images; D, the NDVI images.

4.2.2 Remote sensing data

Landsat 7 Enhanced Thematic Mapper Plus (ETM+) images (Path/Row: 19/37 and 19/38) acquired on 10 September 1999 from the USGS Earth Resource Observation System Data Center were used in this research. Atmospheric conditions were clear at the time of image acquisition, and the data had been corrected for the radiometric and geometric distortions of the images to the standard Level 1G before delivery. Two Landsat images covering this study area were masked after the geometric corrections using U.S. Geological Survey (USGS) digital orthophoto quarterquads (DOQQs) as the sources of control (RMSE is less than 10 m). This resulted in a 4449 pixel by 9010 row 6-band (i.e., 1, 2, 3, 4, 5, and 7) image for analysis.

Band Combinations

Band 1 of Landsat images contributes little for vegetation analysis. Studies indicate that as the leaf coverage changes from 0% to 11.9%, 43.2%, and 87.6%, very little change occurs in the reflectance of band 1 (0.4-0.5 *um*) (Short, 1999). The differences of reflectance increase from 0.5 to 0.8 *um* as leaves change. The differences of reflectance in the mid-infrared ranges are very close to the differences in the near infrared ranges. Band 7 of Landsat images is not used as an independent variable. Bands 2, 3, 4 and 5 are used, and 432 and 543 band combinations are applied to estimate pine basal area.

Principal Component Analysis

Principal component analysis (PCA) is the most frequently used technique for remote sensing data reduction. Generally, remotely sensed data, such as Landsat images, are highly correlated among the adjacent spectral bands (Barnsley, 1999). The Landsat bands are

transformed into orthogonal principal components (PC). The first PC contains the largest percentage of data variation, and the second PC contains the second largest variance of the data, and so on. The higher the PC is numbered, the less useful information the PC contains. In this research, the six Landsat ETM+ bands used (i.e., band 1, 2, 3, 4, 5, and 7) were processed using PCA, and the first three PCs were applied for pine basal area analysis because they accounted for more than 95% total variance.

Normalized Difference Vegetation Index

In this study, the normalized difference of vegetation index (NDVI) is used for pine basal area estimation. NDVI is based on a ratio of the near infra red (NIR) and the red channels, and the standard equation for NDVI is as in equation 4-1.

$$NDVI = \frac{NIR - \mathrm{Re}\ d}{NIR + \mathrm{Re}\ d} \tag{4-1}$$

Healthy forests reflect strongly in the near-infrared portion of the spectrum while absorbing strongly in the visible red. On the other hand, soil, bare ground, and rock show near equal reflectance in both the near-infrared and red portions and have NDVI values close to 0 while water bodies have the opposite trend to vegetation and the index is negative. The NDVI image can significantly enhance the discrimination of vegetation cover from other surface cover types. The values of NDVI generally range from 0.05 for sparse vegetation cover to 0.7 for dense vegetation cover (Tucker, 1979). It not only measures both the amount of green vegetation and vegetation health in an area, but it also is a basic indicator of changes in vegetation over space and time. It has been extensively applied as a proxy for leaf area index (Tucker, 1979),

vegetation biomass (Seller, 1987), and net primary production (Goward et al, 1985). Therefore, NDVI indicates the spatial characteristics of forest stand development, especially the density and health of trees. It has been proven to be an efficient indicator in detecting and quantifying large-scale changes in plant and ecosystem processes (Braswell et al. 1997; Myneni et al. 1997).

4.3 Methodology

4.3.1 Correlation analysis

Correlation analysis was applied to measure the strength of association between the response variable and the independent variables. Pearson's product-moment correlation (r_{xy}, equation 4-2) coefficient and the Pearson partial correlation ($r_{xy \bullet z_1 z_2}$, equation 4-3) coefficient were used to measure the association between the response variable and the independent variables. Pearson's product-moment correlation measures the association without considering the correlation contributions from other independent variables. The Pearson partial correlation measures the strength of a relationship between two variables while controlling the effects of two additional variables. Therefore, it is called the second-order partial correlation indicating the partial correlation between *x* and *y* controlling for both z_1 and z_2.

$$r_{xy} = \frac{\sum (x_i - \bar{x})(y_i - \bar{y})}{\sqrt{\sum (x_i - \bar{x})^2 \sum (y_i - \bar{y})^2}} \tag{4-2}$$

$$r_{xy \bullet z_1 z_2} = \frac{r_{xy \bullet z_1} - r_{xz_2 \bullet z_1} r_{yz_2 \bullet z_1}}{\sqrt{(1 - r^2_{xz_2 \bullet z_1})(1 - r^2_{yz_2 \bullet z_1})}} \tag{4-3}$$

4.3.2 Geostatistical approach

Geostatistical methods are based on the theory of regionalized variables (Matheron, 1965), which makes the assumption that data are observations of stochastic variables. We can consider a spatial variable as a realization of a random function represented by a stochastic model.

One of the key steps in geostatistical modeling is the semivariogram, a function describing the spatial dependence of the spatial variable. The semivariogram has been used widely in remote sensing to determine spatial structures (Curran, 1988; Warren, et al., 1990; Atkinson & Lewis, 2000). Based on the semivariogram, the geostatistical process derives optimal linear unbiased spatial prediction methods (i.e., kriging) by minimizing mean-squared prediction error. However, the assumptions of stationarity, which often are not met by the field-sampled data sets, and the requirement of a large dataset to define the spatial autocorrelation, result in the limitations of univariate kriging. Fortunately, geostatistical methods also provide optimal prediction methods using auxiliary data. Large volumes of auxiliary data for forest research are available now, such as remote sensing data. Incorporating the auxiliary data, co-kriging and regression kriging, as described below, can increase prediction accuracy. The gstat package (Pebesma, 2005) is mainly referenced for variogram and kriging methods as follows.

4.3.3 Variograms

Direct variogram

The direct variogram generally is computed from equation (4-4),

$$\gamma(h) = \frac{1}{2N}\sum_{i=1}^{N}[Z(x_i) - Z(x_{i+h})]^2 \quad (4\text{-}4)$$

where x_i is a data location, h is a vector of distance, $Z(x_i)$ is the data value of one kind of attribute at location x_i, N is the number of data pairs for a certain distance and direction of h units. The equation is used for determining the spatial autocorrelation of the univariate variable.

Cross variograms

A typical cross variogram is calculated as in equation 4-5, and is applied for the joint spatial variability between two kinds of spatial variables. It is defined as half of the average product of the lag distance relative to the two variables Z and Y.

$$\gamma(h) = \frac{1}{2n(h)}\sum_{i=1}^{n(h)}\{[Z(x_i) - Z(x_{i+h})]*[Y(x_i) - Y(x_{i+h})]\} \quad (4\text{-}5)$$

When the direct and cross variogram models are fitted, they also can guarantee that the fitted models follow the linear model of coregionalisation (Goovaerts, 1997). This ensures the cross covariance matrices are always positive. Calculations and visualizations of directional variograms, variogram clouds, and identification through interactive examination in the variogram cloud were finished using the gstat package (Pebesma, 2004).

4.3.4 Kriging

Ordinary kriging and universal kriging

Ordinary kriging (OK) is identical to multiple linear regression with a couple of important differences. The ordinary kriging model is as in equation 4-6. $Z(s_0)$ is the value to be interpolated at location s_0, $z(s_i)$ are the sampled values at their locations, and λ_i are the weights to be assigned to each sampled value. Universal kriging is applied when a trend exists. Universal kriging is often fitted using a polynomial equation, which is similar to the equation 4-6 to analyze the trend across the study area.

$$Z(s_0) = \sum_{i-1}^{n} \lambda_i z(s_i) \qquad (4\text{-}6)$$

Cokriging

For forest applications, a few studies using remote sensing data have been conducted using the geostatistical approach. Dungan et al. (1994) and Dungan (1998) applied co-kriging and a stochastic simulation method for forest management using synthetic remote sensing datasets.

Co-kriging (CoK) is an extension of kriging, and is a method for estimating one or more variables of interest using data from several variables by incorporating not only spatial correlation but also inter-variable correlation. Co-kriging is a very versatile and rigorous statistical technique for spatial point estimation when both primary and auxiliary attributes are available. It is defined as in equation 4-7. If each component of $z(s_0)$ satisfies the intrinsic hypothesis (Journel and Huijbregts, 1978), then equation 4-5 is unbiased if

$$Z(s_0) = \sum_{j=1}^{n} z(s_j)\Lambda_{j\bullet} \tag{4-7}$$

$$\sum_{j=1}^{n} \Lambda_{j\bullet} = \mathrm{I} \tag{4-8}$$

where I is an identity matrix = $[1,0,\ldots,0]^T$ and *T* indicates a transpose, and $\Lambda_{j\bullet}$ are the weights associated with prediction. Equation 4-7 is

$$\sum_{\phi=1}^{v} \Gamma(s_i, s_j) + \Psi = \Gamma(s_i, s_0) \qquad i = 1,\ldots,n \tag{4-9}$$

where $z(s_j)$ is the vector $z_1(s_j)\ldots z_m(s_j)$. $\Gamma(s_i, s_j)$ and $\Gamma(s_i, s_0)$ are the cross variograms, and Ψ is the Lagrange Multiplier for *i* from 1 to n.

According to the sample relations between the primary variable and the auxiliary variables, CoK could be described in several ways as follows. The most efficient way to predict the primary variable is to use the auxiliary variables to cokrig it into dense grid locations. This is named heterotopic cokriging (Wackernagel, 1994). Isotopic cokriging requires that data on both the target variable and co-variables be measured at all sample locations. A variant of both is generalized cokriging (Myers, 1982) that involves simultaneous prediction of all the correlated variables into more dense locations. The complete case is the case where the covariates and the primary variable do not share any common locations. A more general type applied using remote sensing data is collocated cokriging, where covariates are available at all interpolation locations, although the primary variable is available at only a few locations. When CoK is compared to univariate kriging, no new concept is added, but there is heavier notation associated with having several variables (Goovaerts, 1997).

Regression kriging

Regession kriging (RK) is a hybrid method that combines either a simple or multiple-linear regression model (or a variant of the generalized linear model (GLM) and regression trees) with kriging (Odeh et al., 1995; Goovaerts, 1997). In the process of RK, kriging with uncertainty introduces the regression residuals (i.e., the model uncertainty) into the kriging system, which is then applied directly to predict the primary variable. The predictions are combined from two parts; one is the estimation obtained by regressing the primary variable on the auxiliary variables; the second part is the residual estimated from the ordinary kriging. Regression kriging is estimated as follows:

$$\hat{Z}_{rk}(s_0) = \hat{m}(s_0) + \hat{\ell}(s_0) \tag{4-10}$$

$$\hat{Z}_{rk}(s_0) = \sum_{k=0}^{v} \hat{\beta}_k * q_k(s_0) + \sum_{i=1}^{n} \omega_i(s_0) * \ell(s_i) \qquad q_0(s_0) = 1, \qquad i = 1,...,n \tag{4-11}$$

where $\hat{\beta}_k$ are trend model coefficients, optimally estimated using generalized least squares; ω_i are weights determined by the semivariance function, and ℓ are the regression residuals. In the gstat package, univarite kriging and multivariable kriging are applied for pine basal area prediction (Pebesma, 2004, 2005).

4.4 Model Evaluation

In this study, different geostatistical models are developed and applied for pine basal area prediction. There are always discrepancies between true and predicted values. It is necessary to validate the models and check which is more efficient. For this geostatistical approach, two methods for assessing models are applied. One method is cross validation, which is used to

validate whether the model fits the training data. The second method is validation based on random samples outside of the training data set. We developed 200 random points to check which model is more efficient in spatial predictions of pine basal area.

There are many different measures for checking discrepancies and each has its advantages and weaknesses. Details about forecast evaluation were discussed by Murphy and Katz (1985). Typically, four criteria, standard deviation (SD), bias error (BE), root mean square error (RMSE), and mean-absolute error (MAE) are used to directly compare forecast and observation. Standard deviation is the measure of dispersion from the mean of a particular parameter as illustrated by equation 4-12.

$$SD = \left[\frac{1}{N-1} \sum_{n=1}^{N} (X_n - \overline{X})^2 \right]^{1/2} \quad (4\text{-}12)$$

where N is the size of the sample, X_n is the sample values and $\overline{X}$ is the mean of the sample. The bigger the SD, the larger the dispersion of the estimations is from the mean. For the error term, SD typically is used to measure the extent that forecast error differs from the mean. In this study, the SD of errors (SDe) is computed to analyze dispersions of errors across the whole study area.

Bias error is used to measure whether the model under-forecasts or over-forecasts a parameter and is defined in the equation:

$$BE(X) = \frac{1}{N} \sum_{n=1}^{N} (X_f - X_o) \quad (4\text{-}13)$$

where N is the total number of comparisons, X_f is the forecast value, and X_o is the observed value. A positive BE indicates a tendency to overpredict while a negative BE implies under predictions.

The square-root of the individual squared differences between forecast and observation is root mean square error (RMSE). It is defined in equation 4-14.

$$RMSE(X) = \left[\frac{1}{N} \sum_{n=1}^{N} (X_f - X_0)^2 \right]^{1/2} \quad (4\text{-}14)$$

Mean-absolute error is the average of the absolute value of the difference between forecast and observation as defined in equation 4-15. Mean-absolute error values near or equal to 0 indicate perfect or almost perfect forecasts. This measure is not as heavily weighted towards large differences in forecast comparisons as with RMSE.

$$MAE = \frac{1}{N} \sum_{n=1}^{N} \left| X_f - X_o \right| \quad (4\text{-}15)$$

4.5 Results

4.5.1 Correlations between Pine Basal Area and Predictors

Predictors are grouped into four groups: a 432 band combination; a 543 band combination; a three-PCs combination; and an NDVI image. The general Pearson correlation coefficients were calculated and summarized in Table 4.1. Considering the absolute values of these coefficients, for the correlations between pine basal area and different independent variables, PC2 has the highest correlation, the second one is NDVI, the third one is band5, and then, band3, PC1, band2, band4, and PC3.

Since different combinations of predictors were used, the Pearson partial correlation coefficients were calculated and tested in the combinations of bands and PCs in order to better understand the associations between pine basal area and the predictors (Table 4.2). In the 432

band combination, band 3 and band 4 have similar degree correlations but in different directions; one is positive, and another is negative; band 2 is little correlated with the pine basal area, and the coefficient is not significantly different from 0. In the 543 band combination, band 4 and band 5 have similar correlations with pine basal area. However, band 4 is positively correlated, and band 5 is negatively correlated. Band 3 is little correlated with pine basal area. PC2 is highly correlated with pine basal area. The coefficient of PC1 is much smaller. The correlation between PC3 and pine basal area might be little, since its P value is around the boundary of 0.05 and therefore statistically means the partial correlation coefficient is close to 0.

Table 4.1. Correlation Matrix For The Variables Analyzed.

	PINEBA	Band2	Band3	Band4	Band5	NDVI	PC1	PC2	PC3
PINEBA	1								
Band2	-0.3917	1							
Band3	-0.5417	0.8364	1						
Band4	0.3456	0.1221	-0.0724	1					
Band5	-0.5964	0.8067	0.9312	-0.0488	1				
NDVI	0.6365	-0.6517	-0.8794	0.5202	-0.8187	1			
PC1	-0.5195	0.8623	0.9384	0.1197	0.9766	-0.7417	1		
PC2	-0.6520	0.7129	0.9022	-0.3508	0.9448	-0.9269	0	1	
PC3	-0.0315	-0.1852	-0.1287	-0.7872	-0.3163	-0.2450	0	0	1

The second column indicates the correlations between pine basal area (PINEBA) and predictors of four Landsat ETM+ bands, three PCs, and NDVI. The values from column 3 to column 10 indicate some independent variables also are highly correlated, and Pearson partial correlation need conducting to understand the real contributions of independent variables to the estimations of PINEBA.

Table 4.2. Partial Correlations Analysis.

	234 band combination			345 band combination		
	Band2	Band3	Band4	Band3	Band4	Band5
r_{xy}	0.0129	-0.3350	0.3436	0.0828	0.3997	-0.3429
P value	0.4976	<.0001	<.0001	<.0001	<.0001	<.0001

Pearson partial correlation coefficients (*r*) were calculated by eliminating effects due to the correlations between pine basal area and the other two variables in the band combinations. For example, the correlation between pine basal area and band2 is 0.0129 when the contributions from band3 and band4 were removed. This correlation is not significantly different from 0, since the *P* value is 0.4976 which is much bigger than 0.05.

4.5.2 Variograms and Spatial Dependence

Variograms were used to spatially analyze the surface properties of pine basal area. Based on the variogram cloud, the empirical semivariogram model was created. The different types of semivariogram models used to fit the points include exponential, Gaussian, circular, spherical, tetraspherical, pentaspherical, Hole effect, K-Bessel, and J-Bessel models. The spherical model had the best fits and was selected as the theoretical model applied for spatial predictions. The fit of the spherical model has a nugget of 5, a partial sill of 450, and a range of 750. Also, there was no obvious trend existing among the pine basal area across the study area.

The characteristics of the semivariogram also may be affected by the directions, which result from a special geographic phenomenon. For example, a certain kind of species exists and crosses the area in a certain direction. It is therefore necessary to check anisotropy. Semivariogram analyses at directions 0, 45, 90, 135, 180, 225, 270, and 315 were conducted and indicated similar spatial dependence at these eight directions (Figure 4.4). It is not necessary to analyze anisotropic effects in spatial predictions.

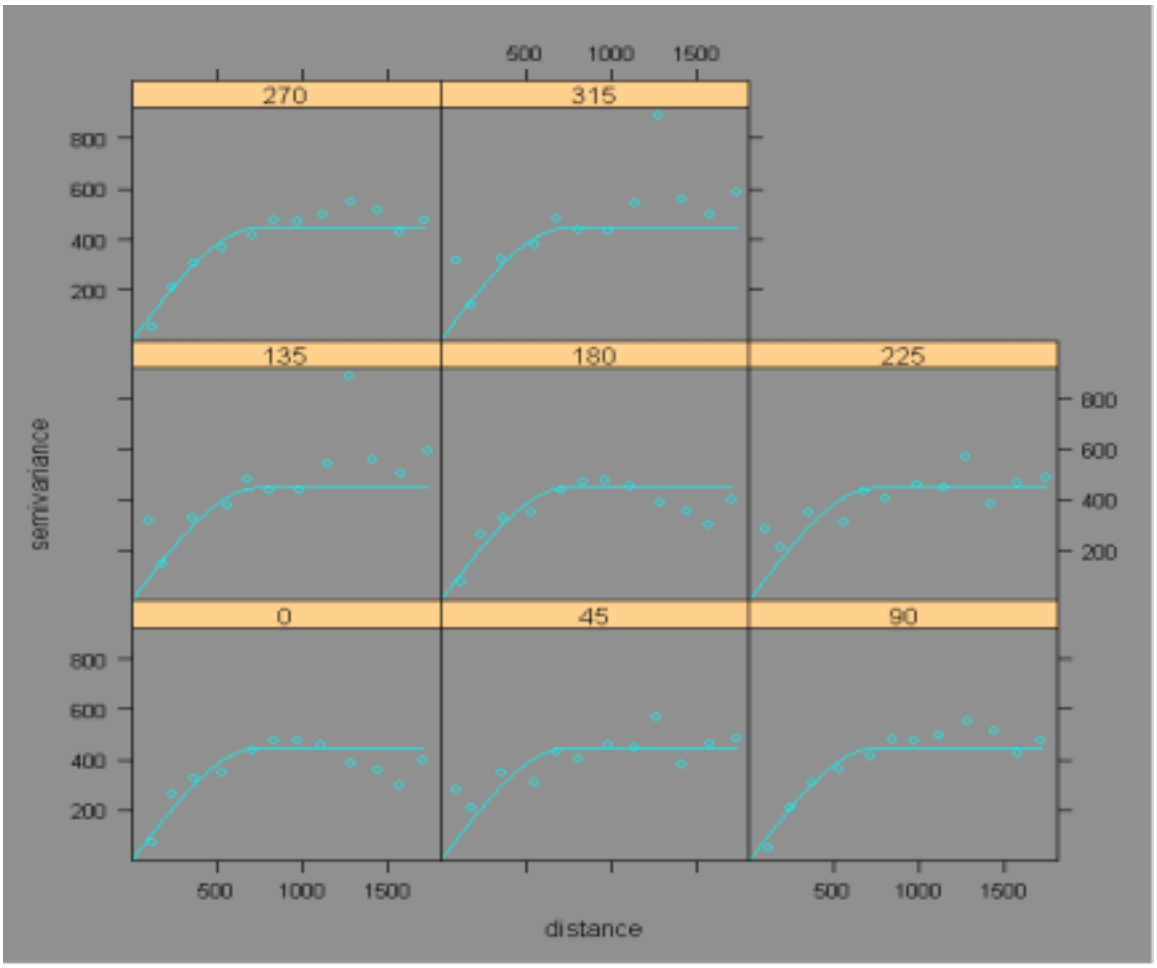

Figure 4.4 Semivariogram Modeling Effects of Eight Different Directions

4.5.3 Assessment of Pine Basal Area Estimation

We first applied Univariate kriging (i.e., OK and UK) to estimate the pine basal area using 2822 ground inventory points. The UK was used to check whether it is effective compared to the OK, though there was no obvious trend of pine basal area existing across the study area. Four types of co-kriging were applied using the 432 band combination, the 543 band combination, NDVI, and PCs as the auxiliary data. At last, four groups of regression kriging were conducted using the 432 band combination, the 543 band combination, NDVI, and PCs as predictors.

The results were evaluated using cross validation (Table 4.3). Bias errors using the kriging methods indicated the values of BE were close to 0, and almost unbiased estimations of pine basal area were obtained. For RMSE, there was not much difference between OK, UK, and the four kinds of co-kriging. However, the RMSEs of the estimations using regression kriging were much smaller than those from OK, UK, and co-kriging. In order to further assess these geostatistical approaches, 200 random sample points outside of the training dataset were selected and used to compare these kriging methods (Table 4.4). The regression kriging methods had the smallest BE, MAE, RMSE, and SDe, which indicated that regression kriging was more efficient than other kriging methods. Pine basal area predictions based on RK resulted in the prediction BE of 27.9~31.5% of the mean (13.99 m^2/ha), the prediction MAE of 39.3~42.1% of the mean, the prediction RMSE of 63.5~68.6% of the mean, and the prediction SDe of 59.3~62.1% of the mean using the 200 random points outside the training datasets.

Table 4. 3. Model Evaluation Using Cross Validation.

	OK	UK	CoK432	CoK543	CoKndvi	CoKPCs	RK432	RK543	RKndvi	RKPCs
BE	-0.076	-0.078	-0.099	-0.100	-0.095	-0.095	-0.078	-0.067	-0.066	-0.070
RMSE	11.310	11.290	10.970	11.000	11.010	11.020	7.020	7.000	7.220	6.890

Ordinary kriging (OK), universal kriging (UK), Co-kriging (Cok), and regression kriging (RK) are used to predict basal area. CoK432 means using the 432 band combination as predictors to krig the basal area, likewise CoK543, CoKndvi, CoKPCs, RK432, RK543, RKndvi, and RKPCs; bias error (BE) and root mean square error (RMSE) are used to measure the discrepancy between observations and predictions.

Table 4.4 Model And Forecast Evaluation Using Validation Based On Random Samples.

	OK	UK	CoK432	CoK543	CoKndvi	CoKPCs	RK432	RK543	RKndvi	RKPCs
BE	10.120	10.130	4.990	4.980	4.760	4.660	4.460	4.010	4.432	3.964
RMSE	13.320	13.390	10.550	10.320	10.560	10.010	9.655	8.980	9.601	9.161
SDe	8.660	8.770	9.300	9.260	9.310	9.210	8.583	8.601	8.700	8.280
MAE	10.330	10.470	6.310	6.290	6.310	6.280	5.929	5.502	5.900	5.727

Stand deviation of errors (SDe), mean-absolute errors (MAE), BE, and RMSE are used to measure the discrepancy between observations and predictions. Other notations are the same as Table 4.3.

4.6 Pine Basal Area Mapping Using Regression Kriging

Regression kriging was the best approach to predict pine basal area using Landsat ETM+ images. The results of regression kriging were transformed and used to map the pine basal area at these 20 counties using ERDAS Imagine® and ArcGIS9.1. The pine basal areas were mapped based on the four types of regression kriging using the 432 band combination, the 543 band combination, NDVI, and PCs as predictors (Figure 4.5). The standard deviations of errors were also mapped in order to indicate the spatial characteristics of errors of pine basal area estimations (Figure 4.6). Using the 432 band combination, we obtained relatively smaller standard errors of predicted pine basal area across the whole study area than those from the 543 band combination, three PCs and NDVI.

4.7 Discussions

Challenges still exist in the field of large area forest inventory using remotely sensed data (Tokola et al. 1996, Trotter et al. 1997, Holmström & Fransson 2003). Spatial diversity of forest stands and landscape makes the spatial prediction of forest parameters a major challenge,

although the remote sensing data are highly associated with forest features. For example, forest stands may have very similar values of biomass/carbon but have different spectral characteristics because of differences in species. The differences of spectral characteristics between plantations and natural stands might exist although the stands have many of the same characteristics, such as same species, same age, and same density. These differences will add noise when the prediction models are fitted based on the associations between remotely sensed data and ground-inventoried data.

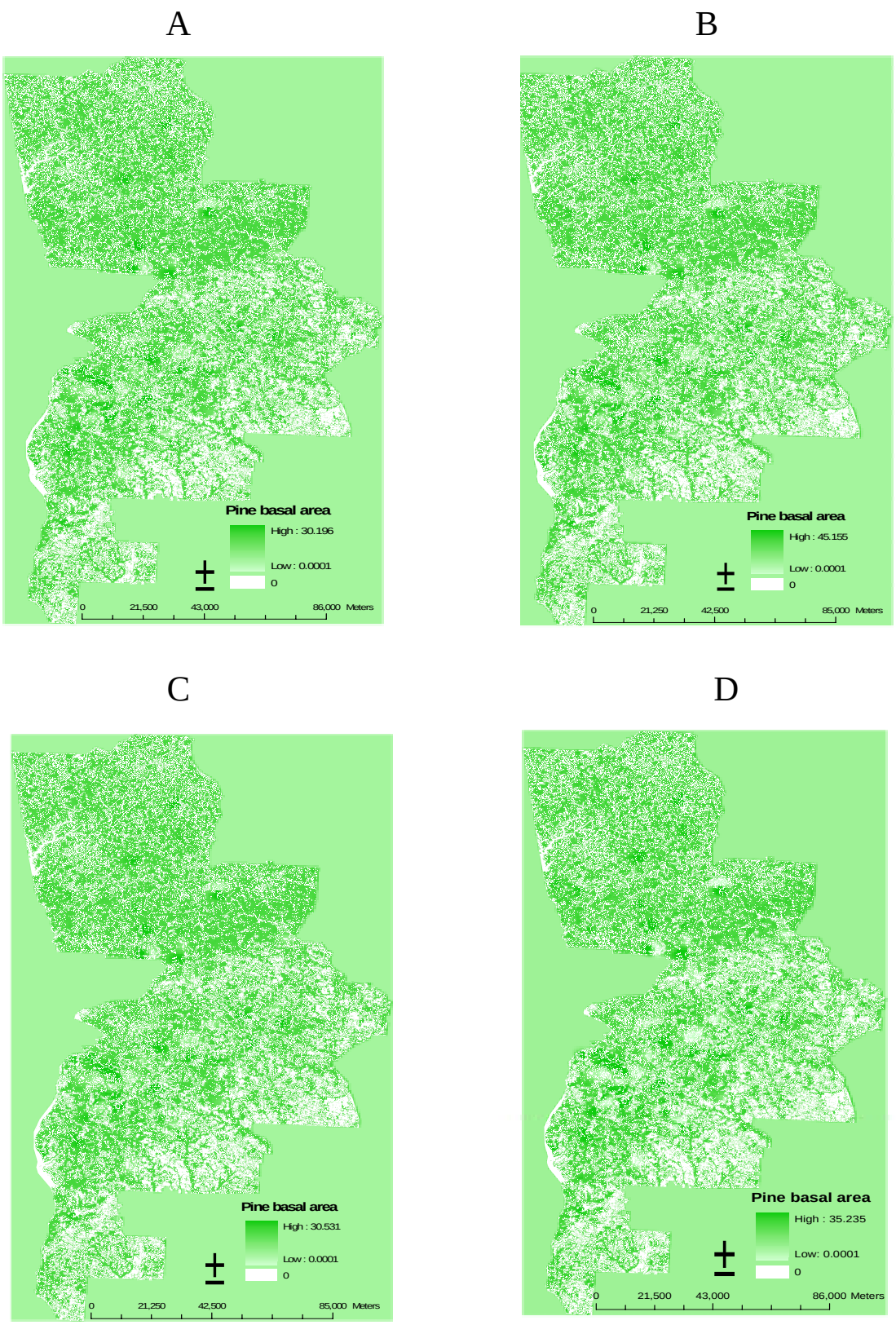

Figure 4.5. Pine Basal Area Estimations Using Regression Kriging.
A, using bands 2, 3, and 4 as predictors; B, using bands 3, 4, and 5 as predictors; C, using NDVI as predictors; D, using three PCs as predictors.

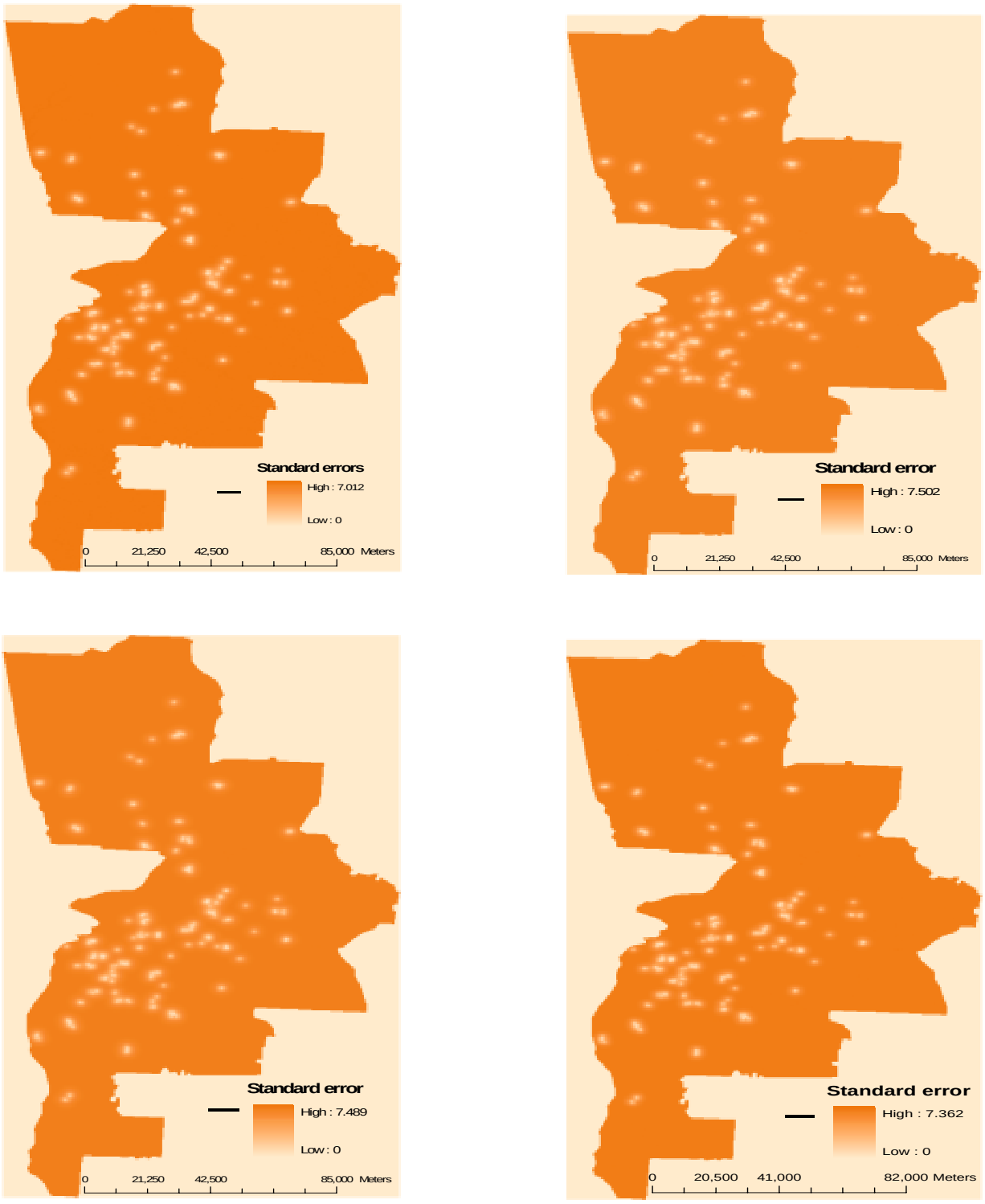

Figure 4.6. Mapping Standard Errors of Spatial Predictions from Regression Kriging.
A, standard errors from regression kriging using bands 2, 3, 4 as predictors; B, standard errors from regression kriging using bands 3, 4, 5 as predictors; C, standard errors from regression kriging using the band of NDVI; D, standard errors from regression kriging using PCs.

Berterretche et al. (2005), Tuominen et al.(2003), and Zhang et al (2004) applied geostatistical models to estimate forest variables, leaf area index, and classify forest lands based on remote sensing data. Compared to their studies, multivariable kriging (i.e., RK in this study) is robust and results in relative smaller errors. Multivariable kriging can be applied for almost all kinds of forest parameters. Also, either numerical or categorical data can be used in the process of kriging, i.e., any kind of variable can be used as auxiliary data or predictors.

Remote sensing data and ground inventory data are collected and stored in different data structures. The discrepancy between remotely sensed data and ground sampling data might be the source of big errors in forest predictions (Tokola et al. 1996, Gilbert & Lowell 1997). The ground inventory data are usually collected at the forest plot level or forest stand level. The plot size may be from several meters to 10 or 20 meters. The stand size may be from 10 meters to dozens of meters, and the stands are assumed to be homogenous. Therefore, some ground data may be finer than remote sensing data in spatial resolution, but generally, remote sensing data has a finer spatial resolution than ground inventory data. This may result in some noise added to the geostatistical modeling and cause bias errors and mean-absolute errors.

4.7 Conclusions

The systematic approach of geostatistical prediction and mapping developed by integrating remote sensing, ground inventory, and GPS data provides a new way to spatially estimate forest parameters using remotely sensed data. It has many applications in forest or natural resource management. Forest metrics, such as stand density, dominant height, species,

stand age, forest health conditions, the probability of forest fire, biomass, carbon, and so on, can be incorporated in the model. They can be estimated spatially at finer spatial resolution using remotely sensed data with higher spatial resolution.

Providing finer spatial information is essential for large area timber, biomass, and carbon budget management and planning. Kriging is an optimum method for spatial interpolation. Regression kriging is the most powerful one among the different kriging methods in this research. It was used to predict the pine basal area at 30m for these 20 counties (about 35000 km^2) using only 2822 ground inventory data points. Four groups of independent variables are used in RK. The 543 band combination resulted in the smallest BE, RMSE, MAE, and had a relatively smaller SDe. Therefore, Compared with OK, UK and CoK using different auxiliary data, RK resulted in the smallest BE, RMSE, SDe, and MAE. Regression kriging using the NDVI as the predictor could be the best method for pine basal area predictions if computation is considered for large area basal area inventory, since it has only one independent variable and can significantly reduce computation time as compared with other band combinations. For other forest parameters, such as dominant height, timber volume, or biomass/carbon, other band combinations, such as PCs or NDVI need to be applied again to check which will result in better estimations.

More research is needed to demonstrate whether the geostatistical approach is more or less efficient than other methods used for large area forest inventory, such as K nearest neighbor methods using remotely sensed data. This will further demonstrate the efficiency and usefulness of this geostatistical approach for forest inventory and management.

CHAPTER 5

FINE SPATIAL RESOLUTION FOREST INVENTORY FOR GEORGIA USING WEIGHTED K NEAREST NEIGHBOR METHOD

5.1 Introduction

The nearest neighbor methods represent one of the simplest and most intuitive techniques in the field of statistical prediction and the field of data mining. The K nearest neighbor method is an extension of the nearest neighbor method. In the field of statistics the K nearest neighbor method is a well known, easy, and successful method for discrimination or prediction. In the field of computer science, the K nearest neighbor method is a powerful instance-based machine-learning algorithm, and it is a typical method for data mining. In Chapter 3 I explored the two major disadvantages of the K nearest neighbor method, which are the selection of K and computation cost.

There are two specific techniques that are especially important in the process of implementing the K nearest neighbor method. The first is distance metrics, and the second is weight schemes of the K nearest neighbors. In applications of the K nearest neighbor method for forest inventory, Euclidian distance often is used as the optimal metric without comparing it with other distance measurements. The average of the values of the K nearest neighbors is then used as the optimal estimation for the predicted locations. I will therefore explore distance metrics and weight schemes in detail.

When the weight scheme is added to KNN, the statistic or machine-learning algorithm is called the weighted K nearest neighbor (WKNN) (Hechenbichler and Schliep 2004). In a general sense, WKNN and the basic nearest neighbor algorithm can be seen as voting or ensemble

methods. In other words, some potential classifiers or regressors (say, the nearest neighbors) are aggregated by a (say, weighted) majority vote and this aggregated result is used as a prediction. In using WKNN, the closest observation and the K most similar (say, K nearest neighbors) cases within the learning set are used for either or both prediction and classification. Also I determine the combined influence I get from the K nearest neighbors and use it for prediction or classification. Therefore, the distance metrics and weight schemes are important techniques and determine the contribution or influence from the nearest neighbors once the value of K has been determined.

5.2 Distance Metrics

Distance is an important criterion to determine the nearest neighbors (say, most similar objects) in a multidimensional space. Several kinds of distance metrics could be used to determine this type of similarity. The smaller the distances are between objects, the more similar the objects are. Two objects are identical to each other if the distance between them is 0. The distance from object to object measured in multidimensional space is a kind of point-to-point distance. Three kinds of distance metrics are often used in the measurement of the nearest neighbor. These are Euclidian distance (Minkowski distance with an order of 2), Manhattan distance (Minkowski distance with an order of 1), and Minkowski distance with order of 3, These are expressed by equations (5-1), (5-2), and (5-3) respectively.

These distance measures can be summarized in one type of measure as in equation (5-4). If the order is 1, equation (5-4) is Manhattan distance. If the order is 2, equation (5-4) is Euclidian distance. If the order is 3, it is simply Minkowski distance with an order of 3. The Manhattan distance (equation 5-2) computes the distance that would be traveled to get from one

point to the other if a grid-like path is followed. The Manhattan distance between two items is the sum of the differences of their corresponding components. Computationally speaking, Manhattan distance is a cheaper distance measure.

$$D = \sqrt{\sum_{b=1}^{n} (i_b - j_b)^2} \tag{5-1}$$

$$D = \sum_{b=1}^{n} |i_b - j_b| \tag{5-2}$$

$$D = \sqrt[\lambda]{\sum_{b=1}^{n} (i_b - j_b)^{\lambda}} \qquad \lambda = 3 \tag{5-3}$$

$$D = \sqrt[\lambda]{\sum_{b=1}^{n} (i_b - j_b)^{\lambda}} \tag{5-4}$$

5.3 Weight Schemes

The weight schemes are designed for transforming each distance measure into a weight according to any arbitrary kernel function (say, $K(.)$). These are functions $K(.)$ of the distance d with maximum value when $d = 0$. The value decreases as the absolute value of d increases. Therefore, the weight schemes should have the following properties:

1) $K(d) \geq 0$ for all $d \in \Re$
2) $K(d)$ is maximized when $d = 0$
3) $K(d)$ declines monotonously when $d \to \pm\infty$

Since domains of K functions are defined as positive, only the positive ones have to be applied. Some typical examples of the kernel functions are listed as follows:

1) Rectangular kernel (1/2)* I($|d| \leq 1$)
2) Triangular kernel (1 - $|d|$) * I($|d| \leq 1$)

3) Epanechnikov kernel $(3/4)*(1 - d^2) * I(|d| \leq 1)$

4) Quartic or biweight kernel $(15/16)*(1 - d^2)^2 * I(|d| \leq 1)$

5) Triweight kernel $(35/32)*(f - d^2)^3 * I(|d| \leq 1)$

6) Cosine kernel $(\pi/4)*\cos(\pi d/2) *I(|d| \leq 1)$

I have already explored throughout this paper the three parameters of the weighted K nearest neighbor. These are the values of K, the distance metric, and the weight schemes in WKNN. Using Landsat TM imagery as predictors, I applied the WKNN to predict volume of trees in the State of Georgia with a 25-meter cell size.

5.4 Results

After classifying the Landsat TM imagery into hardwoods, softwoods and non-forest area, I used the TM bands in the hardwood and softwood areas as predictors for estimation. I applied the above weighted K nearest neighbor method to spatially forecast the hardwood and softwood volumes. The objective was to obtain the unbiased estimations of volume of hardwoods and softwoods based on a 25-meter cell size for the State of Georgia.

For this study I assumed the mean estimation of the volume of hardwoods/softwoods for the entire state of Georgia by the US Forest Inventory and Analysis (FIA) was an unbiased estimation. In order to get the unbiased estimation at a 25-meter cell size, I needed to use the FIA mean estimation to adjust my estimations at the cell-size level for the whole state. The comparisons of the FIA hardwood and softwood estimations with those using WKNN are summarized in Table 5.1. The mean estimation of volume of softwoods using the weighted K nearest neighbor is very close to the FIA mean, while the mean estimation of volume of

hardwoods is higher than that by FIA. I then applied the ratios of the mean FIA estimation to the mean WKNN estimation to all estimations at the cell size level for Georgia, and then obtained the unbiased estimations. In other words, assuming the mean estimation by FIA was an unbiased estimation, I obtained estimations for hardwood and softwood at the 25-meter cell size using the weighted K nearest neighbor method. I then used the ratio of the FIA mean to the KNN mean as a balance index to multiply by my estimations at each cell in a raster dataset. Cieszewski et al (2003) proofed this approach to obtaining unbiased estimations.

Table 5.1. Simple Comparisons of Volume with the Inventory by FIA

	FIA		Estimation		Ratio of
	Mean	Total	Mean	Total	Mean
Softwoods	140.4	503877695	147.4	692269753	0.95
Hardwoods	112.1	536589533	141.9	646415865	0.79

FIA, US Forest Inventory and Analysis Program;
Mean is cubic meters per hectare, and Total is cubic meters.

I summarize this fine spatial resolution forest inventory (i.e., the 25-meter cell) to the county level in Table 5.2. Figures 5.1 and 5.2 display the total volume of hardwoods and

softwoods at the county level. These figures generally display the total production of hardwoods and softwoods. I also display the volume per hectare (i.e., total volume over the area of forest lands) at the county level, which indicates the production potentials of hardwoods and softwoods for the 159 counties in Georgia (Figures 5.3 and 5.4). The volume of hardwoods and softwoods for each county and the relative difference between my estimation and the FIA summarization also are listed in Table 5.2.

Volume per hectare mapping indicates economic value (i.e., the timber productivity) as well as value to the ecosystem in the form of biomass and carbon production, which play important roles in land use dynamics and land resource management. The 30 counties having high hardwood volume per hectare are aggregated in northern Georgia. Another sub-region, with 4 counties located along the Florida boundary, also has high values of hardwood volume per hectare. Twenty counties of lower values of hardwood volume per hectare lay like a belt across central Georgia. There are several other lower values of hardwood volume per hectare counties in southern Georgia (Figure 5.3).

For spatial distribution of softwood volume per hectare is different in Georgia (Figure 5.4) from that of hardwood. A region of about 20 counties with high values of softwood volume per hectare exists in south central Georgia. A region of about 20 counties of lower values of softwood volume per hectare is located in central Georgia. The counties located in northern Georgia have relatively high values of softwood volume per hectare.

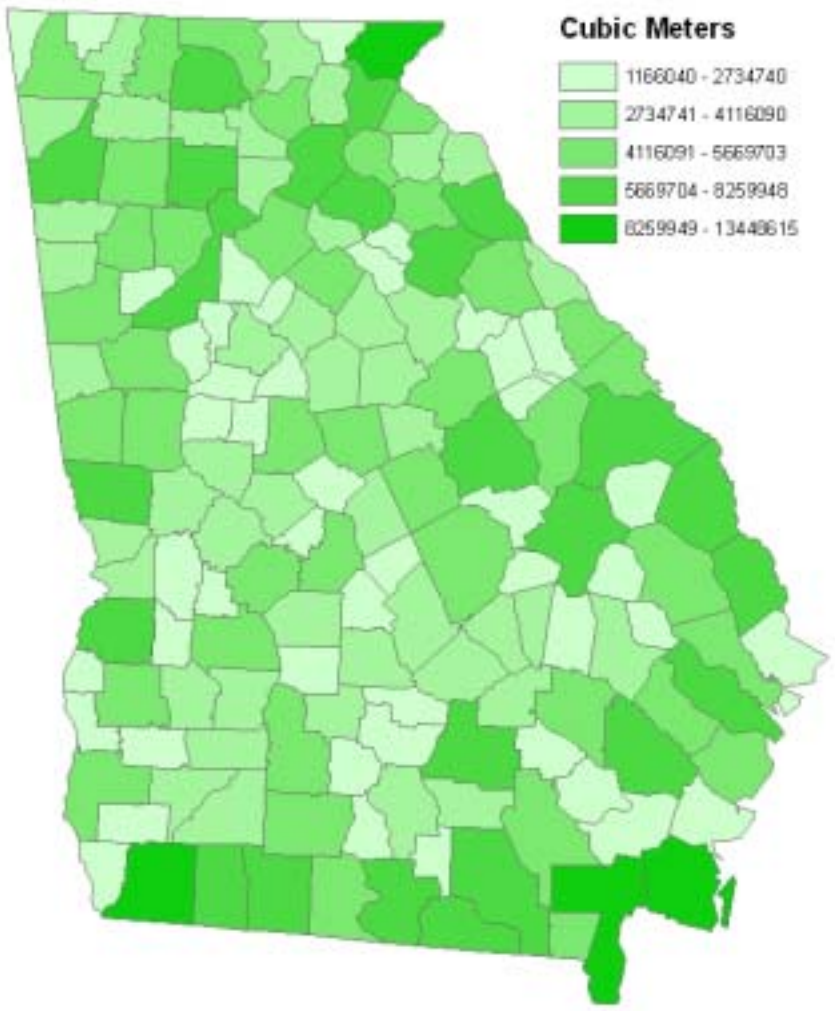

Figure 5.1. Total Hardwood Volume by County, Georgia.

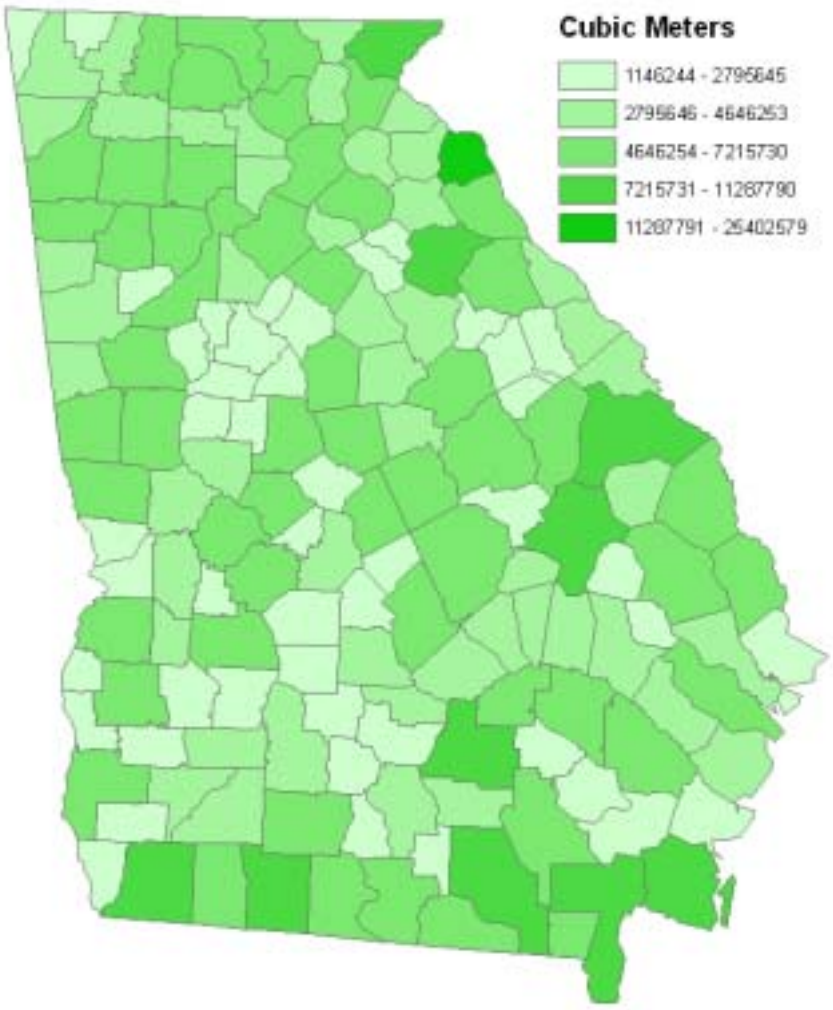

Figure 5.2. Total Softwood Volume by County, Georgia.

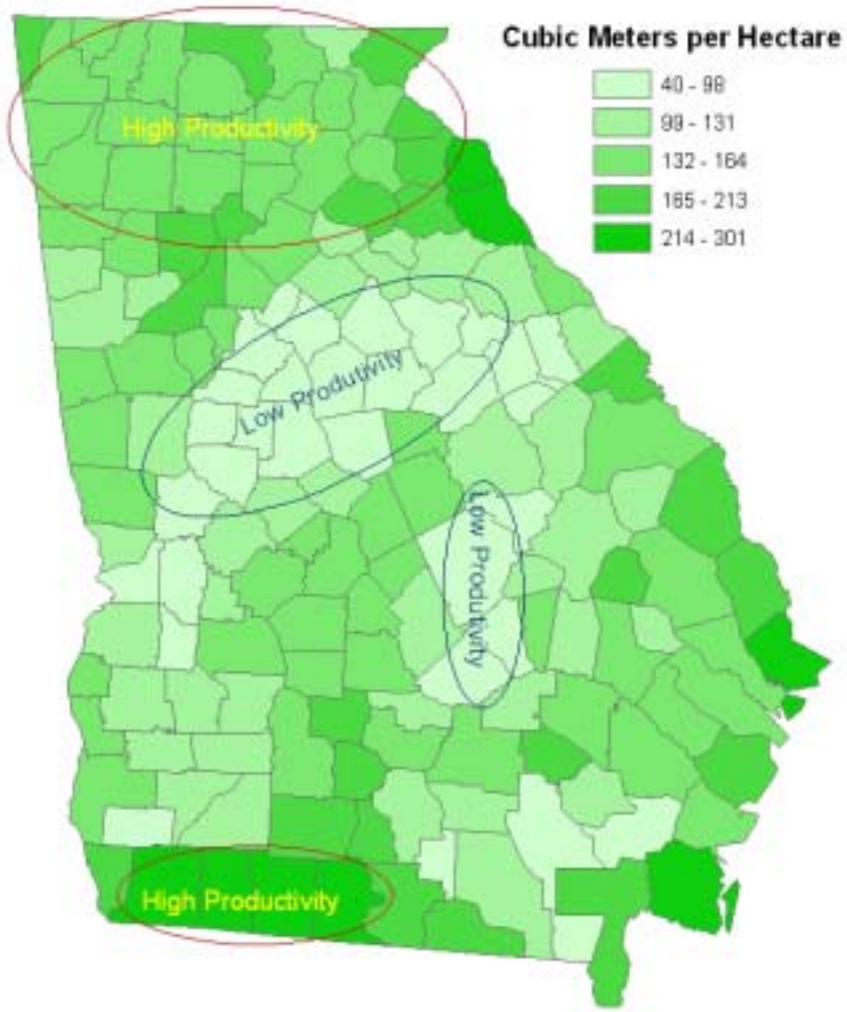

Figure 5.3. Hardwood Volume per Hectare by County, Georgia.

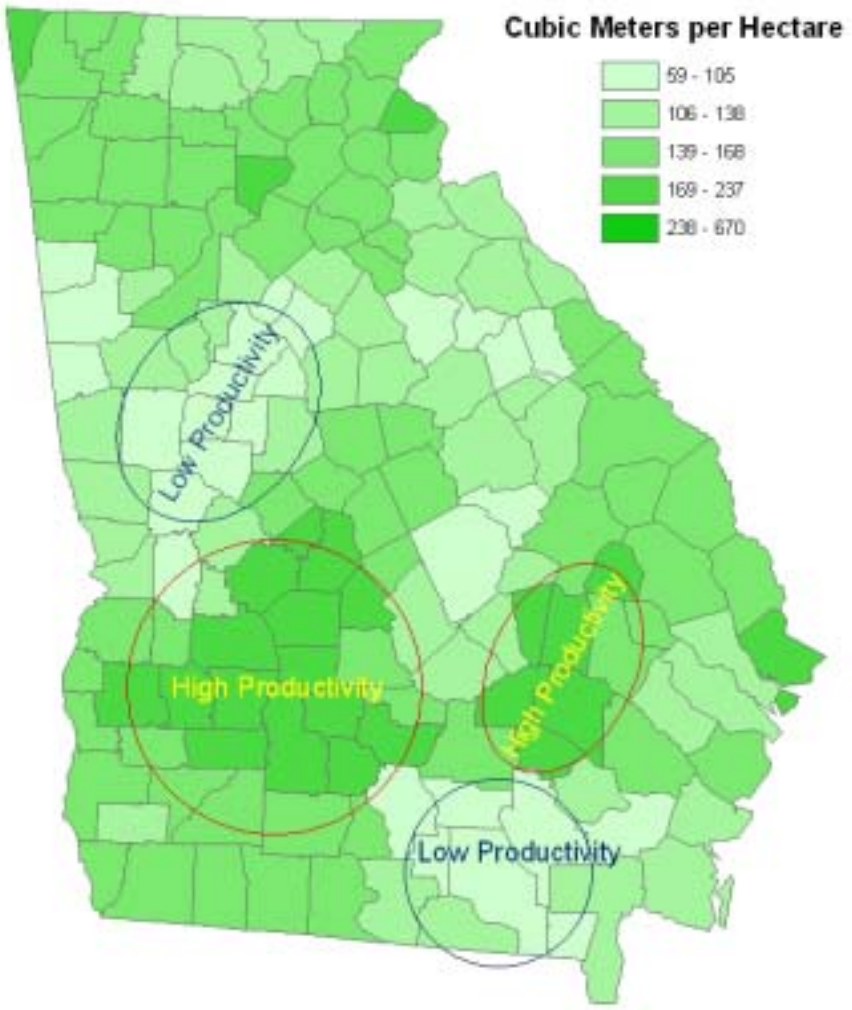

Figure 5.4. Softwood Volume per Hectare by County, Georgia.

Table 5.2. Estimated Volume by Hardwoods, Softwoods, County, Georgia (Cubic Meters).

	Estimation		FIA		Different Ratio	
NAME	Softwoods	Hardwoods	Softwoods	Hardwoods	Softwoods	Hardwoods
Appling	5083417	4403658	6016532	3662752	0.18	0.17
Atkinson	3049399	3225220	3399343	1105478	0.11	0.66
Bacon	2371567	2734740	3101425	1331242	0.31	0.51
Baker	3664154	3435917	1631234	3421286	0.55	0.00
Baldwin	3334114	4040996	2282606	2325894	0.32	0.42
Banks	4214981	5361755	1316282	4093769	0.69	0.24
Barrow	3325637	2874034	1135648	1750386	0.66	0.39
Bartow	7178345	5588570	3100807	2940419	0.57	0.47
Ben Hill	2846236	2061727	2267286	1556610	0.20	0.24
Berrien	3593434	2959091	5301857	1196606	0.48	0.60
Bibb	2206787	2551107	943101	2601769	0.57	0.02
Bleckley	2054820	1974947	1601092	2949974	0.22	0.49
Brantley	2148367	1422828	5331578	2345198	1.48	0.65
Brooks	5004572	4601797	4470639	2666426	0.11	0.42
Bryan	4336247	5130674	6102257	4277365	0.41	0.17
Bulloch	5603165	5373387	5143303	5558034	0.08	0.03
Burke	8049920	8259948	7419552	8626070	0.08	0.04
Butts	2035593	1535292	1666883	1790529	0.18	0.17
Calhoun	2121768	2594260	1592985	1341775	0.25	0.48
Camden	7974059	10518535	7104717	6044734	0.11	0.43
Candler	2502960	2323087	1187487	1651763	0.53	0.29
Carroll	4400194	5033222	4086508	4974538	0.07	0.01
Catoosa	1541004	2214359	477972	1596386	0.69	0.28
Charlton	9521053	10034505	4643752	2175374	0.51	0.78
Chatham	1687121	2139339	3163140	2926558	0.87	0.37
Chattahoochee	2150312	3003126	2348432	2899968	0.09	0.03
Chattooga	3190863	3482028	1764515	3788176	0.45	0.09
Cherokee	6161890	6798385	3656125	7888668	0.41	0.16
Clarke	2511216	1990722	692211	857316	0.72	0.57
Clay	2755780	2452430	887965	2231877	0.68	0.09
Clayton	1146244	1166040	457391	790013	0.60	0.32
Clinch	11287790	8163144	10849490	3538427	0.04	0.57
Cobb	6291280	4440499	2497006	2334694	0.60	0.47
Coffee	7466600	7576623	6346912	2259286	0.15	0.70
Colquitt	4881335	4714019	5058710	2560838	0.04	0.46
Columbia	4437711	4579707	5682009	3036049	0.28	0.34
Cook	1524902	1474893	1211353	2210139	0.21	0.50
Coweta	4923558	5110905	4563210	4941464	0.07	0.03
Crawford	6126272	3646142	3042784	1758292	0.50	0.52

Table 5.2. Continued

NAME	Estimations		FIA		Different Ratio	
	Softwoods	Hardwoods	Softwoods	Hardwoods	Softwoods	Hardwoods
Dawson	3176520	3790215	2163165	4303894	0.32	0.14
Decatur	10525557	13448615	4908589	3572737	0.53	0.73
De Kalb	3306986	2544900	1156613	1337589	0.65	0.47
Dodge	4884068	4116090	6010453	3461016	0.23	0.16
Dooly	2758580	2995838	3055076	1518602	0.11	0.49
Dougherty	2882220	3772678	2286919	3639257	0.21	0.04
Douglas	1743921	2691935	1375040	4426952	0.21	0.64
Early	4737868	5081096	3306104	2383210	0.30	0.53
Echols	6674322	7196916	5583604	1241454	0.16	0.83
Effingham	5304618	6013583	4637785	4959846	0.13	0.18
Elbert	5677923	6138844	2041057	5233068	0.64	0.15
Emanuel	9173208	6238050	8505657	5306592	0.07	0.15
Evans	1627066	1429179	1472059	3030769	0.10	1.12
Fannin	6695893	4501463	2244992	8035994	0.66	0.79
Fayette	1917730	2100691	1541297	2463735	0.20	0.17
Floyd	7215730	6093188	3155856	4706663	0.56	0.23
Forsyth	2892924	3114473	778726	2485169	0.73	0.20
Franklin	3145135	3917079	427355	2915058	0.86	0.26
Fulton	6944691	6434531	3568389	5917771	0.49	0.08
Gilmer	6929291	6184364	5036919	10211574	0.27	0.65
Glascock	1743257	1425591	1559847	1140395	0.11	0.20
Glynn	2451272	2585326	5339236	1920721	1.18	0.26
Godon	3943891	4022595	1837250	2074137	0.53	0.48
Grady	5422486	6465888	2821790	3608326	0.48	0.44
Greene	4012067	3136057	4352248	4193302	0.08	0.34
Gwinnett	6586172	5421955	1563920	4049900	0.76	0.25
Habersham	5631737	5904218	2258411	7823126	0.60	0.33
Hall	6264888	6597817	2206621	4923296	0.65	0.25
Hancock	6407442	5069010	6435916	3790617	0.00	0.25
Haralson	2927403	3085838	2287901	3686113	0.22	0.19
Harris	6659758	6388821	5706178	4405585	0.14	0.31
Hart	2540257	3279633	632702	2469062	0.98	0.25
Heard	3813981	3951499	3398909	1827381	0.11	0.54
Henry	2349514	2895956	2316695	3464087	0.01	0.20
Houston	3557289	4520500	2307741	4381654	0.35	0.03
Irwin	2658690	2570103	2897872	2102029	0.09	0.18
Jackson	6128703	6704442	1442026	4311739	0.76	0.36
Jasper	5306064	3783993	5328897	4440335	0.00	0.17
Jeff Davis	5498660	3874926	3631097	1373964	0.34	0.65

Table 5.2. Continued

	Estimations		FIA		Different Ratio	
NAME	Softwoods	Hardwoods	Softwoods	Hardwoods	Softwoods	Hardwoods
Johnson	2795645	2276601	3570696	1657181	0.28	0.27
Jones	5675634	4352180	4789485	3534908	0.16	0.19
Lamar	1525178	1879005	1130597	1336468	0.26	0.29
Lanier	1591448	2109824	2334720	1877109	0.47	0.11
Laurens	7030069	5212435	6927622	5489747	0.01	0.05
Lee	2718313	3133144	1551371	3219087	0.43	0.03
Liberty	5148181	5922343	9177459	3848603	0.78	0.35
Lincoln	4646253	3733679	3235647	1848440	0.30	0.50
Long	4391712	4264416	6252860	6067001	0.42	0.42
Lowndes	5015587	5846477	4879266	2478158	0.03	0.58
Lumpkin	4857084	4265875	3027844	7459994	0.38	0.75
McDuffie	2618834	1917750	4385871	2337935	0.67	0.22
McIntosh	4059266	4449580	3561245	2135816	0.12	0.52
Macon	6088824	5235112	2442943	5782362	0.60	0.10
Madison	2980148	4230881	2634234	2256213	0.12	0.47
Marion	4031144	2669190	2142901	2225659	0.47	0.17
Meriwether	6084904	4949269	5654964	3944686	0.07	0.20
Miller	1382958	1264343	747950	1846812	0.46	0.46
Mitchell	3797967	3933746	2341485	1143487	0.38	0.71
Moroe	6776475	4639425	4300141	4070624	0.37	0.12
Montgomery	4209117	3526026	1888718	1778075	0.55	0.50
Morgan	2936578	3302430	2863361	4584931	0.02	0.39
Murray	5007477	4348840	3057029	4828426	0.39	0.11
Muscogee	2536349	2768119	1963366	1328534	0.23	0.52
Newton	2717865	3011136	2467586	3706571	0.09	0.23
Oconee	2463059	2522156	747299	2088280	0.70	0.17
Oglethorpe	7647027	6226983	3973524	7849413	0.48	0.26
Paulding	5802460	4915221	2079173	5219372	0.64	0.06
Peach	1332297	1370527	339051	520321	0.75	0.62
Pickens	3056552	3720132	1282013	4704248	0.58	0.26
Pierce	2239241	2294305	3558719	2704637	0.59	0.18
Pike	1746569	1648801	1230953	2894702	0.30	0.76
Polk	5803229	4040875	1852563	2968542	0.68	0.27
Pulaski	1699980	2158833	1519467	1401673	0.11	0.35
Putnam	4191632	2764186	4667982	1711259	0.11	0.38
Quitman	2786740	2229393	1412974	2290330	0.49	0.03
Rabun	9328378	12017244	4665912	10918604	0.50	0.09
Randolph	4990766	5623791	2550515	3537369	0.49	0.37
Richmond	3445657	4749719	2258433	2278556	0.34	0.52
Rockdale	1366177	1435223	1013357	1174459	0.26	0.18
Schley	2417654	1888281	1355834	1264264	0.44	0.33

Table 5.2. Continued

	Estimations		FIA		Different Ratio	
NAME	Softwoods	Hardwoods	Softwoods	Hardwoods	Softwoods	Hardwoods
Spalding	1648597	1764084	1014370	2083413	0.38	0.18
Stephens	3766400	4448398	1255117	2146529	0.67	0.52
Stewart	6220946	5806041	2805287	3723743	0.55	0.36
Sumter	5493438	4942247	3086635	2112093	0.44	0.57
Talbot	4200675	3190313	4307520	2939658	0.03	0.08
Taliaferro	1678061	1581084	2669247	1544499	0.59	0.02
Tattnall	3723638	3385125	3953411	2562107	0.06	0.24
Taylor	5185842	3834356	3151183	1897990	0.39	0.51
Telfair	4342908	4101921	2864386	4261613	0.34	0.04
Terrell	2530604	3494067	1670114	2356031	0.34	0.33
Thomas	7770509	7191097	5789963	3429186	0.25	0.52
Tift	1611158	2185616	1740553	1780206	0.08	0.19
Toombs	3200175	2404310	2381491	2104974	0.26	0.12
Towns	2851844	2510203	1526826	3788948	0.46	0.51
Treutlen	3164420	2349841	2916967	1159417	0.08	0.51
Troup	5416568	5652611	4156782	5515206	0.23	0.02
Turner	2244338	2892550	2140879	221649	0.05	0.92
Twiggs	4831200	3449732	3112624	5117781	0.36	0.48
Union	5314470	3571436	1290692	7045709	0.76	0.97
Upson	3634197	3097581	2755050	4364648	0.24	0.41
Walker	3100454	4575248	2261089	7431837	0.27	0.62
Walton	5168850	4394978	1841353	4244044	0.64	0.03
Ware	5910980	5439308	7526986	1532503	0.27	0.72
Warren	2732406	1792120	4525620	2685283	0.66	0.50
Washington	6005720	5919557	5873825	6717704	0.02	0.13
Wayne	6468992	6204952	6329761	3188298	0.02	0.49
Webster	2932349	1660861	1526642	723560	0.48	0.56
Wheeler	4041251	2970380	3001535	4550765	0.26	0.53
White	4291314	3943074	2284622	4805498	0.47	0.22
Whitfield	3178822	3979490	1257591	2980369	0.60	0.25
Wilcox	3790978	3653803	3802680	2978876	0.00	0.18
Wilkes	6908272	5279787	6229458	3996584	0.10	0.24
Wilkinson	4860092	5346287	4089518	6249206	0.16	0.17
Worth	4582856	5162361	6132641	4287324	0.34	0.17

FIA, US Forest Inventory and Anlaysis Program;
Different Ratio is equal to the difference between estimation and FIA value divided by the estimation value.

5.5 Forecast Evaluation

Ten thousand pixels (Figure 5.5) outside the training dataset are randomly selected to evaluate the forecasts using the weighted K nearest neighbor method. The criteria included bias error (BE), rote mean square error (RMSE), and relative RMSE are applied. The results for the regions of path/row of 17/37, 17/38, 17/39, 18/36, 18/37, 18/38, 18/39, 19/37, 19/38, and 19/39 are summarized in Table 5.3 and Table 5.4. The estimations at regions of 17/39, 18/36, 18/37, 18/38, 19/37, 19/38, and 19/39 have small bias errors, while estimations at 17/37, 17/38, and 18/39 have relatively large errors. Generally, the values of relative RMSE are in the range of 40% to 70%.

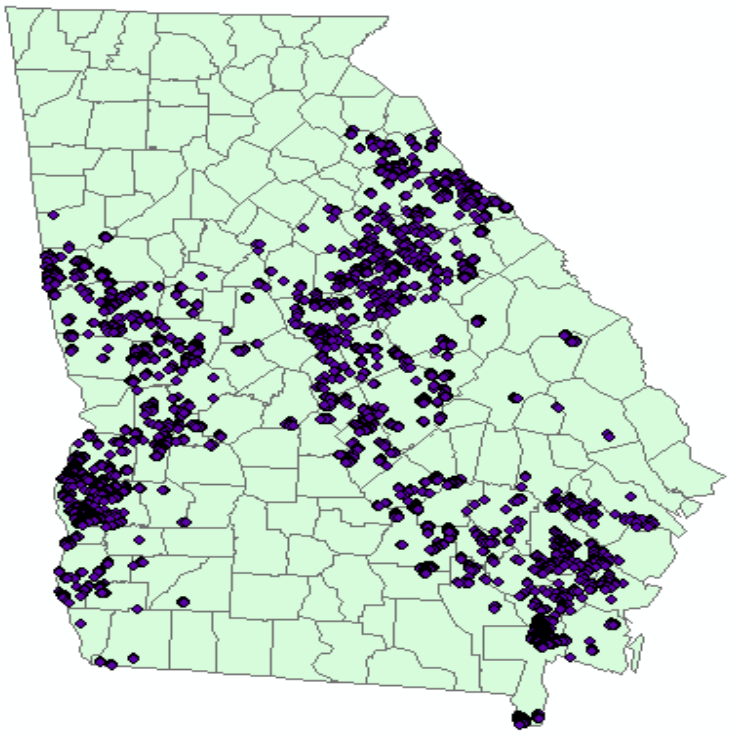

Figure 5.5. Random Sample Points Used for Forecast Evaluation

Table 5.3. Spatial Estimation Evaluation for Hardwoods

	P17R37	P17R38	P17R39	P18R36	P18R37	P18R38	P18R39	P19R37	P19R38/39
BE	24.50	-69.48	2.07	3.06	0.82	0.54	63.43	0.77	-2.67
RMSE	117.55	69.63	83.71	85.19	119.50	100.18	63.60	74.05	64.49
R_RMSE	0.79	0.60	0.75	0.56	0.74	0.58	0.60	0.60	0.51

P17R37 is Path17 Row 37, and so on;
RMSE, root mean square error;
R_RMSE is the relative RMSE, and it is the ratio of RMSE to the mean obtained through ground inventory.

Table 5.4. Spatial Estimation Evaluation for Softwoods

	p17r37	p17r38	p17r39	p18r36	p18r37	p18r38	p18r39	p19r37	p19r38r39
BE	-5.29	-7.73	5.53	3.06	-0.82	-2.79	-61.87	0.10	1.06
RMSE	151.34	64.69	97.49	97.64	143.14	131.06	62.02	119.99	76.00
R_RMSE	0.72	0.47	0.84	0.63	0.78	0.70	0.64	0.73	0.52

Notes are the same as those in Table 5.3.

The results I obtained in this research are compatible with other studies. I obtained values of R_RMSE ranges from 0.51 to 0.79 for hardwoods and from 0.47 to 0.84 for softwoods. Tomppo pointed out at the stand level the highest relative RMSE is 54% (Tomppo et al, 1999). For standwise forest inventory, Tomppo used a cross validation process to check the difference of estimation using different K values. The RMSE values for merchantable volume range from 118.4 to 160.3 cubic meters per hectare. ToKola et al (2001) obtained a relative RMSE of 0.65 at the stand level. Using Aerial photography to estimate volume of trees at the stand level, Paivinen et al (1993) obtained an RMSE of 55.6 cubic meters per hectare and a relatively small R_RMSE of 0.29. The best results for volume estimation using remotely sensed data with a relatively high

spatial resolution still have a high RMSE and a high R_RMSE. For example, the best results using JETS-1 (Japanese Earth Resources Satellite-1 with 18 m resolution) have an RMSE of 60 cubic meters per hectare (Schemullius et al 2005); while Tomppo et al (1995) using ERS SAR (i.e., European Space Agency, Synthetic Aperture Radar) images to estimate volume achieved an RMSE of 90 cubic meters per hectare and an R_RMSE of 0.584. In my research, the study unit is 25-m, and the RMSE for hardwood is in the range of 63.6 to 119.5, and RMSE of softwoods is in the range of 62.02 to 151.34. Reese et al (2003) conducted a countywide forest inventory, and reported the R_RMSE values are 0.58, 0.59, 0.66, and 0.69 at selected areas; they also listed the values of RMSE in Remniingstorp (e.g. a test region in Sweden) as 21, 32, 52, 87, 109, and 159 cubic meters per hectare.

However, most of the study areas in the previously mentioned publications are smaller than my study area. They usually used one scene or a small part of a scene of Landsat imagery, and the forest types in their study areas are simple. For example, the forest species in northern Europe are relatively more uniform compared to forests in the southern US. The study area in the research conducted by Tomppo et al is 1000 ha (1999), and ToKola et al used parts of one scene of Landsat imagery (2001). Using Landsat TM data to predict volume typically will result in relatively low accuracy at the pixel level (Tomppo 1993, Mouer and Stage 1995, ToKola et al 1996) yet relatively high accuracy for large areas such as the stand or landscape level (Franklin 1986, Poso et al 1987, Ahern et al 1991). It is also of significance that when trees become mature, the volume increases but the canopy closes, while the relationship between spectral reflectance and wood volume can be asymptotic and relationships for those higher volumes become less accurate. Therefore, in the applications of Landsat TM imagery, there is limited information content for denser and older forests.

Another approach to checking the performance of the weighted K nearest neighbor regression is to calculate R-squared using equation 5-5 (e.g., y_i is the ground truth, $\hat{y}_i$ is the predictions, and $\bar{y}$ is the mean of the ground truth). R-squared is calculated using both the training datasets and test datasets for hardwood and softwood, and the results were summarized in Tables 5.5, 5.6, 5.7, and 5.8.

$$R^2 = 1 - \frac{\sum_{i=1}^{n}(y_i - \hat{y}_i)^2}{\sum_{i=1}^{n}(y_i - \bar{y})^2} \tag{5-5}$$

Table 5.5. R^2 for Hardwood Volume Estimation Using Training Data

	P17R37	P17R38	P17R39	P18R36	P18R37	P18R38	P18R39	P19R37	P19R38R39
R^2	0.3436	0.3058	0.2123	0.3493	0.3218	0.3629	0.4869	0.3241	0.3876
r	0.5861	0.5521	0.4677	0.591	0.5673	0.6025	0.6978	0.5693	0.6226

r is the square root of R^2;
P17R37 is the Landsat image of Path 17 Row 37, and so on.

Table 5.6. R^2 for Softwood Volume Estimation Using Training Data

	P17R37	P17R38	P17R39	P18R36	P18R37	P18R38	P18R39	P19R37	P19R38R39
R^2	0.3325	0.2575	0.33	0.3905	0.2507	0.3589	0.5155	0.2559	0.3025
r	0.5766	0.5075	0.5745	0.6249	0.5507	0.5991	0.7179	0.5059	0.55

Notes are the same as Table 5.5.

Table 5.7. R^2 for Hardwood Volume Estimation Using Test Data

	P17R37	P17R38	P17R39	P18R36	P18R37	P18R38	P18R39	P19R37	P19R38R39
R^2	0.251	0.0039	-0.0294	0.3934	0.1909	0.1361	0.4936	0.1094	0.1546
r	0.501	0.0624	------	0.6272	0.437	0.3689	0.7026	0.3307	0.3932

Notes are the same as Table 5.5.

Table 5.8. R^2 for Softwood Volume Estimation Using Test Data

	P17R37	P17R38	P17R39	P18R36	P18R37	P18R38	P18R39	P19R37	P19R38R39
R^2	0.1937	0.0038	0.1919	0.3794	0.0614	0.1545	0.4938	0.0647	-0.08242
r	0.4401	0.0623	0.4381	0.6159	0.2478	0.3931	0.7027	0.2544	------

Notes are the same as Table 5.5.

The R^2 values calculated using training datasets were bigger than those using test datasets. The smaller the errors in the estimated wood volume, the bigger are the R^2 values. Therefore, the predictions using images of Path 18 Row 36 and Path 18 Row 39 have smaller errors, while the inventories using other images have relatively big errors. The R^2 values using images Path 17 Row 38 and Path 17 Row 39 for hardwood volume inventory were close to 0 (Tables 5.7), which indicates big errors in the estimations. For softwood inventory using K nearest neighbor regression, the R^2 values using images Path 17 Row 38 and Path 19 Row 38 and 39 were close to 0, and there were big errors in the estimations. The performance of the K nearest neighbor regression was also indicated using scatter plots of predictions versus observations for hardwood and softwood volume using both training datasets and test datasets (Figures 5.6, 5.7, 5.8, and 5.9).

5.6 Conclusions

Using the FIA mean estimation of volume, I adjusted the estimations using the weighted K nearest neighbor method and obtained the unbiased estimations. I then summarized the estimations for hardwoods and softwoods by county for the state of Georgia. I assessed total volume and mean volume of hardwoods and softwoods at the county level and identified the regions with high and low volume per hectare in Georgia. Volume per hectare also is an important indication for forest ecosystems in the state of Georgia. Using 10,000 random pixels, I evaluated my estimations, and compared these assessments with other available studies. This research is compatible with other studies.

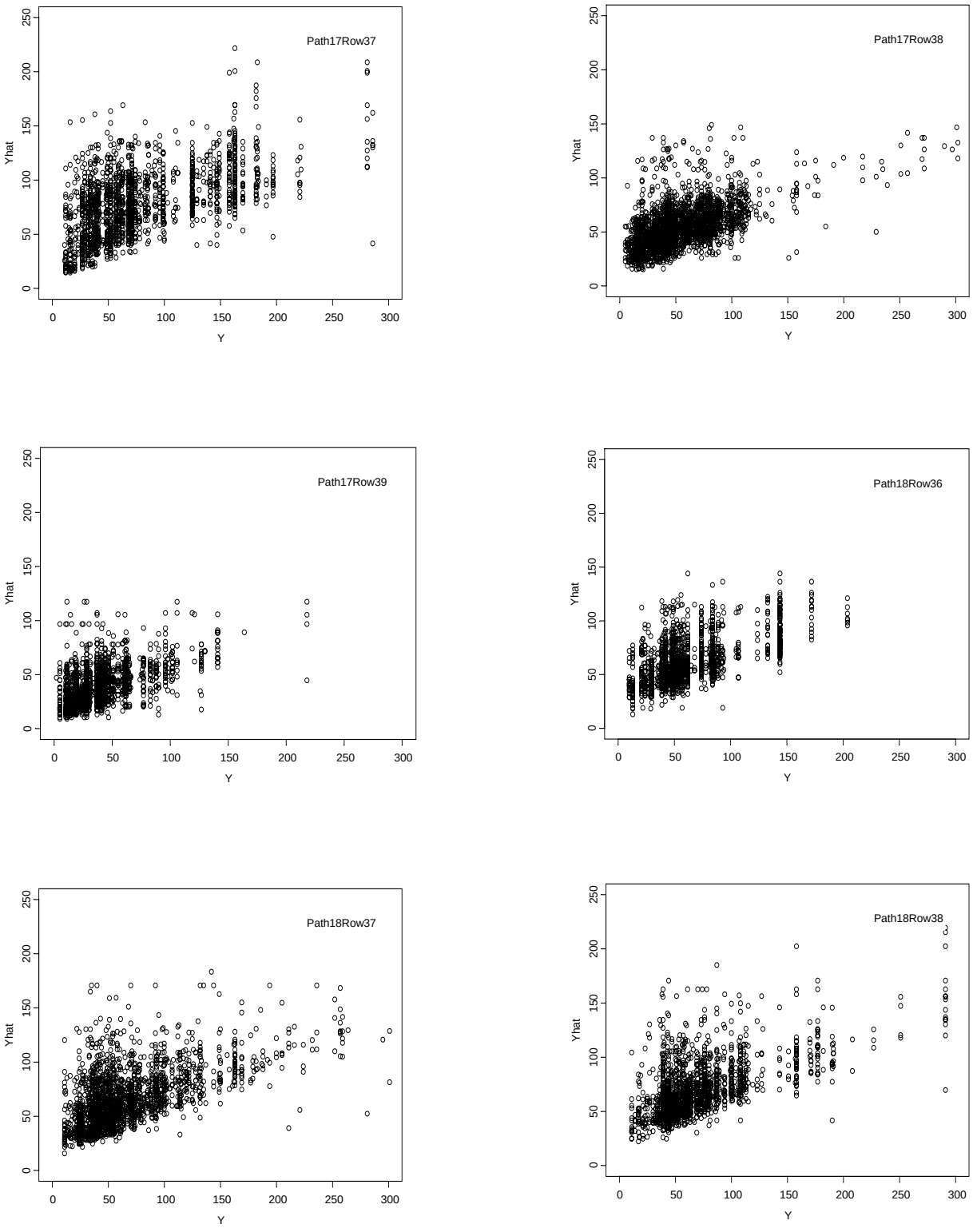

Figure 5.6. Predictions (i.e., Yhat) versus Observations (i.e., Y) of Hardwood Volume Using Training Data.

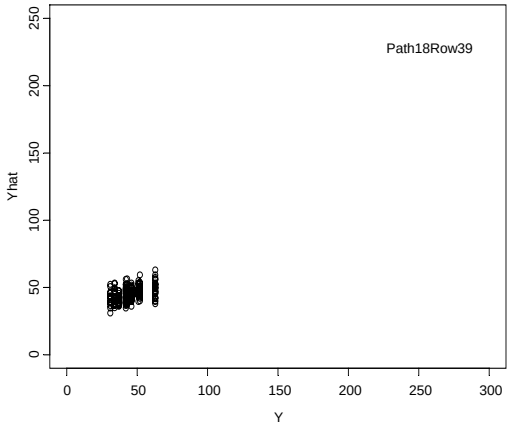

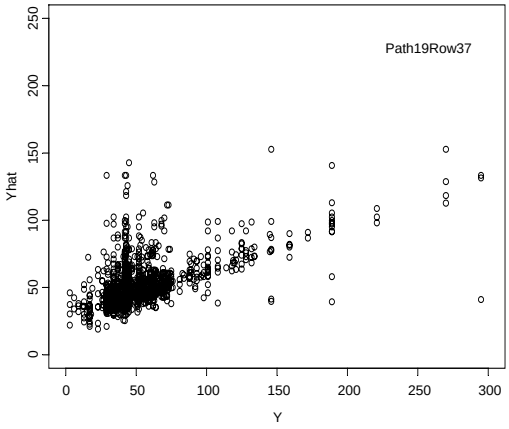

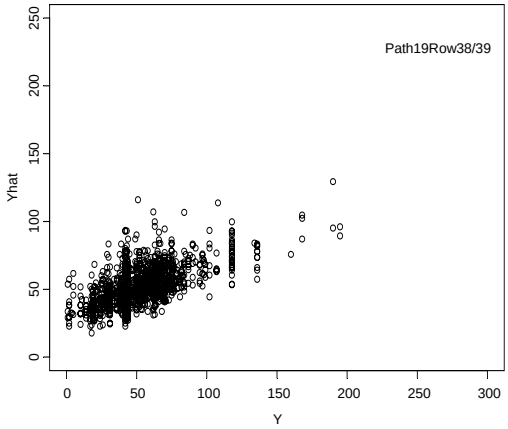

Figure 5.6. Continued.

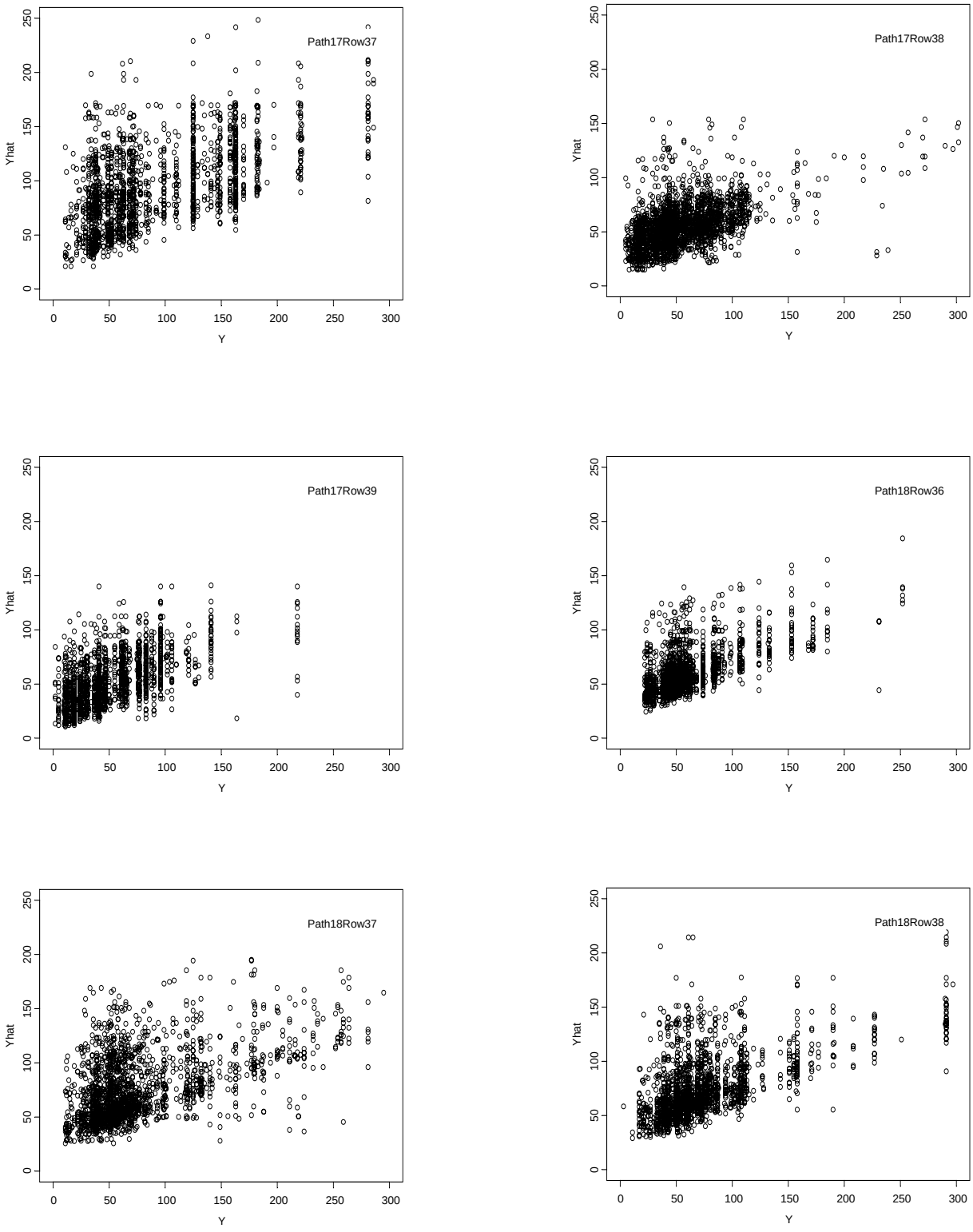

Figure 5.7. Predictions (i.e., Yhat) versus Observations (i.e., Y) of Softwood Volume Using Training Data.

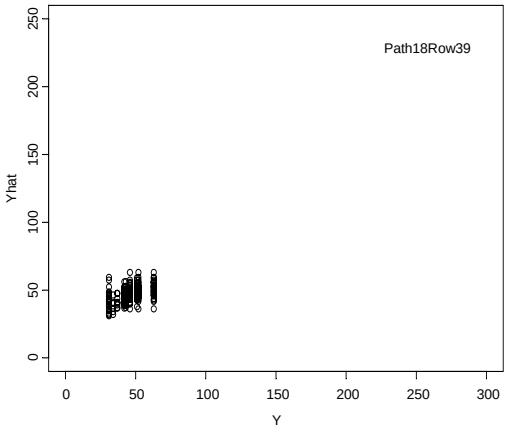

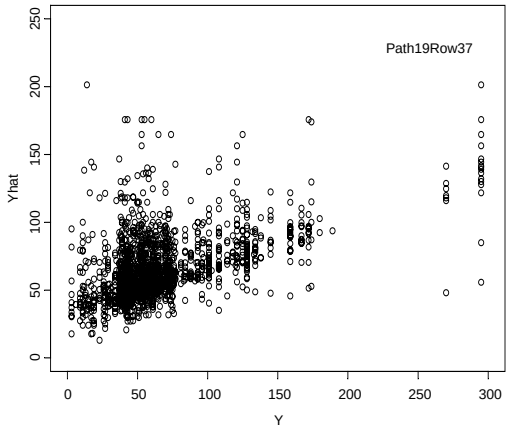

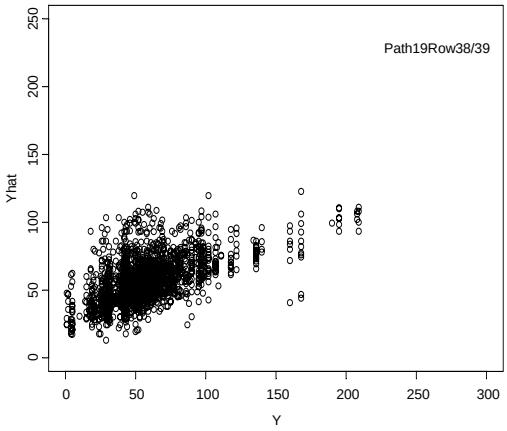

Figure 5.7. Continued

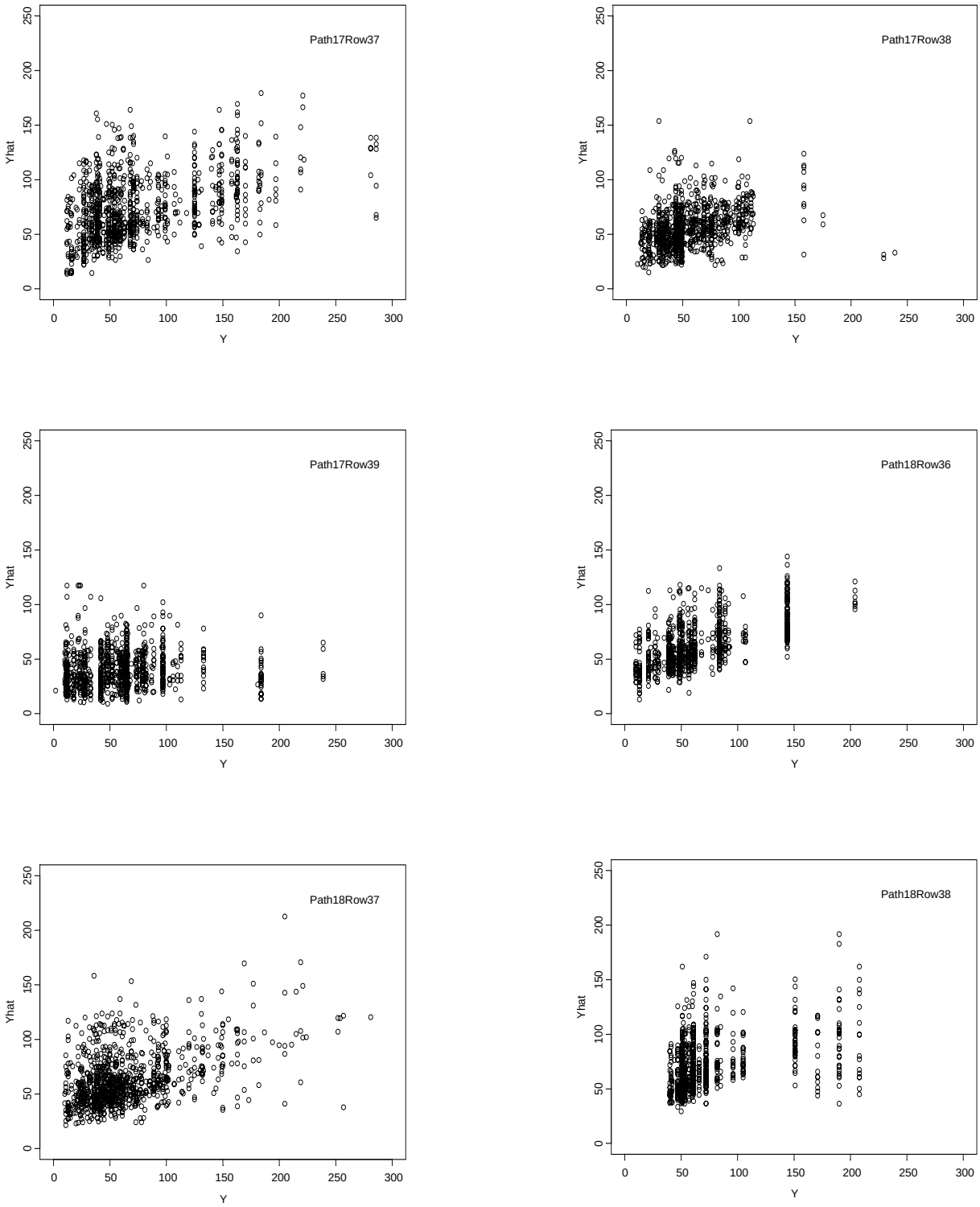

Figure 5.8. Predictions (i.e., Yhat) versus Observations (i.e.,Y) of Hardwood Volume Using Test Data.

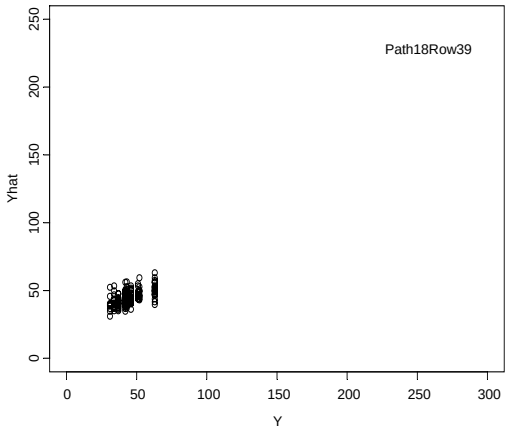

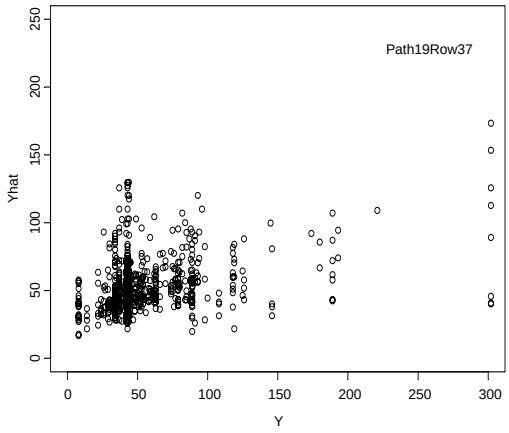

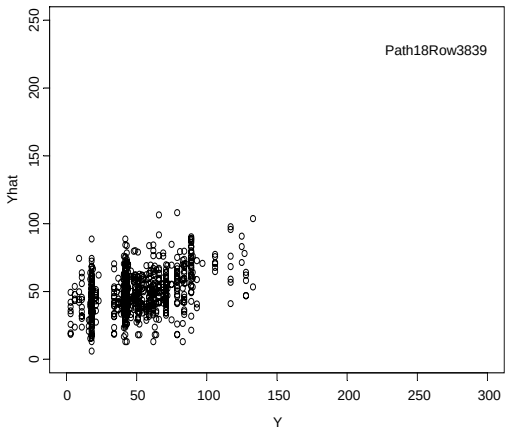

Figure 5-8. Continued.

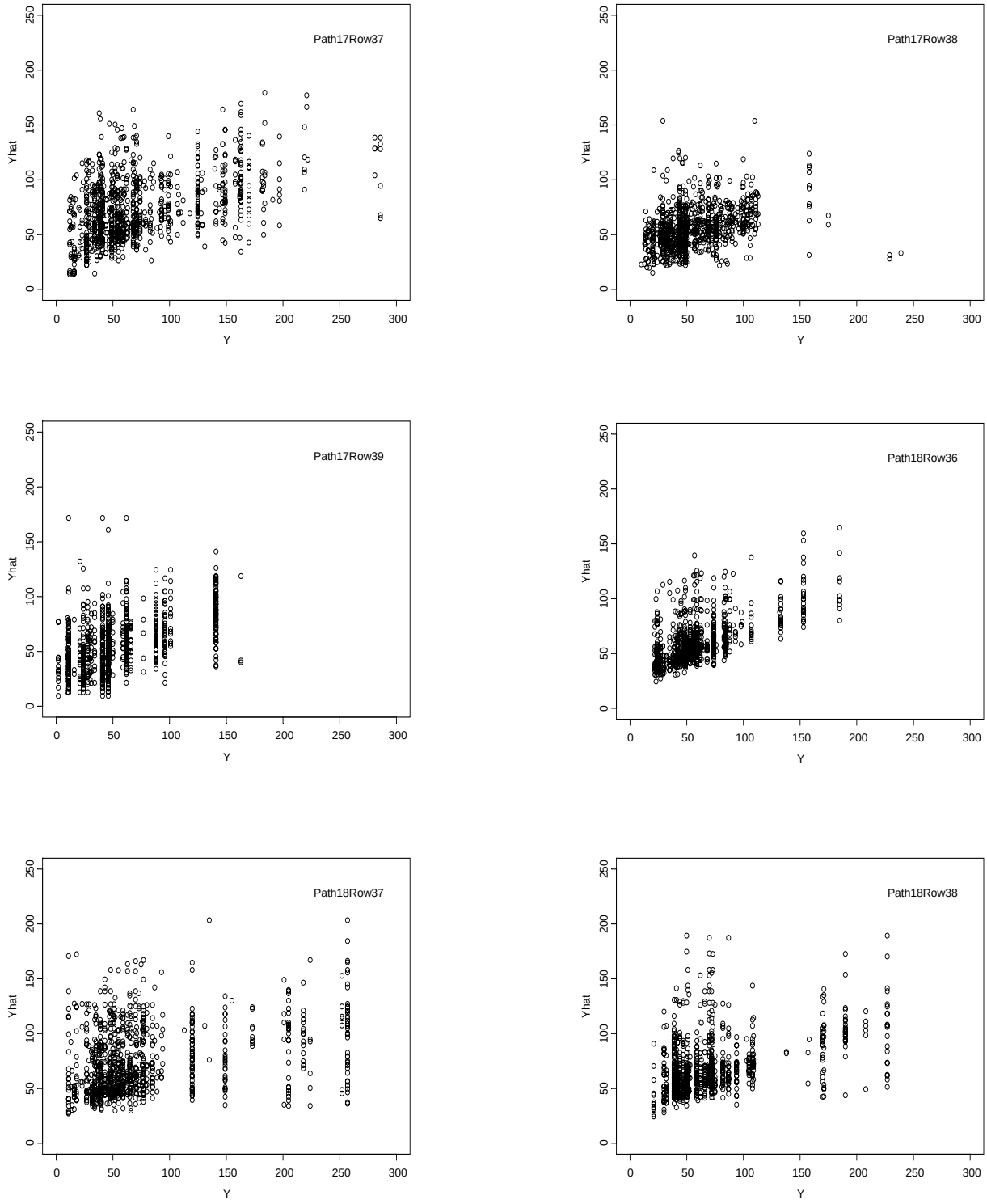

Figure 5.9. Predictions (i.e.,Yhat) versus Observations (i.e., Y) of Softwood Volume Using Test Data.

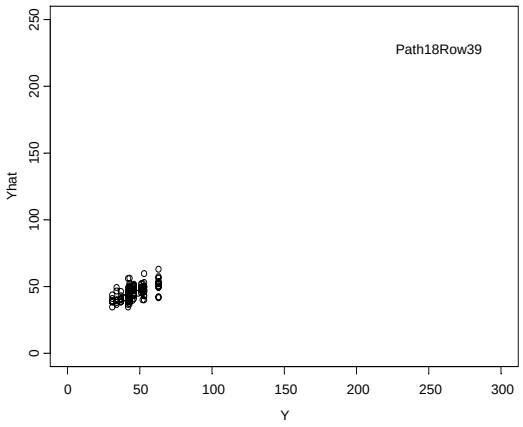

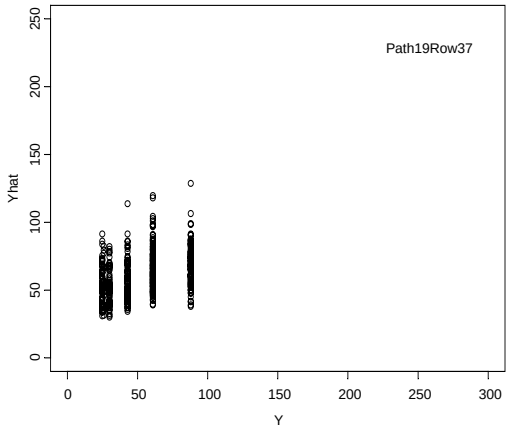

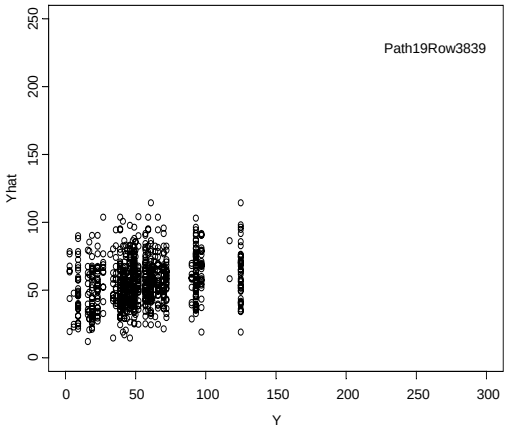

Figure 5.9. Continued.

CHAPTER 6

CONCLUSION AND DISCUSSION

6.1 Conclusions

The objective of this research is to develop and apply a remote sensing based approach for large area forest inventory in order to estimate forest variables with fine spatial resolution (i.e., a 25-m cell size). The K nearest neighbor method is a popular method and is widely applied for forest inventory. However, current research of applying K nearest neighbor method for forest inventory overlooks some of its disadvantages.

Forest is one of the main geographical phenomena, and its attributes have a typical geographical characteristic, spatial dependence. Therefore, a geostatistical approach is developed so that forest variables can be predicted using these spatial BLUP methods, i.e., a group of kriging methods.

Four sub-objectives are addressed in order to obtain the main objective of fine spatial resolution forest inventory. First, a powerful approach based on the nearest neighbor algorithm is developed to remove cloud and cloud shadow from the Landsat images so that the Landsat imagery can be applied as predictors for forest inventory. Second, two disadvantages of K nearest neighbor method is explored. The selection of K values is improved using statistical tests and comparisons of cumulative distribution functions. The computation cost can be reduced using remote sensing data reduction methods while the most useful information is still maintained in the reduced dataset. Third, a systematic geostatistical approach is developed for forest inventory. This approach includes spatial/aspatial data exploration, semivriogram

modeling, and kriging modeling. The kriging modeling typically includes ordinary kriging, universal kriging, Cokriging, and regression kriging. Regression kriging is the robust one that can incorporate both the correlation between predictors and response variables and the spatial association between predictors and response variables. Regression kriging takes advantages of regression and kriging. Fourth, for K nearest neighbor method, I explored the distance metrics and weight schemes. The estimations of K nearest neighbor are improved using improved distance measurements and weight schemes.

Finally, I use the weighted K nearest neighbor method to forecast volume of hardwoods and softwoods for each 25-meter pixel across the whole state of Georgia. The estimations are adjusted using the FIA unbiased mean estimate in order to obtained unbiased estimation. The estimates are then summarized at county level. Spatial patterns of forest productivity are characterized using the hardwood and softwood volume per hectare.

6.2 Contributions and Limitations

This study makes several contributions to forest biometrics, natural resources management, and GIS research. First, remote sensing based up-to-date forest inventory for the state of Georgia (i.e., state level or larger regions) with fine spatial resolution can be achieved using geostatistcal modeling or the K nearest nearest neighbor method in a short time. Geostatistical modeling needs the basic assumption that the variables applied in the models should be random variables, while there is no assumption for the K nearest neighbor method.

Second, a systematic geostatistical approach is developed and explored in detail for forest inventory. This geostatistical approach extends from the methods of ordinary and universal kriging that are applied in the current studies to Cokriging and regression kriging using remote

sensing imagery as predictors. The geostatistical approach developed in this research, as one of the main geospatial technologies, can be applied for any type of natural resources management including timber, wildlife, range, recreation, and hazards.

Third, the disadvantage of K nearest neighbor (i.e., the selection of K) is addressed using statistical methods. Typically, using 2 or 3 nearest neighbors resulted in good estimations since a large value of K in application of K nearest neighbor for prediction will result in relatively smooth spatial estimations of forest variables, while spatial variability is lost. Additionally, I develop a SAS program and extend the K nearest neighbor method for remote sensing data preprocessing, i.e., cloud and cloud shadow removal from Landsat TM imagery. The results indicate that nearest neighbor is a powerful method for removing clouds and cloud shadows in Landsat images, and this method can be applied for preprocessing other types of remote sensing imagery.

There are some limitations of this research. First, the accuracy of inventory estimates obtained in this work needs improving. Although it is compatible with other studies for forest inventory and its results are adjusted to the unbiased estimation, its accuracy is rather low. Second, the estimations at county level are obtained using remote sensing (i.e., Landsat TM imagery) and modeling. The applications of these results to a specific county need additional ground truthing and finer resolution data, for example up-to-date aerial photos. Third, there is not an integrated automatic approach for forest inventory using either the geostatistical approaches or K nearest neighbor method developed and applied in this research. Applying these approaches requires use of ArcGIS, Leica Geosystems ERDAS Imagine, ENVI, SAS, Splus and R programming.

6.3 Further Study

Combining Landsat TM imagery with other higher spatial resolution data can improve the accuracy of spatial estimations. One type higher spatial resolution data is Quick Bird, and using one scene of Landsat TM image as an example is a practicable approach. This way will significantly increase the data size. Therefore, the next question to be solved is to develop fast computation algorithms for processing remote sensing data.

Another interesting step is to understand the difference between the estimations and FIA values at county level. There are obvious errors in the FIA data. For example, the land area of softwoods for county Catoosa is 0, while the volume of softwoods is 477971 cubic meters. Maybe this error resulted from typos in the process of data input by FIA staff. There are certain uncertainties in the estimations using K nearest neighbor method. Using geospatial simulation and trying to understand the uncertainty in the predictions also are meaningful.

REFERENCES

Anselin, L. 1995. Local indicators of spatial association – LISA. *Geographical Analysis*, 27: 93-115.

Ahern, F.J., Erdle, T., Maclean, D.A. and I.D. Kneppeck. 1991. A quantitative relationship between forest growth rates and Thematic Mapper reflectance measurements. *International Journal of Remote Sensing*, 12:387-400.

Arana, E., P. Delicado, L. and Marti-Bonmati. 2005. Validation procedures in radiological diagnostic models, neural network and logistic regression. Http://www.econ.upf.es/deehome/what/wpapers/postscripts/414.pdf. Accessed on August 2, 2006.

Ardö, J. 1992. Volume quantification of coniferous forest compartments using spectral radiance recorded by Landsat Thematic Mapper. *International Journal of Remote Sensing*, 13: 1779-1786.

Atkinson, P.M. and P. Lewis. 2000. Geostatistical classification for remote sensing: an introduction. *Computers & Geosciences, 26*: 361-371.

Atkinson, P.M., Webster, R. and P.J. Curran. 1994. Cokriging with airborne MSS imagery. *Remote Sensing of Environment*, 50: 335-345.

Atkinson, P. M. 1993. The effect of spatial resolution on the experimental variogram of airborne MSS imagery. *International Journal of Remote Sensing*, 14: 1005–1011.

Atta-Boateng, J. and J.W.M. Jr. 1998. A method for classifying commercial tree species of an uneven-aged mixed species tropical forest for growth and yield model construction. *Forest Ecology and Management*, 104: 89-99.

Baath, H., Andreas Gallerspang Goran Hallsby, Lundstrom, A., Lofgren, P., Nillsson, M. and Goran Zstahl. Remote sensing, field survey, and long-term forescasting: an efficient combination for local assessments of forest fuels. *Biomass and Bioenergy*, 22:145-147.

Barnsley, M.J. 1999. Digital remote sensing data and their characteristics, In: Paul A. Longley, Michael F. Goodchild, David J. Maguire and David (Eds) *Geographical Information Systems: Principles, Techniques, Applications, and Management*, John Wiely & Sons: New Jersey.

Berterretche, M., Hudak, A.T., Cohen, W.B., Maiersperger, T. K., Gower, S.T. and J. Dungan. 2005. Comparison of regression and geostatistical methods for mapping Leaf Area Index (LAI) with Landsat ETM+ data over a boreal forest. *Remote Sensing of Environment*, 96: 49-61.

Braswell, B.H., Schimel, D.S., Linder, E. and B. III. Moore. 1997. The response of global terrestrial ecosystems to interannual temperature variability. *Science*, 278: 870-872.

Breiman, L. 1996. Heuristics of instability and stabilization in model selection. *Annals of Statistics*, 24: 2350-2383.

Caselles, V. 1989. An alternative simple approach to estimate atmospheric correction in multitemporal studies. *International Journal of Remote Sensing*, 10:1127- 1134.

Chica-Olmo, M. and F. Abarca-Hernandez. 2000. Computing geostatistical image texture for remotely sensed data classification. *Computer & Geosciences*, 26: 373-383.

Chanda, B. and D.D. Majumder. 1991. An iterative algorithm for removing the effects of thin cloud cover form Landsat imagery. *Mathematical Geology*, vol.23, no.6, pp 853-860.

Chander, G. and B. Markham. 2003. Revised Landsat-5 TM Rasiometric Claibration Procedures and Postcalibration Dynamic Ranges. *IEEE Transactions on Geoscience and Remote Sensing*, 41: 2674-2677.

Chica-Olmo, M. and F. Abarca-hernandez. 2000. Computing geostatisitcal image texture for remotely sensed data classification. *Computers and Geosciences*, 26:373–383.

Cieszewski, C.J., K. Iles, Lowe R.C. and M. Zasada. 2003. Proof of concept for an approach to a finer resolution inventory. *Proceedings of the 5th Annual Forest inventory and Analysis Symposium*. New Olance, LA. November 18-20, 2003.

Cihlar J. and J. Howarth.1994. Detection and removal of cloud contamination from AVHRR Images. *IEEE Transactions on Geoscience and Remote Sensing*. 32:583-589.

Clutter, J.L., Fortson, J.C., Pienaar, L.V., Brister, G.H. and R.L. Bailey. 1983. *Timber Management: A Quantitative Approach*. John Wiley and Sons, New York.

Coburn C.A. and A.C.B. Roberts. 2004. A multiscale texture analysis procedure for improved forest stand classification. *International Journal of Remote Sensing*, 20:4287-4308.

Cressie, N.A.C. 1993. *Statistics for spatial data*. John Wiley & Sons, New York.

Curran, P.J. and P.M. Atkinson. 1998. Geostatistics and remote sensing. *Progress in Physical Geography*, 22: 61-78.

Curran, P.J. 1988. The semivariogram in remote sensing: an introduction. *Remote Sensing of Envrironment*, 24: 493-507.

Czaplewski, R.L., Reich, R.M. and Bechtold, W.A. 1994. Spatial autocorrelation in growth of undisturbed natural pine stands across Georgia. *Forest Science*, 40:314-328.

Curran P.J. and P.M. Atkinson.1998. Geostatistics and remote sensing. *Progress in Physical Geography*, 22:61-78.

Dungan, J.L., Peterson, D.L. and P.J. Curran. 1994. Alternative approaches for mapping vegetation quantities using ground and image data. In: Michener, W., Stafford, S. & Brunt, J. (eds.). *Environmental information management and analysis: ecosystem to global scales*. Taylor and Francis, London, UK. pp. 237-261.

Dungan, J.L. 1998. Spatial prediction of vegetation quantities using ground and image data. *International Journal of Remote Sensing*, 19: 267-285.

Efron B, and R. Tibshirani. 1997. Cross-validation and the bootstrap: Estimating the error rate of a prediction rule. *Journal of the American Statistical Association*, 92:548-560.

Fazakas, Z. and M. Nilsson. 1996. Volume and forest cover estimation voer southern Sweden using AVHRR data calibrated with TM data. *International Journal of Remote Sensing*, 17:1701-1709.

Franklin, J. 1986. Thematic Mapper analysis of coniferous forest structure and composition. *International Journal of Remote Sensing*, 7: 1287-1301.

Foody, G.M. and D.S. Boyd. 1999. Fuzzy mapping of tropical land cover along an environmental gradient from remotely sensed data with an artificial neural network. *Journal of Geographical Systems*, 1: 23-35

Foody, G.M. 2000. Mapping land cover from remotely sensed data with a softened feed forward neural network classification. *Journal of Intelligent and Robotic Systems*, 29: 433-449.

Fotheringham A. S. and P. Rogerson. 1994. *Spatial Analysis and GIS*, London: Taylor and Francis, Ch.2, pp.25-27,

Franco-Lopez, Ek, A.R. and M.E. Bauer. 2001. Estimation of forest stand density, volume, and cover type using the K-nearest neighbors method. *Remote Sensing of Environment*, 77: 251-274.

Gilbert, B. and K. Lowell. 1997. Forest attributes and spatial autocorrelation and interpolation: effects of alternative sampling schemata in the boreal forest. *Landscape and Urban Planning*, 37: 235-244.

Goodchild, M.F. 2004. The validity and usefulness of laws in geographic information science and geography. *Annals of the Association of American Geographers*, 94: 284–289.

Goodchild M. F.2003.
Http://www.csiss.org/aboutus/presentations/files/goodchild_ucgis_jun03.pdf. University of California, Santa Barbara.

Goovaerts, P. 1997. *Geostatistics for natural resources evaluation*. Oxford University Press, New York.

Goward, S.N., Tucker, C.J. and D.G. Dye. 1985. North American vegetation patterns observed with the NOAA-7 advanced very high resolution radiometer. *Vegetatio*, 64: 3-14.

Gunnarsson, F., Holm, S., Holmgren, P., and T. Thuresson. 1998. On the potential of kriging for forest management planning. *Scand. J. For. Res*. 13: 237–245.

Hardin P.J. and C.N. Thomson. 1992. Fast Nearest Neighbor Classification Methods for Multispectral Imagery. *Professional Geographer*, 44: 191-201.

Hastie, T., Tibshirani, R. and J. Friedman. 2001. *The Elements of Statistical Learning: Data Mining, Inference, and Prediction.* New York: Springer press. 415-420 p.

Hechenbichler K. and K.P. Schliep. 2004. Weighted k-Nearest-Neighbor Techniques and Ordinal Classification. http://www.stat.uni-muenchen.de/sfb386/papers/dsp/paper399.ps. Accessed on October 15, 2006.

Heikkila, J., Nevalainen, S. and T. Tokola. 2002. Estimating defoliationin borealconiferous forests by combining Landsat TM, aerial photographs and field data. Forest Ecology and Mangement 158:9-23

Hock, B.K., Payn, T.W. and J.W. Shirley. 1993. Uisng a geographic information system and geostatistics to estimate site index of Pinus radiata for Kaingaroa Forest. New Zealand. *N. Z. J. For. Sci*., 23:264-277.

Holmström, H. and J.E.S. Fransson. 2003. Combining remotely sensed optical and radar data in *k*NN estimation of forest variables. *Forest Science*, 10: 409-418.

Holmstrom, H. 2002. Estimation of single-tree characteristics using the KNN method and plotwise aerial photograph interpretations. *Forest Ecology and Management*, 167:303-314.

Holmstrom, H. 2002. Estimation of single-tree characteristics using the KNN method and plotwise aerial photograph interpretations *Forest Ecology and Management*, 167:303-314.

Holmgren, P. and T. Thuresson. 1997. Applying objectively estimated and spatially continuous forest parameters in tactical planning to obtain dynamic treatment units. *Forest Science*, 43:317-326.

Holmgren, J., Joyce, S., Nilsson, M. and H. Olsson. 2000. Estimating stem volume and basal area in forest compartments b combining satellite image data with field data. *Scandinavian Journal of Forest Research*, 15:103-111.

ITT Company. ENVI Add-Ons FLAASH. http://www.ittvis.com/envi/flaash.asp. Accessed on July 28, 2006.

James M. 1985. *Classification Algorithms*. New York: John Wiley & Sons. 168 p.

Jensen, J.R. 1986. *Introductory Digital Image Processing: A Remote Sensing Perspective*. Englewood Cliffs, NJ: Prentice-Hall. 151-169 p.

Journel, A. G., Kyriakidis, P.C. and S. Mao. 2000. Correcting the Smoothing Effect of Estimators: A Spectral Postprocessor. *Mathematical Geology*, 32: 787-813.

Jupp, D. B., Strahler, A. H. and C. E. Woodcock. 1988. Autocorrelation and regularization in digital images I. Basic theory. *IEEE Transactions on Geoscience and Remote Sensing*, 26: 463–473.

Kramer, E. Conroy, M.J., Anderson, E.A. Bumback, W.R. and J. Epstein. 2003. *The Geogorgia Gap Analysis Project*. Institute of Ecology and Georgia Cooperative Fish & Wildlife Research Unit, University of Georgia.

Katila, M. and E. Tomppo. 2002. Stratification by ancillary data in mutisource forest inventries employing k-nearest-neighbour estimation. *Canadian Journal of Forest Research*, 32:1548-1561.

Katila, M., Heikkinen, J. and E. Tomppo. 2000. Calibration of small-area estimation for map errors in multisource forest inventory. *Canadian Journal of Forest Research*, 30:1329-1339.

Katila, M., E. Tomppo. 2001. Selecting estimation parameters for the Finnish Mulisource national forest inventory. *Remote Sensing of Environment*, 76:16-32.

Kleinn, C. New technologies and methodologies for national forest inventories. http://www.fao.org/docrep/005/y4001e/Y4001E03.htm. Accessed on November 22, 2006.

Lark, R. M. 1996. Geostatistical description of texture on an aerial photograph for discriminating classes of land cover. *International Journal of Remote Sensing*, 17, 2115–2133.

Liu Z.K. and B.R. Hunt. 1984.A new approach to removing cloud cover from satellite imagery. *Computer vision, Graphics, and Image Processing*, 25: 252-25.

Matheron, G. 1965. Les Variable Regionalisees et leur Estimation. Masson, Paris.

McRoberts, R.E., Nelson, M.D. and D.G. Wendt. 2002. tratified estimation of forest area using satellite imagery, inventory data, and the K-nearest neighbor technique. *Remote Sensing of Environment*, 82:457-468.

Meng, Q. and C.J. Cieszewski. 2006. Spatial variability and cluster analysis of tree mortality. *Physical Geography*, (In press).

Miller, H.J. 2004. Tobler's First Law and Spatial Analysis. *Annals of the Association of American Geographers*, 94: 284–289.

Mitchell, O.R., Delp, E.J. and P.L.Chen. 1977. Filtering to remove cloud cover in satellite Imagery. *IEEE Transactions on Geoscience Electronics*, Vol. GE-15, no.3, pp. 137-141.

Moeur, M. and A.R. Stage. 1995. Most similar neighbor: an improved sampling inference procedure for natural resource planning. *Forest Science*, 41:337-359.

Myers, D.E. 1982. Matrix formulation of cokriging. *Mathematic Geology*, 14: 249-157.

Myers, B. 1996. Http://www.ai-geostats.org/archives/1996/AI-11-96/0039.html. Accessed on May 1, 2006.

Myneni R.B., C.D. Keeling, C.J. Tucker, Asrar, G. and R.R. Nemani. 1997. Increased plant growth in the northern high latitudes from 1981 to 1991. *Nature*, 386: 698-702.

Murphy, A.H. and R.W. Katz. 1985. *Probability, Statistics, and Decision Making in the Atmospheric Sciences*. Boulder, Colo: Westview Press.

Nanos, N. and G. Montero. 2002. Spatial prediction of diameter distribution models. *For. Ecol. Manage*. 161: 147–158.

Nanos N., Calama R., Montero G., and L. Gil. 2004. Geostatistical prediction of height/diameter models. *Forest Ecology and Management*, 195: 221-235.

Odeh, I.O.A., McBratney, A.B. and D.J. Chittleborough. 1995. Further results on prediction of soil properties from terrain attributes: heterotopic cokriging and regression-kring. *Geoderma*, 67: 215-226.

Odeh, I.O.A. and A.B. McBratnery. 2000. Using AVHRR images for spatial prediction of clay content in the lower Namoi Valley of eastern Australia. *Geoderma*, 97: 237-245.

Paivinen, R., Pussinen, A. and E. Tomppo. 1993. Assessment of boreal forest stands using field assessment and remote senign, *Proceedings of Earsel Conference*. ITC Enshedene, the Netherlands. Aprial 19-23, 1993.

Pebesma, E. J. 2004. Multivariable Geostatistics in S: the Gstat Package. *Computer & Geosciences*, 30: 683-691.

Pebesma, E.J. 2005. The Gstat Package. http://cran.r-project.org/doc/packages/gstat.pdf. Accessed on November 25, 2005.

Poso, S., Paananen, R. and M. Simila 1987. Forest inventory by compartments using satellite imagery, *Silva Fennica*, 21: 69-94.

Reese, H., Nilsson, M., Pahlen, T.G., Hagner, O., Joyce, S., Tingelof, U., Egberth, M. and H. Olsson. 2003. Countywide estimation of forest variables using satellite data and field data from the national forest inventory. AMBIO, 32: 542-548.

Reese, H., Nilsson, M., Sandstrom, P. and H. Olsson. 2002. Applications using estimates of forest parameters derived from satellite and forest inventory data. *Computers and Electronics in Agriculture*, 37:37-55.

Samra, J.S., Gill, H.S. and V.K. Bhatia. 1989. Spatial stochastic modeling of growth and forest resource evaluation. *Forest Science*, 35:663-676.

Shao, J. and D. Tu. 1995. *The Jackknife and Bootstrap*, New York: Springer-Verlag.

Short, N.M. 1999. The remote sensing tutorial. Http://www.fas.org/irp/imint/docs/rst/Sect3/Sect3_1.html. Accessed on May 1, 2005.

Simonett, D. S. 1983. *Theory, instruments, and techniques. Vol. 1 of Manual of Remote Sensing*. Falls Church, VA: American Society of Photogrammetry, p170.

Simpson J.J. and J.R. Stitt. 1998. A procedure for the detection and removal of cloud shadow form AVHRR data over land. *IEEE Transactions on Geoscience and Remote Sensing*, 36: 880-897.

Song, M. and D.L. Civco. 2002. A knowledge-based approach for reducing cloud and shadow. ASPRS-ACSM Annual Conference and FIG XXII Congress, April 22-26.

Schmullius C. Lecture 4 Introducing to Modeling. http://earth.esa.int/dragon/Schmullius4_SAR_Introduction_to_Modelling.PDF. Accessed on Nov.11, 2006.

Tatem, A.J., Lewis, H.G., Atkinson, P.M. and Nixon, M.S. 2001. Land cover mapping from remotely sensed images at the sub-pixel scale using a Hopfield neural network. *IEEE Transactions on Geoscience and Remote Sensing*, 39: 781-796.

Tobler, W. R. 1970. A computer movie simulating urban growth in the Detroit region. *Economic Geography*, 46: 234–40.

Tobler, W. 2004. On the first law of geography: a reply. *Annals of the Association of American Geographers*, 94: 304–310.

Tokola, T., Pitkänen, S., Partinen, S. and E. Muinonen. 1996. Point accuracy of a non-parametric method in estimation of forest characteristics with different satellite materials. *International Journal of Remote Sensing*, 17: 2333-2351.

Tokola, T. 2000. The influence of field sample data location on growing stock volume estimation in Landsat TM-based forest inventory in eastern Finland. *Remote Sensing of Environment*, 74:422-431.

Tokola, T., Pitkanen, J., Partinens, S. and E. Muinonen. 1996. Point accuracy of a non-parametric method in estimation of forest characteristics with different satellite materials. *International Journal of Remote Sensing*, 17:2333-2351.

Tomppo, E. 1991. Satellite imagery-based national inventory of Finland. *International Archives of Photogrammetry and Remote Sensing*, 28: 419-424.

Tomppo, E. 1993. Multi-source national forest inventory of Finland. In: *Proceedings of Ilvessalo Symposium on National Forest Inventories*, August 17-21, Finland. pp. 52-59.

Tomppo, E., Goulding, C. and M. Katila. 1999. Adapting Finnish multi-source forest inventory techniques to the New Zealand preharvest inventory. *Scandinavian Journal of Forest Resaearch*, 14:182-192.

Tomppo, E., Nilsson, M., Rosengren, M., Aalto, P. and P. Kennedy. 2002. Simultaneous use of Landsat-TM and IRS-1C WIFS data in estimating large area tree stem volume and aboveground biomass. *Remote Sensing of Environment*, 82:156-57.

Tomppo E. and M. Halme. 2004. Using coarse scale forest variables as ancillary information and weighting of variables in K-NN estimation: a genetic algorithm approach. *Remote Sensing of Environment*, 92: 1–20.

Tomppo E., Mikkela, P., Veijanen, A., Makisara, K., Henttone, H., Katila, M., Pullianinen, J., Hallikainen, M. and J. Hyyppa. 1995. Application of ERS_1 SAR data in large area forest inventory. *Proceedings of the Second ERS Applicatioins Workshop*, London, UK. December 6-8, 1995.

Trotter, C.M., Dymond, J.R. and C.J. Goulding. 1997. Estimation of timber volume in a coniferous plantation forest using Landsat TM. *International Journal of Remote Sensing*, 18: 2209-2223.

Tucker, C.J. 1979. Red and photographic infrared linear combinations for monitoring vegetation. *Remote Sensing of Environment*, 8: 127-150.

Tuominen, S., Fish, S. and S. Poso. 2002. Combining remote sensing, data from earlier inventories, and geostatistical interpolation in multisource forest inventory. *Canadian Journal of Forest Research,* 33: 624–634.

Tuominen, S., Fish, S. and S. Poso. 2003. Combining remote sensing, data from earlier inventories, and geostatistical interpolation in multisource forest inventories. *Canadian Journal of Forest Research*, 33: 623-634

Tuominen, S., Fish, S. and S. Poso. 2003. Combining remote sensing, data from earlier inventories, and geostatistical interpolation in multisource forest inventory. *Canadian Journal of Forest Research*, 33:624-634.

Wackernagel, H. 1994. Multivariate spatial statistics. *Geoderma*, 62: 83-92.

Warren, B.C., Spies, T.A. and G.A. Bradshaw. 1990. Semivariograms of digital imagery for analysis of conifer canopy structure. *Remote Sensing of Environment 34*: 167-178.

Woodcock, C. E., Strahler, A. H. and Jupp, D. 1988a. The use of variograms in remote sensing: I. Scene models and simulated images. *Remote Sensing of Environment*, 25: 323–348.

Woodcock, C. E., Strahler, A.H. and Jupp, D. 1988b. The use of variograms in remote sensing: II. Real digital images. *Remote Sensing of Environment*, 25:348–379.

Wulder, M., Lavigne, M. and Franklin, S. 1996. High spatial resolution optical image texture for improved estimation of forest stand leaf area index. *Canadian Journal of Remote Sensing*, 22: 441–449.

Wulder, M., Ledrew, E. F., Franklin, S. E. and Lavigne, M. B. 1998. Aerial image texture information in the estimation of northern deciduous and mixed wood leaf area index (LAI). *Remote Sensing of Environment*, 64:64–76.

Zhang, C., Franklin, S.E. and M.A. Wulder. 2004. Geostatistical and texture analysis of aribore-acquired images used in forest classification. *International Journal of Remote Sensing*, 25: 859-865.

APPENDIX A

HARDWOOD AND SOFTWOOD CLASSIFICATION ACCURACY

Table 1. Classification Check at 25-m Pixel Level for Georgia

Class	Reference Totals	Classified Totals	Number Correct	Producers Accuracy	Users Accuracy
Non-forest	0	330	0	-----	-----
Hardwoods	60	153	49	81.67%	31.82%
Softwoods	1495	1072	1060	70.90%	98.88%

Table 2. Error Matrix of Classification Evaluation at 25-m Pixel Level

Classified Data	Non-forest	Hardwoods	Softwoods
Non-forest	0	0	330
Hardwoods	0	49	105
Softwoods	0	11	1060

APPENDIX B

SPATIAL DISTRIBUTION OF SOFTWOOD AND HARDWOOD, GEORGIA

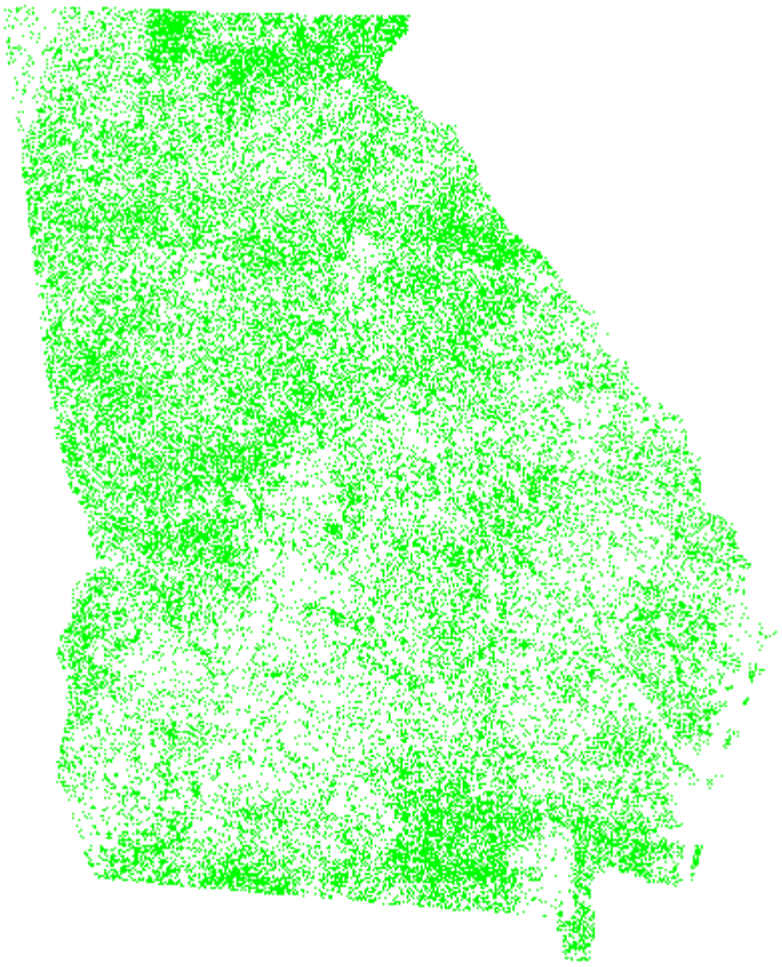

Figure 1. Softwood Spatial Distribution with a 25-m Resolution in Georgia.

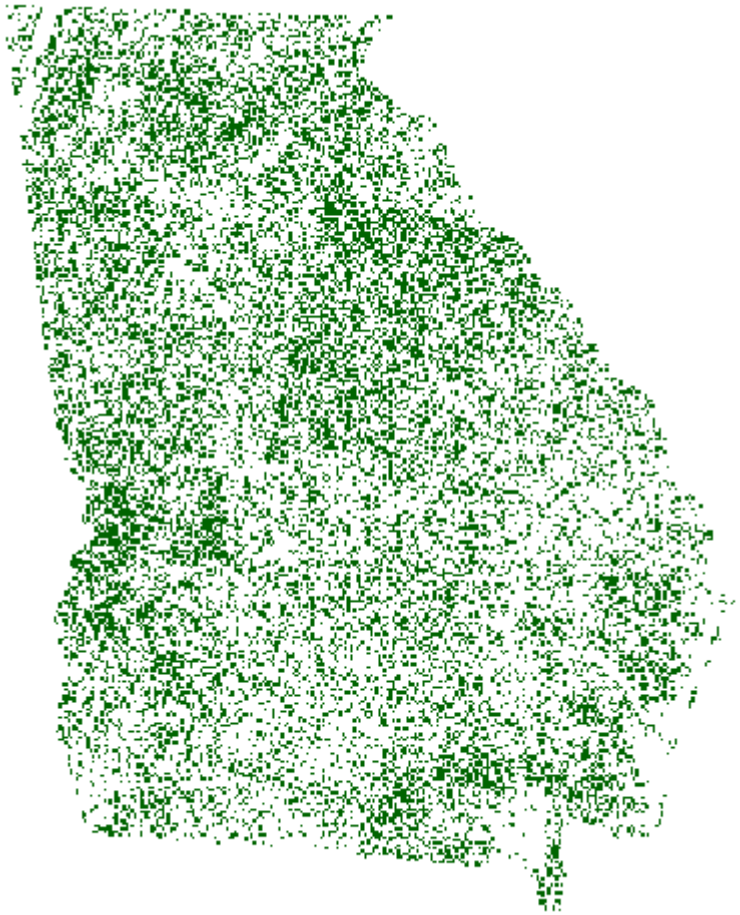

Figure 2. Hardwood Spatial Distribution with a 25-m Resolution in Georgia

APPENDIX C

ESTIMATED AREA BY HARDWOODS, SOFTWOODS, AND COUNTY, GEORGIA

	Estimation		FIA		Different ratio	
COUNTY	Softwoods	Hardwoods	Softwoods	Hardwoods	Softwoods	Hardwoods
Appling	29555	29555	49931	40664	0.69	0.38
Atkinson	35051	31933	51884	17766	0.48	0.44
Bacon	13475	13472	34491	16458	1.56	0.22
Baker	23339	28873	9547	37950	0.59	0.31
Baldwin	20207	30157	23485	22116	0.16	0.27
Banks	26509	33097	6516	29792	0.75	0.10
Barrow	21879	21939	5616	14999	0.74	0.32
Bartow	45433	34929	36277	33949	0.20	0.03
Ben Hill	18363	17039	28004	17597	0.53	0.03
Berrien	34552	22939	41527	32157	0.20	0.40
Bibb	13707	24530	11193	23319	0.18	0.05
Bleckley	12843	13166	15232	18825	0.19	0.43
Brantley	36413	35571	58257	39811	0.60	0.12
Brooks	32925	18407	39028	36935	0.19	1.01
Bryan	33101	33101	51731	36620	0.56	0.11
Bulloch	36384	34892	42096	64020	0.16	0.83
Burke	47916	59000	68665	74433	0.43	0.26
Butts	24233	23989	11367	21805	0.53	0.09
Calhoun	13959	21801	10286	25851	0.26	0.19
Camden	58205	44570	51210	55494	0.12	0.25
Candler	13385	13428	11760	27742	0.12	1.07
Carroll	44002	40921	28035	39511	0.36	0.03
Catosa	9753	14286	------	14797	------	0.04
Chalton	72129	51724	76855	42679	0.07	0.17
Chatham	8697	8697	12784	26408	0.47	2.04
Chattahoochee	19029	35752	25491	34164	0.34	0.04
Chattooga	19339	24181	20167	37432	0.04	0.55
Cherokee	37573	43302	22870	56457	0.39	0.30
Clarke	15794	16452	2181	10505	0.86	0.36
Clay	17224	15328	10808	23190	0.37	0.51
Clayton	10713	8098	1538	9232	0.86	0.14
Clinch	120083	67464	120064	72641	0.00	0.08
Cobb	38597	24947	8319	10460	0.78	0.58
Coffee	46090	52615	54409	45243	0.18	0.14

Appendix C. Continued

	Estimation		FIA		Different ratio	
COUNTY	Softwoods	Hardwoods	Softwoods	Hardwoods	Softwoods	Hardwoods
Colquitt	29056	26937	40030	40120	0.38	0.49
Columbia	31473	41259	28927	23150	0.08	0.44
Cook	10099	8779	7485	23472	0.26	1.67
Coweta	46015	37306	31638	36043	0.31	0.03
Crawford	42841	35399	34702	36770	0.19	0.04
Crisp	7653	14323	6056	26316	0.21	0.84
Dade	5150	9972	4521	22734	0.12	1.28
Dawson	19853	25960	10801	27966	0.46	0.08
Decatur	62652	54011	39020	45826	0.38	0.15
De Kalb	24679	16966	6502	5819	0.74	0.66
Dodge	37570	37419	47461	44526	0.26	0.19
Dooly	12891	18608	16856	32295	0.31	0.74
Dougherty	15836	29706	18315	30036	0.16	0.01
Douglas	15711	21365	4893	26304	0.69	0.23
Early	30178	34101	40917	22655	0.36	0.34
Echols	52971	37484	58989	40654	0.11	0.08
Effingham	37890	33595	52059	43845	0.37	0.31
Elbert	42059	22653	17955	48421	0.57	1.14
Emanuel	63264	57230	69335	64039	0.1	0.12
Evans	10994	10994	10194	21669	0.07	0.97
Fannin	59256	26636	8181	66381	0.86	1.49
Fayette	15466	15005	9910	15541	0.36	0.04
Floyd	45960	40621	16602	59399	0.64	0.46
Forsyth	16626	18991	2550	18743	0.85	0.01
Franklin	19535	19684	3591	27422	0.82	0.39
Fulton	47566	38530	13874	31677	0.71	0.18
Gilmer	51711	42071	12379	80073	0.76	0.9
Glascck	15993	16018	16971	12784	0.06	0.2
Glynn	19151	19151	37153	19028	0.94	0.01
Gordon	25777	24985	17232	28178	0.33	0.13
Grady	34538	24585	29348	40277	0.15	0.64
Greene	43141	38717	51509	30667	0.19	0.21
Gwinnett	46710	39867	9070	27147	0.81	0.32
Habersham	36101	39626	8863	42287	0.75	0.07
Hall	39651	43407	11476	43638	0.71	0.01

Appendix C. Continued

	Estimation		FIA		Different ratio	
COUNTY	Softwoods	Hardwoods	Softwoods	Hardwoods	Softwoods	Hardwoods
Hancock	52954	53358	56135	52968	0.06	0.01
Haralson	28984	26375	17050	34158	0.41	0.3
Harris	53278	48036	50208	48625	0.06	0.01
Hart	15211	12237	9342	15021	0.39	0.23
Heard	36324	28025	32948	25732	0.09	0.08
Henry	29741	31139	16224	25153	0.45	0.19
Houston	18922	28978	18994	31165	0	0.08
Irwin	15458	17973	21499	22476	0.39	0.25
Jackson	40587	38754	7795	41392	0.81	0.07
Jasper	46140	49789	37415	39033	0.19	0.22
Jeff Davis	31066	30038	45120	18867	0.45	0.37
Jefferson	43144	52016	36017	52749	0.17	0.01
Jenkins	21701	22166	28324	28329	0.31	0.28
Johnson	30721	31186	33476	20716	0.09	0.34
Jones	37838	44410	50241	35367	0.33	0.2
Lamar	21788	24724	17343	17242	0.2	0.3
Lanier	24866	21529	19293	21958	0.22	0.02
Laurens	70301	65155	68592	68684	0.02	0.05
Lee	14773	24288	17046	24511	0.15	0.01
Liberty	38708	38708	54254	40704	0.4	0.05
Lincoln	34164	26861	18139	24575	0.47	0.09
Long	31824	31824	50419	48294	0.58	0.52
Lowndes	46015	33408	40739	48673	0.11	0.46
Lumpkin	31955	30041	6802	49931	0.79	0.66
McDuffie	27860	31963	29301	16483	0.05	0.48
McIntosh	26021	26021	28272	39182	0.09	0.51
Macon	31713	35372	19502	46240	0.39	0.31
Madison	22577	21586	14717	30335	0.35	0.41
Marion	40311	33365	32462	43221	0.19	0.3
Meriwether	58509	43037	47329	48437	0.19	0.13
Miller	12239	15419	4349	21637	0.64	0.4
Mitchell	24662	30974	27595	14866	0.12	0.52
Monroe	57428	55897	38244	34423	0.33	0.38
Montgomery	23915	26314	19410	30058	0.19	0.14
Morgan	24886	35510	22838	36174	0.08	0.02

Appendix C. Continued

	Estimation		FIA		Different ratio	
COUNTY	Softwoods	Hardwoods	Softwoods	Hardwoods	Softwoods	Hardwwods
Murray	40383	26680	20394	38134	0.49	0.43
Muscgee	20962	26875	13190	18051	0.37	0.33
Newton	30199	36279	14349	20134	0.52	0.45
Oconee	15299	22929	6358	23681	0.58	0.03
Oglethorpe	60691	48271	46177	46014	0.24	0.05
Paulding	38943	33437	20703	35239	0.47	0.05
Peach	7443	10228	4222	10321	0.43	0.01
Pickens	19720	27154	12414	37604	0.37	0.38
Pierce	18354	18354	29324	27688	0.6	0.51
Pike	19847	17540	12103	20116	0.39	0.15
Polk	37200	29712	22763	29564	0.39	0
Pulaski	9770	14686	4825	28393	0.51	0.93
Putnam	32747	37866	49142	20601	0.5	0.46
Quitman	17097	15270	11011	20315	0.36	0.33
Rabun	62607	66029	6259	73734	0.9	0.12
Randolph	28357	45722	38145	40917	0.35	0.11
Richmond	21139	27141	15966	29038	0.24	0.07
Rockdale	14850	16497	6615	8594	0.55	0.48
Schley	18742	18883	13748	22375	0.27	0.18
Screven	41338	35803	58081	51944	0.41	0.45
Seminole	9617	8171	9483	8266	0.01	0.01
Spalding	18524	18186	7808	18469	0.58	0.02
Stephens	20470	21700	5588	26297	0.73	0.21
Stewart	41751	55827	50048	50950	0.2	0.09
Sumter	31036	36882	36656	33046	0.18	0.1
Talbot	48284	34304	50843	41166	0.05	0.2
Taliaferro	22080	21081	19324	22354	0.12	0.06
Tattnall	22568	22568	37349	42378	0.65	0.88
Taylor	43948	38344	40691	44992	0.07	0.17
Telfair	38096	46089	33148	57013	0.13	0.24
Terrell	13389	30383	17497	35050	0.31	0.15
Thomas	49494	23891	37976	47784	0.23	1
Tift	8305	11266	7947	12601	0.04	0.12
Tombs	18392	18638	26277	31353	0.43	0.68
Towns	26653	19765	4155	28431	0.84	0.44

Appendix C. Continued

	Estimation		FIA		Different ratio	
COUNTY	Softwoods	Hardwoods	Softwoods	Hardwoods	Softwoods	Hardwoods
Treutlen	24156	23266	28478	9676	0.18	0.58
Troup	47514	36235	34522	37776	0.27	0.04
Turner	10587	17015	18129	18223	0.71	0.07
Twiggs	29280	24466	27551	53475	0.06	1.19
Union	47451	22748	3242	53953	0.93	1.37
Upson	43264	37320	19452	43414	0.55	0.16
Walker	19021	31337	13749	59932	0.28	0.91
Walton	38006	36625	11586	31677	0.7	0.14
Ware	70369	58487	102534	43707	0.46	0.25
Warren	30360	26748	38101	22063	0.25	0.18
Washington	53623	51926	69071	65758	0.29	0.27
Wayne	44007	44007	74168	62856	0.69	0.43
Webster	20506	16948	20040	18687	0.02	0.1
Wheeler	31821	33754	34313	32626	0.08	0.03
White	30009	27768	7717	34873	0.74	0.26
Whitfield	20119	24565	14711	23775	0.27	0.03
Wilcox	22976	27267	31096	36660	0.35	0.34
Wilkes	65172	50284	53853	40213	0.17	0.2
Wilkinson	30956	37387	35403	72896	0.14	0.95
Worth	22247	31478	52334	39385	1.35	0.25
Total	5002797	4820674	4355052	5418535	0.129	0.124

Area in hectares;
Different ratio is equal to the absolute value of the difference between estimation and the FIA area over the estimated value.

APPENDIX D

SPATIAL ESTIMTION OF HARDWOOD VOLUME FOR GEORGIA

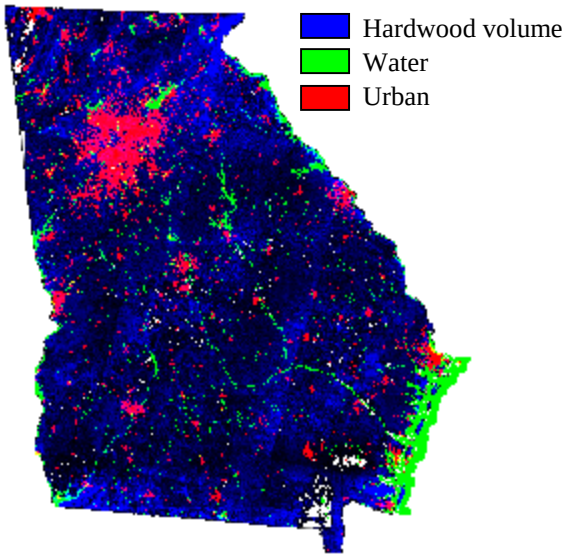

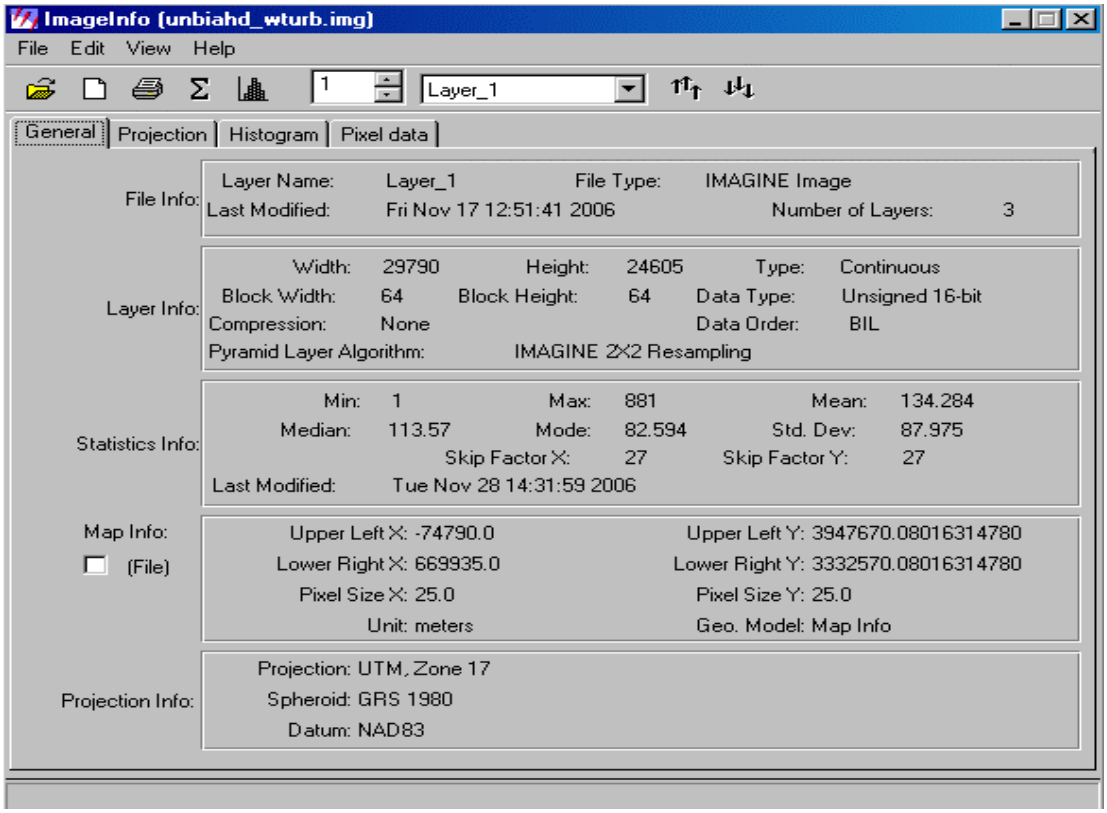

APPENDIX E

SPATIAL ESTIMATION OF SOFTWOOD VOLUME FOR GEORGIA

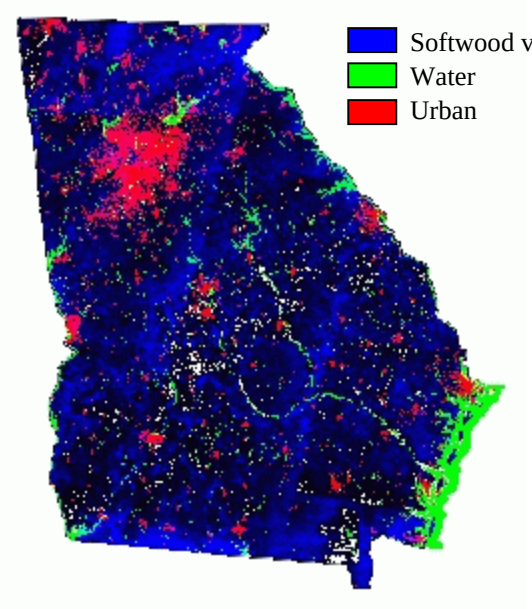

ImageInfo (unbiastallprj1121.img)

File Edit View Help

1 Layer_1

General | Projection | Histogram | Pixel data

File Info:
Layer Name: Layer_1 File Type: IMAGINE Image
Last Modified: Tue Nov 21 14:57:07 2006 Number of Layers: 3

Layer Info:
Width: 29790 Height: 24605 Type: Continuous
Block Width: 64 Block Height: 64 Data Type: Unsigned 16-bit
Compression: None Data Order: BIL
Pyramid Layer Algorithm: IMAGINE 2X2 Resampling

Statistics Info:
Min: 1 Max: 1190 Mean: 128.112
Median: 116.21 Mode: 97.617 Std. Dev: 85.459
Skip Factor X: 27 Skip Factor Y: 27
Last Modified: Tue Nov 28 14:53:39 2006

Map Info:
(File)
Upper Left X: -74790.0 Upper Left Y: 3947670.08016314780
Lower Right X: 669935.0 Lower Right Y: 3332570.08016314780
Pixel Size X: 25.0 Pixel Size Y: 25.0
Unit: meters Geo. Model: Map Info

Projection Info:
Projection: UTM, Zone 17
Spheroid: GRS 1980
Datum: NAD83